Using AASHTOWare Pavement ME Design Tools to Evaluate Flood Impact on Concrete Pavement Performance

by

Oluremi Oyediji

A thesis
presented to the University of Waterloo
in fulfillment of the
thesis requirement for the degree of
Master of Applied Science
in
Civil Engineering

Waterloo, Ontario, Canada, 2019

Author's Declaration

This thesis consists of material all of which I co-authored: see Statement of Contributions included in the thesis. This is a true copy of the thesis, including any required final revisions, as accepted by my examiners.

I understand that my thesis may be made electronically available to the public.

STATEMENT OF CONTRIBUTION

Chapter 2 of this thesis contains parts of a paper that was submitted for publication and co-authored by myself, my supervisor (Professor Tighe) and Donghui Lu, a PhD Candidate. I developed the methodology for the analysis, with inputs from Professor Tighe. Donghui Lu advised on the research methodology and data collection and I wrote the paper based on the findings. I documented the findings and the co-authors also provided editing and review during paper production.

Chapter 3 of this thesis consist of a paper that will be submitted for publication. The paper is coauthored by myself, my supervisor, Dan Pickel, Research Engineer, and Warren Lee. My supervisor, initiated the project, I developed the methodology for the study, Warren Lee collected and provided data for the analysis, Dan Pickel provided guidance on the analysis and assisted in the compilation of data for the study. The co-authors provided technical inputs regarding the analysis of the data. I analyzed the data and developed the new calibration coefficients, and I wrote the paper based on my findings.

Chapter 4 of this thesis contains parts of a paper that will be submitted for publication. The paper is co-authored by myself, my supervisor, and Jessica Achebe, a Ph.D Candidate. My supervisor, provided guidance on the research methodology, I developed the methodology for the analysis, collected and analyzed the research data by myself. I wrote the paper based on the findings and Jessica Achebe provided editing and review during paper writing.

ABSTRACT

The resilience of concrete pavement to flood impact has remained positive based on previous experimental investigations and overtime recommended as a pre-flood adaptation strategy in countries such as Australia and the United States. However, no study on concrete pavement flood impact performance has been conducted in Canada until now. Flood impact assessment under Canadian climate conditions was therefore conducted on typical concrete pavement designs common to the provinces of Ontario and Manitoba.

In the Ontario study, representative arterial and collector pavement designs were modelled, and cycles of flood hazards simulated on these pavements to evaluate changes in performance under climate change scenarios using the AASHTO Pavement ME Design (PMED) program. Percentage damage was estimated by observing changes in International Roughness Index (IRI) prediction values under flood and no-flood conditions. Results indicate a slight reduction in pavement performance across road classes, and minimal increases in damage as event cycles increased. Estimated flood damage on pavement performance was more pronounced in collector (non-dowelled) pavements than arterial (dowelled) pavements. The major distress indicator which contributed to damage was faulting, being that it increased across event cycles irrespective of return periods.

In the Manitoba case study, a total of 27 pavement design classes was developed based on a matrix of representative traffic levels, subgrade conditions and slab thicknesses common to the province. Projected climate-induced flood hazards under climate change scenarios were further modelled on the design classes to evaluate flood impact on concrete pavement performance. Results also indicated diminutive flood damage and loss of life in all of the concrete pavement classes. Increases in flood cycles induced no further damage or loss in pavement performance. In all of the pavement classes considered, there was no positive change or damage to faulting and fatigue cracking under flood conditions. The IRI parameter was the only parameter influenced by inundation, which could further suggest the possible build-up of permanent moisture-induced

warping. The observed low flood damage ratios further reiterates the resilience and adaptive capacity of the Jointed Plain Concrete Pavement (JPCP) to withstand extreme precipitation or flood conditions.

A local calibration of the AASHTOWare Pavement ME Transverse Cracking Transfer Function was successfully completed to fit observed concrete pavement performance in Ontario. As bias existed in cracking predictions using default AASHTOWare Pavement ME cracking calibration coefficients, a need for local calibration was pertinent to provide better predictions of cracking performance under Ontario conditions. This achievement is pivotal to the delivery of reliable and economical pavement design and construction projects across the province. The derived local calibration factors have been accepted and published by the Ministry of Transportation Ontario (MTO) for industry use.

ACKNOWLEDGEMENT

I would like to expresses my deep and sincere gratitude to Professor Susan Tighe for granting me the opportunity to conduct research at the best engineering university in Canada. Studying here was a lifelong dream. I am deeply grateful for her guidance and encouragement all through my research study.

I am also very grateful to Professor Hassan Baaj, the Director of CPATT. I always admire his great technical knowledge and unique teaching styles.

My gratitude also goes to the supporters of this research,

- Cement Association of Canada (CAC)
- Concrete Ontario
- The Natural Sciences and Engineering Research Council of Canada Collaborative Research and Development Program, (NSERC CRD)
- Ministry of Transportation Ontario (MTO)

I would like to specially thank Donghui Lu, Ph.D Candidate, Dan Pickel, Research Engineer, Mr. Warren Lee, MTO, and Jessica Achebe, Ph.D Candidate. Donghui Lu provided me with various suggestions on this research study. Dan Pickel engaged and provided guidance on the MTO calibration study and Jessica Achebe helped to refine ideas and strategies on this research.

A big thank you to Abimbola Grace Oyeyi for helping me settle in Canada so easily at the beginning of my program.

Furthermore, I thank all my CPATT and University colleagues, Ali Qabur, Edward Abreu, Rob Aurilio, Dandi Zhao, Hawraa Kadhim, Huyan Ju, Luke Zhao, Wei Yi, Frank Liu, Oladotun Alade, Tunde Adubiobi, Abdulrahman Hamid, and Saeid Salehiashani for always responding to my requests.

Last, but not the least, my gratitude goes my Creator, the Maker of Heaven and Earth, my Helper and my Friend, the Lord Jesus Christ, for always answering the most insignificant prayers of mine. Thank you for making everything beautiful in your time.

DEDICATION

I dedicate this thesis to my loving father of blessed memory, Late Honorable Olubunmi Oyediji (MFR) and the blessed family he left behind, Bimpe Oyediji (Mother), Aduragbemi Oyediji (Brother) and Tunde Olubode (Brother).

TABLE OF CONTENT

LIST OF FIGURES

LIST OF TABLES

Chapter 1
General Introduction

1.1 Background and Motivation

Climate change is increasing the reoccurrence of climate hazards across Canada and this is threatening the sustainability of critical infrastructures as most assets were not designed to withstand the aggression imposed by climate hazards. Flooding is a major Canadian climate hazard limiting the performance of critical assets as it results in rapid deterioration and early aging of infrastructure due to flood loads. Highly vulnerable infrastructures include water and transportation. Road infrastructure, which is a major transportation asset, has been reported vulnerable to flood hazards. With increases in flood frequency, these vulnerabilities may likely turn into a risk with heavy cost implications. As Canada is faced with aging infrastructure, flood hazards, heavy traffic due to migration, ever increasing business activities and population growth, a heavy toll is taken on our road way system and its condition is gradually deteriorating. Road pavements are a critical component of sustainable socio-economic activities and a loss of their performance can come with heavy user and non-road user costs. Therefore there is a need to conscientiously give considerations to road measures, materials and alternatives that provide resilience and sustained performance in the wake of reoccurring extreme climate events.

Based on previous investigations into how pavements types, classes and configuration respond to extreme events, concrete pavements have been reported to provide better performance in the wake of flood hazards in various countries that have experienced hurricanes, typhoons, intense flooding and inundation. Although Canada has experienced some of the worst flood incidences in history and owns a number of concrete pavement infrastructure, no study on flood impact has been conducted on concrete pavements to better understand their response to extreme events under the Canadian climate. To get insight into concrete pavement flood response, the use of state of the art AASHTOWare Pavement ME Design (PMED) program was employed to model various flood scenarios on concrete pavement types and configurations common to two Canadian provinces. Furthermore, to improve PMED pavement performance prediction, a local calibration of Jointed

Plain Concrete Pavement (JPCP) transverse cracking model was performed for the province of Ontario and calibration coefficients recommended for industry use by the Ministry of Transportation Ontario (MTO).

1.2 General Research Objectives

The primary goal of this thesis is to investigate the impact of flooding and inundation on the performance of concrete pavements in Canada to further enhance use of concrete pavements in provincial and municipal applications. This is accomplished by accessing future climate-induced extreme precipitation magnitudes under climate change, modelling flood cases on representative concrete pavement designs using AASHTOWare PMED program and evaluating pavement performance changes under flood and no-flood conditions.

Additionally, for the delivery of reliable and economical pavement design and construction projects across the province of Ontario, a local calibration of the AASHTOWare Pavement ME transverse cracking transfer function for better concrete pavement distress prediction was performed, aiding the use of the sophisticated PMED program for concrete pavement designs.

The general objectives of this study are as follows:

1. To investigate the impact of flooding and inundation on concrete pavement performance
2. To evaluate how various concrete pavement designs respond to flood and inundation
3. To gain insight into optimal concrete pavement designs with good flood resilience, service life and cost feasibility

1.4 Thesis Organization

This thesis has been written in a "manuscript-based" style, arranged into five chapters, starting with a general introduction followed by the main body from Chapter 2 to 4 organized in an integrated article format. Then, the last chapter presents a general conclusion for the study.

Chapter 1: General Introduction – This chapter provides a background of the study, which is a review of the influence of flood events on concrete pavement performance. This chapter informed on the problem statement and details the research objectives for all articles in this thesis.

Chapter 2: Manuscript 1 – The title of the first technical paper is "Impact of Flooding and Inundation on Concrete Pavement Performance – Ontario Case Study". This paper explores the previous field investigative studies conducted on concrete pavement flooding outside Canada. No study currently exist on the topic in Canada, therefore a modelling approach through pavement design and analysis is conducted to investigate concrete pavement flood impact. As JPCP is the dominant concrete pavement type in Ontario, representative Ontario arterial and collector JPCP and likely flood cases under a climate change scenario were modelled using the AASHTOWare Pavement ME Design (PMED) Tool. Performance results of the two JPCPs provided insight on the response of JPCP pavement types to various flood hazards in Ontario.

Chapter 3: Manuscript 2 – The title of the second technical paper is "Calibration of Ontario AASHTOWare Pavement ME Transverse Cracking Transfer Function". This paper describes the local calibration of the Pavement ME JPCP transverse cracking distress prediction model to Ontario conditions. Derived calibration coefficients from this paper have been published by the Ministry of Transportation Ontario (MTO) for Ontario JPCP pavement design, analysis and forensic investigative studies.

Chapter 4: Manuscript 3 – The title of the third technical paper is "Towards a Flood Resilient Pavement System in Canada – A Rigid Pavement Design Approach. Case of Ontario and Manitoba". This paper provides a deeper insight into the resilient capacity of rigid pavements

under flood conditions considering service life and cost feasibility. A matrix of twenty-seven (27) JPCP designs was developed based on typical traffic, slab thickness and subgrade parameters common to the province of Manitoba and flood impact modelled to estimate performance change. A more robust analysis of flood performance results of Ontario arterial and collector JPCP was also conducted.

Chapter 5: Conclusions and Recommendations for Future Work – This chapter provides a summary of findings, contributions to the state of knowledge and recommendations for future work.

Chapter 2

Impact of Flooding and Inundation on Concrete Pavement Performance

2.1 Overview

Pavement infrastructure have become vulnerable to damage as they were not designed to withstand the aggressions of extreme weather events such as flooding, induced by climate change. In Ontario, flooding tops the list of climate change hazards having a consequential impact on pavement performance. Rigid pavements are recorded to provide resilience to flood hazard in literature but knowledge about its behaviour and response to flood impact is currently scarce. The objective of this study is to investigate the impact of flood hazards on the performance of concrete pavement examining a case study of Jointed Plain Concrete Pavement (JPCP) road classes in Ontario. Subsequent to this, the AASHTOWare Pavement ME Design (PMED) program was employed to simulate JPCP performance under climate change using a conservative Representative Concentration Pathway (RCP) of 4.5W/m^2. Flood depth, duration and event cycles were used to define flood loading. Typical designs of JPCP collector and arterial road classes in the province were chosen and modelled. The result indicated lower damage ratios and loss of pavement life based on changes in faulting and International Roughness Index (IRI). Increases in flood frequency resulted in additional damages and loss of pavement performance and analysis showed that arterial pavement was more resilient to flood damage than collector pavements. The inference is that concrete pavements may not have their life shortened at lower cycles of extreme precipitation. However, at higher frequencies of extreme precipitation, damage may increase and resilience to flood hazards in JPCP pavement altered.

2.2 Introduction

Based on historical studies, climate is changing due to anthropogenic activities (IPCC 2013) thereby increasing the frequent occurrence of natural hazards. A number of infrastructural systems are being threatened by these hazards as they were not designed to cater for the extreme conditions brought about by climate change. Roadways critical infrastructure pivotal to socio-economic growth, is not exempted from this threat and has been declared susceptible to the impact of the

changing climate (Schweikert *et al.* 2014). Therefore, given its importance, potential climate change impacts need to be addressed (Tighe 2015).

Natural hazards classified into hydrological, meteorological, geological, and biological hazards have increased over the years. In Ontario, hydrological hazards such as flooding are more pronounced as it tops the list of natural hazards in the province for over a century. Public Safety Canada and Environment Canada reported a total of 160 disasters occurring between the year 1900 to 2013, out of which flood hazard occurred 56 times amidst 12 other climate disasters recorded. (Nirupamaa N. and Sheybanib 2014, PSC 2014). This portrays flooding as a major threat and investigation into its possible impact on road infrastructure is pertinent.

Following the July 8, 2013 extreme precipitation of over 126 mm of rainfall which flooded major parts of the city of Toronto, the Insurance Bureau of Canada evaluated socio-economic damages to be approximately $1 billion, describing the event as the most expensive natural disaster in the history of Toronto and Ontario (Environment Canada 2014). Similarly, a previous event washed out a portion of Finch Avenue in the same city on August 19, 2005. According to a publication by Clean Air Partnership, predictions indicates increases in the frequency of these types of events over the next 50 years (CAP 2006).

For pavement infrastructure, increased frequency in rainfalls may lead to pavement flooding and higher groundwater levels, causing soil erosion, slope instability, reduced pavement strength, and lowering of pavement's load bearing capacity. Furthermore, flooding and freezing rain are liable to cause safety hazards for the transportation sector, and potentially loss of pavement infrastructure (Tighe 2015). Sequel to the vulnerability of pavements to flooding, interests have grown in the study of the impact of flood on road pavements especially in flexible pavements, due to its general use. Chen and Zhang (2014) assessed the performance of submerged pavements during the 2005 Hurricane Katrina and Rita in Louisiana, using before and after flood pavement management system data. Their study primarily reported slight increases in road roughness in both flexible and rigid surfaces as a result of the flood event. This increase was further intensified by debris-carrying

heavy trucks traversing the submerged roadways immediately after the hurricane event. The inundation of the pavement weakened subgrade strength and could not sustain heavy vehicle load. Evaluation of pavement structural performance using falling weight deflectometer (FWD) testing to obtain Deflection at the plate (D1), Effective Structural Number (SN_{eff}) and subgrade Resilient Modulus M_r of inundated pavements was done months after the same flood event to estimate structural damages. Loss of structural strength was recorded in both flexible and concrete pavements with AC suffering more damage and concrete pavements recording a diminutive loss in SN_{eff} strength and Mr after the hurricane event. (Gaspard *et al*. 2006).

With emphasis on functional performance, Khan *et al.* (2014, 2017) explored the changes in International Roughness Index (IRI) of 34,000 km of Queensland roads inundated in the 2011 extreme flood event in Australia. Using before-flood and after-flood performance data to develop a new roughness and rutting-based road deterioration model, he reported that high strength rigid pavements provided the highest resilience to flooding and further proposed concrete pavement to be employed as a preflood strategy. This resiliency of concrete pavements can be further justified considering the response of Continuously Reinforced Concrete Pavement (CRCP) roads to flooding in the 2017 Hurricane Harvey event (an over 1000mm storm which lasted for over four (4) days) in South East Texas and South West Louisiana. Despite event extremities, no CRCP repairs were needed on the submerged CRCP roads. Based on a damage evaluation subsequently conducted to the event (TRB 2018), CRCP was reported to be resilient to both flood hazard and traffic loading during and after inundation. The presence of heavily stabilized base in the CRCP structure could have therefore contributed to this resilience (Lukefahr 2018, Powell 2018).

The resiliency of concrete pavement to flood hazard is receiving attention amid the need for flood adaptation measures. Therefore, an intensive study to provide insight on its response to flood hazard is desired. In 2017, a Research Need Statement (RNS) was issued by the Transportation Research Board (TRB), under its Committee for Design and Rehabilitation of Concrete Pavements AFD50, on the impact of flooding and inundation on concrete pavement performance and an

assessment of any modifications that could improve the resiliency of concrete pavements (Mack 2017).

This paper investigates the impact of flood hazards on concrete pavements performance using the PMED program. This modelling technique uses an Enhanced Integrated Climate Model (EICM) in its simulation of pavement performance and has been employed in previous studies relating to climate change hazards on flexible pavements. (Tighe *et al.* 2008, Mills *et al.* 2007, Meagher *et al.* 2012, Qiao 2015, Gudipudi *et al*. 2017, Lu *et al*. 2018a, Lu *et al*. 2018b). Therefore, specific analysis on the impact of flood hazard on rigid pavements using PMED simulation should be carried out, and this is presented in this paper. Typical arterial and collector Jointed Plain Concrete Pavement (JPCP) designs common to the province of Ontario were selected as case study. The aim of this study is to investigate the impact of flood hazard on concrete pavements performance.

2.2.1 Framework for Flood Impact Assessment of Rigid Pavement Performance

To properly evaluate flood impact on the concrete pavements, this paper takes the approach shown in Figure 2-1:

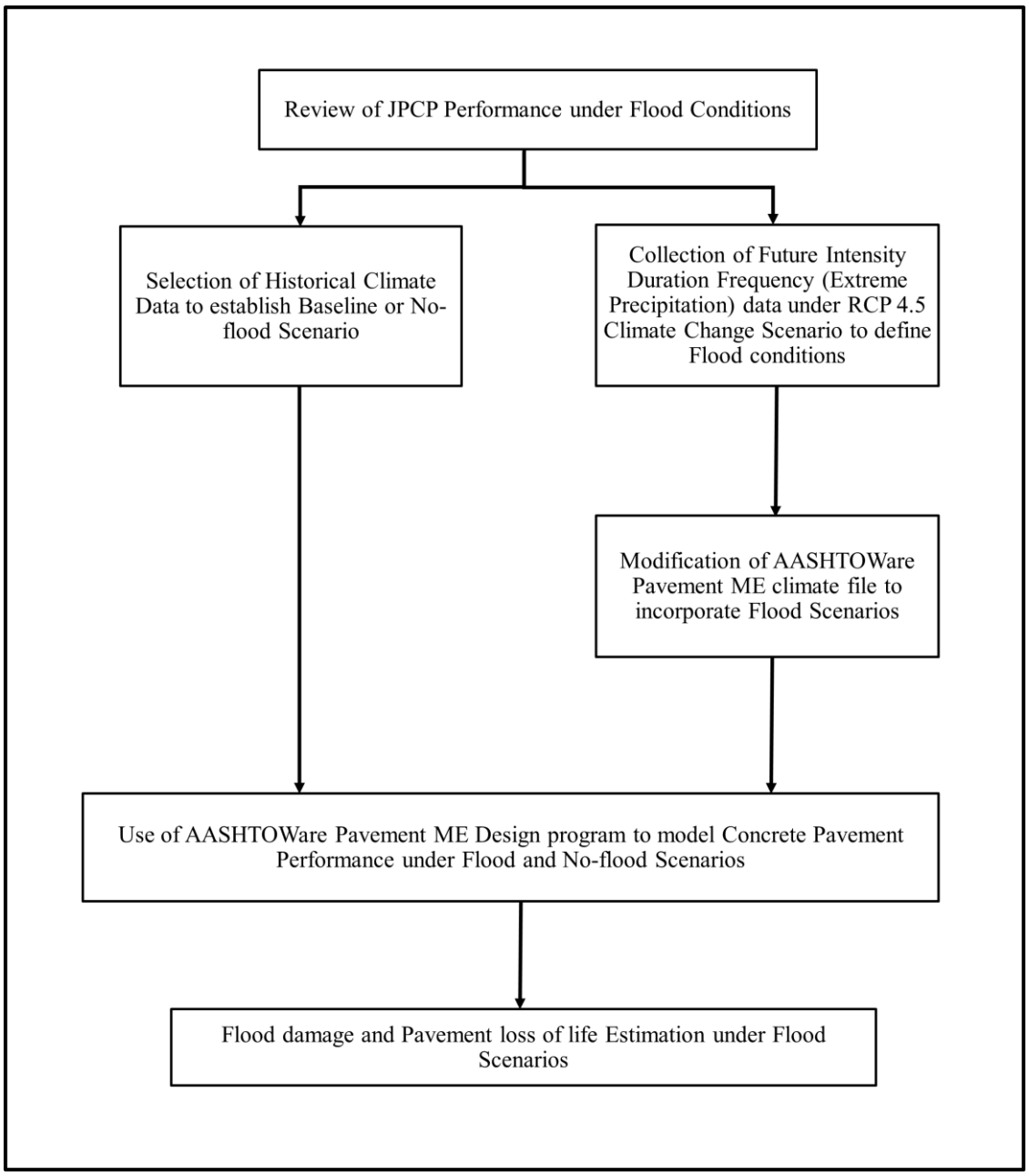

Figure 2-1 Methodological Approach of Evaluating Flood Impact on JPCP.

2.3 Flooding of Concrete Pavement Structure

Concrete pavements can provide improved resistance to damage in the presence of excessive water due to the rigid nature of the structure. In his study, Zhang *et al.* (2008) reported that AC pavements had a Mr loss of subgrade and deflection of 20% and 46%, while concrete pavements had 1% Mr loss of subgrade and 9% deflection following Hurricane Katrina event. (Kahn *et al*. 2017). This reveals Portland Cement Concrete (PCC) pavement as being resilient to flooding, and a choice to

be considered in flood plain areas. The resistance to flood damage in a dowelled and non-dowelled JPCP may have different magnitude. Resistance can be less if compared to non-jointed PCC such as CRCP due to the presence of joints in JPCP, as concrete pavement structural failures can occur at the joints. Thus, resulting in the development of different failure patterns. Lu *et al.* (2018b) proposed four different pavement flood damage patterns namely delayed effect, jump effect, jump and delayed effect, and direct failure effect to describe the possible effect of flood impact. Flooded concrete can potentially experience pavement failure patterns depending on its level of resilience which is a function of traffic, pavement age, existing distresses, PCC pavement type, sub-layer support and structural strength. The PMED practically helps to integrate all these design variables for performance prediction hence the reason why it is employed to model flood performance in this paper. With regards to pavement type, CRCP is not as common as JPCP in Ontario and as there are no PMED typical inputs for CRCP, it is difficult to estimate its flood resilience. Nevertheless, future research should be conducted to compare the flood performance of these two rigid pavement types.

Generally, the detrimental impact of flooding in pavements are pronounced in the sublayers. Studies have shown that inundated roads experience 15 times more damage compared to well-drained soil, (Yuan and Nazarian 2008) causing more deformation and loss of strength. Unbound sublayer soils tend to be at their weakest state during and after a flood event and heavy traffic loading such as those imposed by debris carrying trucks may permanently damage the pavement. Although the sublayer soils under the rigid pavement offers no structural strength, it may lose its ability to provide a uniform foundation to the PCC slab under flood conditions. Floods of high velocity can entirely erode the base and subgrade layer of the PCC leaving no sublayer support. In some cases, a flood may carry large boulders, rocks and other heavy matter known as flood debris to collide with PCC pavements at high speeds, leading to collapse, large spalls, massive edge breaks and in some cases, entire damage of the concrete pavement. It could be difficult to quantify the extent of these loadings due to the dynamic nature of flooding which can be characterized by flood velocity, flood debris and hydrogeological conditions. Inundation is typically considered

when evaluating flood impact, as it basically describes flood depth and duration. Flood loading types are further highlighted under the flood modelling section of this paper.

2.4 Flood Induced Distresses in JPCP

2.4.1 Pumping and Joint Faulting

Unbound underlying soils are common to JPCP and inundation of these layers combined with the action of fast-moving traffic may increase the hydraulic pressure under the JPCP slab. Pushing underlying fine materials into PCC joints or underneath adjacent slab at the joint in a process referred to as pumping. Soil depletion under the slab may initiate large voids and lead to the depression of one adjacent PCC slab to another, initiating the development of faulting distresses. Joint faulting is described as the difference in elevation between adjacent joints at a transverse joint (ARA 2004b). As flood events increase moisture in unbound underlying layers, migration of saturated and soft fines underneath the JPCP slabs may cause elevation and depression at joints, consequently inducing faulting distresses. The influence of traffic on affected joints could intensify these distresses and hence reduce pavement performance and overall service life.

2.4.2 Warping

After an extreme precipitation event and water is allowed to drain, a moisture gradient will most likely develop in the slab, increasing from top to bottom. Concrete pavements are sensitive to volumetric changes in the presence of moisture and temperature. Therefore, tensile stresses develop in a PCC slab with moisture gradient, causing movements that deflect the slab along its edges compared to the middle in a distress known as warping. As shown in Figure 2-2, downward curvature and upward curvature or warping is as a result of negative and positive moisture gradient respectively (FHWA Techbrief 2015). Increased frequency of flood event may potentiality worsen this situation by instigating higher groundwater tables and longer drainage days (Daniel et al. 2014). impacting the service life and smoothness of the PCC pavement. This is indicative based

on a seventeen (17) year study of the LTPP SPS-2 site. Analysis of the study revealed long-term increases in slab curvature is more associated with moisture-induced warping as it independently increased IRI by an average of 0.58m/km with no other distress observed. (Karamihas and Senn 2012). Therefore, one could infer that the repeatability or increase in flood occurrences, which heightens water table, may in the long-term add to permanent warping after repeated slab wetting and drying cycles. Therefore, proliferate roughness and reducing pavement functional performance.

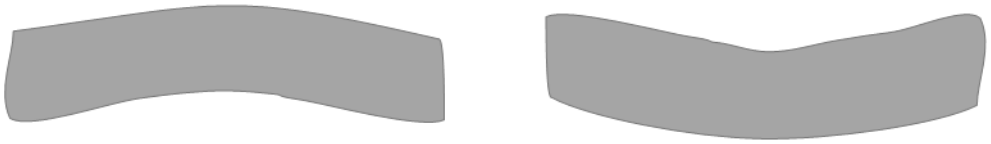

a. Downward Warping - Negative Moisture Gradient. b. Upward Warping - Positive Moisture Gradient

Figure 2-2 Moisture Warping in JPCP

2.5 Flood Performance Modelling for JPCP

Based on the types of flood load considered, performance modelling of pavement under flood conditions could be complex. Flood loads such as flood depth, flood duration, flood velocity, flood debris and contaminants (van de Lindt *et al*. 2009) all have a damaging impact on pavement, but a modelling method to integrate all these stressors is yet to exist. However, extreme precipitation in the form of flood depth could be used to properly describe flood potential (Lu *et al*. 2018a). Certain modelling programs have tried to incorporate hydrological conditions in rigid pavement design. An instance is the ACPA PerviousPave program strictly for pervious concrete pavements. (ACPA 2010).

To model extreme precipitation on concrete pavement, the use of PMED which combines the Enhanced Integrated Climate Model (EICM) and other design parameters to predict performance indicators such as faulting, fatigue cracking, spalling and roughness under extreme precipitation is reasonable. The PMED can assess the impact of pavement structure, material characteristics,

traffic loads and change in incremental and terminal pavement deterioration and performance (ARA 2004a cited Tighe 2015). EICM in PMED consists of Temperature, Relative humidity, Precipitation, Wind, and Sunshine. Thus, to incorporate flooding, precipitation data could be modified to account for extreme precipitation scenarios. The AASHTOWare Pavement ME Design 2.5.3 tool was employed to model these flood scenarios and event frequency on typical arterial and collector JPCP roads in the province of Ontario using global calibration coefficients.

The PMED EICM processes climatic data to calculate monthly Thornwaite Moisture Index (TMI). TMI estimates equilibrium suction for the base and sub-base layers. TMI is determined from average monthly precipitation, average monthly temperature, monthly potential evapotranspiration, day length correction factor, number of days for each month and Average Water storage Capacity of soil (AWC). (Yue and Bulut 2014, Zareie *et al* 2016). Therefore, influential climate parameters such as temperature, average water storage capacity of soil, and potential evapotranspiration, which affect the wetting and drying cycles of soils are well accounted for in TMI monthly estimation. Correlated suction values from TMI estimates are used to obtain underlying soil water content and further determine resilient modulus values. As climate becomes wetter, more positive TMI values are derived and a decrease in matric soil suction occurs. As climate gets drier, more negative TMI values are estimated and an increase in matric suction occurs. (Yue and Bulut 2014). Under extreme precipitation conditions, high water content would most definitely decrease underlying soil stiffness.

2.6 Climate Data

2.6.1. Historical Climate Data

Hourly Climate Data (HCD) files of the North American Regional Reanalysis (NARR) data were accessed via the open-source AASTHO M-E design database (AASHTOWare Pavement ME Design Climatic Data) for two climate stations in Toronto. These two stations were then synchronized to create a virtual station as shown in Table 2-1, interpolating climate data for the area under consideration. This interpolated climate data was harnessed in the PMED program for

pavement performance prediction. With the recent calibration of the PMED to use the Modern-Era Retrospective Analysis for Research and Applications (MERRA) climate data, developed by the National Aeronautics and Space Administration (NASA) in its flexible pavement analysis (ARA 2018), an upgrade from NARR to MERRA for rigid pavements will be evident in the nearest future. Translating to better performance predictions from historical climate data. NARR's historical data was integrated into the program to establish a base-case or no-flooding scenario.

Table 2-1 Climate Data Input for Collector and Arterial Pavement

Pavement Type	Climate station reference	Latitude	Longitude	Elevation
Collector	Virtual station: Toronto_NARR_GRID (94791); Toronto_NARR_GRID (54753)	43.67	-79.63	173.43
Major Arterial		43.86	-79.37	198.12

2.6.2 Climate Change Extreme Precipitation Scenario

Climate models were employed to evaluate future flood cases as a result of climate change under a Representative Concentration Pathway (RCP) with a radiative forcing of 4.5 watts per metre square (W/m^2). Radiative forcing is the additional energy absorbed by the earth due to increases in the effect of greenhouse gases, while RCPs are time and space dependent trajectories of greenhouse gas concentration resulting from anthropogenic activities. There are other radiative forcing values associated with possible RCP scenarios such as RCP 2.6 W/m^2, RCP 6.0 W/m^2 and RCP 8.5 W/m^2. However, RCP 4.5 scenario is assumed realistic and conservative as it is reported to have the least uncertainty in projected increase or decrease in flood frequencies across Canada compared to other RCP scenarios (Gaur *et al* 2018). Also, greenhouse gas concentrations may peak in the year 2040 (Meinshausen *et al.* 2011) and considering that the design life of the JPCP pavement classes used as case study ends by year 2043, the extremities of RCP 4.5 climate scenario

would, therefore be represented in the pavement analysis. In all, the purpose of using this scenario is not to predict the future of the Canadian climate, but to explore scientific and real-world implications of different plausible futures (Bjørnæs 2013).

The precipitation scenario under RCP 4.5 scenario was obtained using the Intensity Duration Frequency Climate Change Tool (IDF_CC Tool 3.0). The IDF_CC tool is an open source information which estimates precipitation accumulation depths for a variety of return periods (2, 5, 10, 25, 50 and 100 years) and durations (5, 10, 15 and 30 minutes and 1, 2, 6, 12 and 24 hours) for the Canadian environment. The tool engages 24 Global Circulation Models (GCMs) and 9 downscaled GCMs using rigorous downscaling method such as spatial and temporal downscaling, statistical analysis and optimization to update pre-estimated IDF from historical precipitation data (Simonovic et al., 2016) to IDF under RCP scenarios. The idea is to identify future local extreme precipitation data for a specific location from repositories of Global Circulation Models (GCM) and Regional Circulation Models (RCM) using climate forcing scenarios as inputs.

An ensemble of these models was selected to obtain future return floods of 50-years and 100-years under RCP 4.5 scenario. Precipitation values obtained were 151.94 mm and 168.84 mm respectively as shown in Table 2-2 for the future return year of 2018-2100. These downscaled data is gridded at a resolution of 300 arc-seconds (0.0833 degrees, or roughly 10 km) (PCIC 2017). Considering the flood event of July 8th, 2013 in Toronto, PMED's integrated climate file was modified to include future return floods under RCP 4.5 starting on this date. A 7-day flood duration was assumed based on a previous study by Gaspard *et al.* (2006) who reported that flooding durations beyond seven (7) days did not cause additional damage on inundated pavements during the Hurricane Katrina event. Whereas, a recent study has identified increases in damage of Asphalt Concrete (AC) pavements due to increase in extreme precipitation cycles (Lu. *et al.* 2018b). Hence, considerations were both given to flood duration and event cycle (1, 2 and 3) alongside precipitation depth to properly define flood scenarios. One event cycle of flood represents seven days pavement inundation. Event is futher repeated to simulate second and third cycles of extreme

precipitation. Datasets of other climate parameters such as temperature, wind, relative density and sunshine were sourced from the historical data of the virtual climate station for the year 2012/2013.

Table 2-2 Return Flood under RCP 4.5

Location (Lat, Long)	Duration	RCP 4.5 50-year return period	RCP 4.5 100-year return period
(43.81174, -79.41639)	24hr	151.94mm	168.84mm

2.7 Ontario Concrete Pavement Design

Typical arterial and collector JPCP road designs and PMED inputs common to Ontario were obtained from the Ontario Pavement Structural Design Matrix for Municipal Roadways document prepared by Applied Research Associates (ARA 2015a, ARA 2015b).

Table 2-3 Typical Ontario JPCP Pavement Design Inputs (ARA 2011a, ARA 2011b)

	Design parameters	Collector	Arterial
Traffic inputs	Two-way AADTT	500	5000
	Truck traffic in design lane	90%	90%
	No. of lanes in design direction	2	2
	% of trucks in design direction	50%	50%
	Reliability	75%	90%
Concrete slab properties	Dowel diameter(mm)	**Non-Dowelled**	**Dowelled** (32mm)
	Slab length	4.0m	4.5m
	Tied shoulder/curb	Tied	Tied

	Load transfer efficiency	70%	70%
Performance trigger values	International Roughness Index (IRI)	2.70m/km	2.70m/km
	Mean joint faulting	3.00mm	3.00mm
	JPCP transverse cracking	20%	10%
	Design life	25years	25years

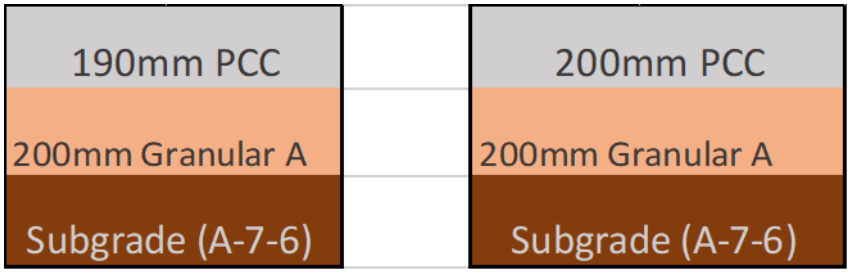

(a) Collector Design (non-dowelled) (b) Arterial Design (dowelled)

Figure 2-3 Typical Collector and Arterial JPCP Pavement Design in Ontario. [1]

Table 2-3 shows JPCP design inputs and Figure 2-3, the cross-section of the pavement classes. Pavement performance is then predicted under no-flood and flood scenario under RCP 4.5.

2.8 Discussion - Flood Impact on Arterial and Collector Pavement in Ontario

As earlier stated, high positive TMI values indicate wetter or humid climate, lower matric suction and a relative decrease in soil stiffness. While negative TMI values indicate a drier climate, higher matric suction and relative increase in soil stiffness. Figure 2-4 shows a plot of average monthly TMI of 50- year and 100-year floods at one, two and three event cycles. At the first and second cycle, average monthly TMI values of 50-year and 100-year extreme precipitation remain same.

[1] *Granular A is a well graded sandy soil and *A-7-6 is a low plasticity soil

While at the third cycle, TMI at 100-year had a higher magnitude to 50-year TMI values. Generally, TMI values increased as return floods and event cycles increased at the case study location.

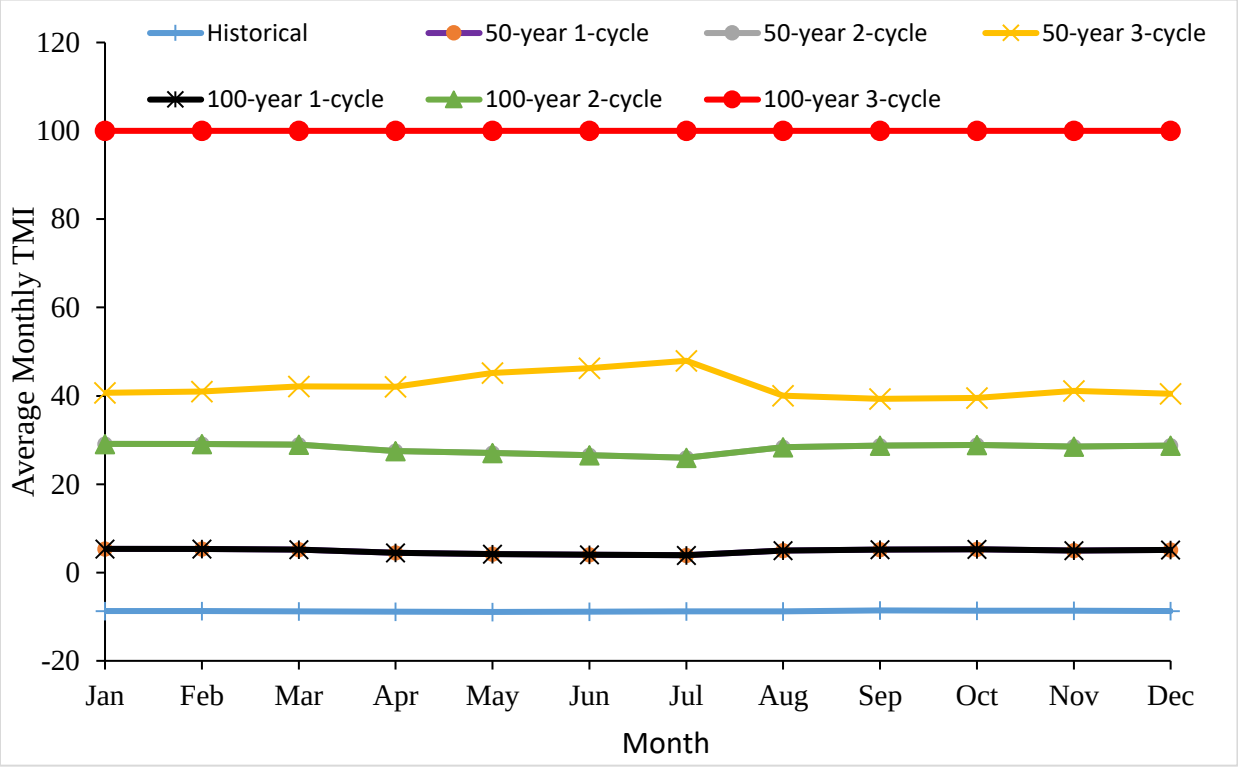

Figure 2-4 Comparison of average monthly TMI at return floods and event cycles under RCP 4.5

Analysis of performance under flooding conditions indicated changes in faulting and IRI values. IRI change is more preferred in describing damage as it is a function of faulting, cracking, spalling, site factors, and initial IRI. Nevertheless, damage was calculated for both IRI and faulting performance indicators to show how each responded to flood impact. Damage ratio is the percentage (%) change in the terminal IRI of pavement under flooding conditions with respect to its no-flood state at a given design life.

$$\delta_{IRI}\,(\%) = \frac{IRI_f - IRI_{nf}}{IRI_{nf}}$$

$$LS_m\ (days) = 365 * \left[\left(\frac{IRI_f\ *\ n}{IRI_{nf}}\right) - n\right]$$

$$\delta_{Fault}\ (\%) = \frac{Mn.Fault_f\ -\ Mn.Fault_{nf}}{Mn.Fault_{.nf}}$$

Where δ_{IRI} (%) is the IRI or overall damage ratio, IRI_f is the terminal IRI (m/km) under RCP 4.5 Extreme Precipitation (EP) or flood conditions, IRI_{nf} is the terminal IRI (m/km) at base-case or no-flood scenario. δ_{Fault} (%) is the percentage change in faulting or faulting damage ratio, n is the pavement design life in years, LS is the loss of pavement service life (days), $Mn.Fault_f$ is the mean joint faulting (mm) under RCP 4.5 Extreme Precipitation (EP) scenario or flood conditions, and $Mn.Fault_{.nf}$ is mean joint faulting (mm) at historical or no-flood scenario.

Below are the comparative graphs indicating IRI and faulting performance of collector and arterial pavements at one, two and three-cycles of 50-year and 100-year flood events over pavement design life.

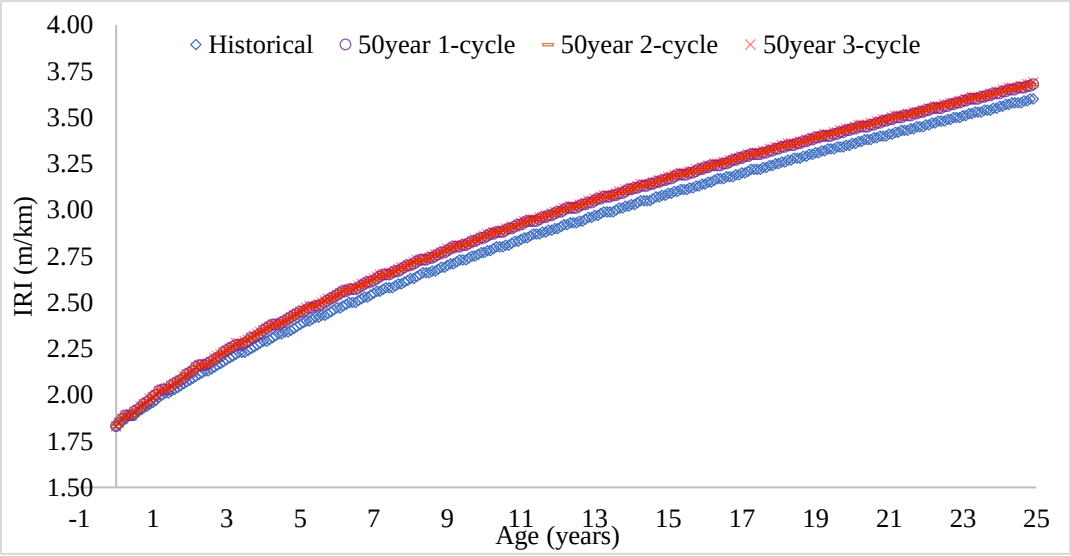

Figure 2-5 50-year Flood Collector IRI performance at one, two, and three event cycles

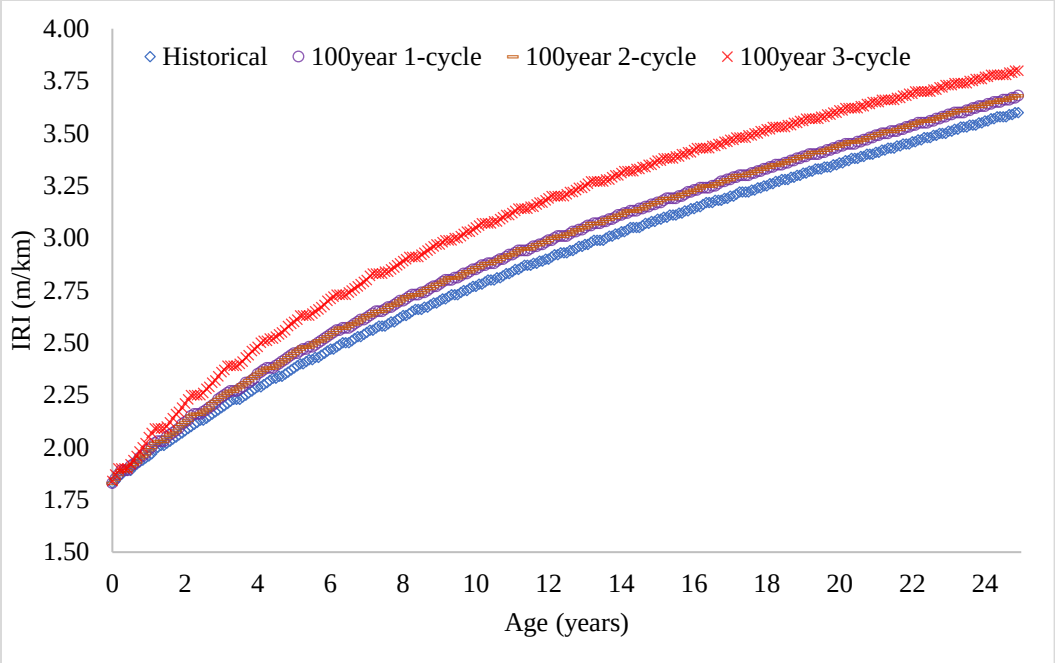

Figure 2-6 100-year Flood Collector IRI Performance at One, Two, and Three Event Cycles

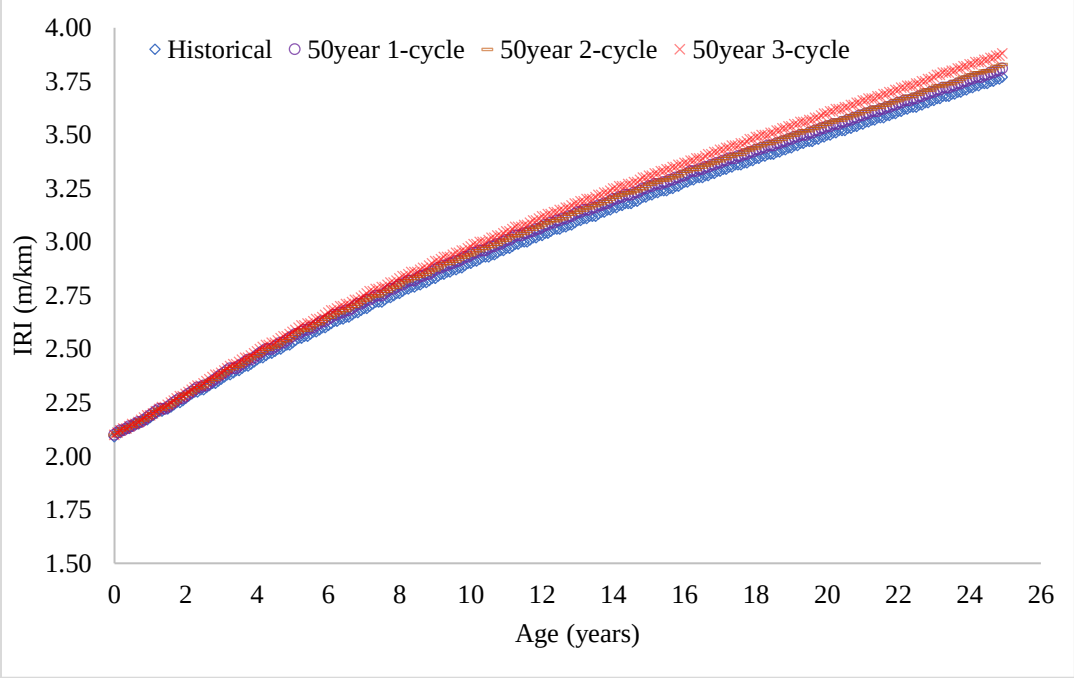

Figure 2-7 50-year Flood Arterial IRI Performance at One, Two, and Three Event Cycles

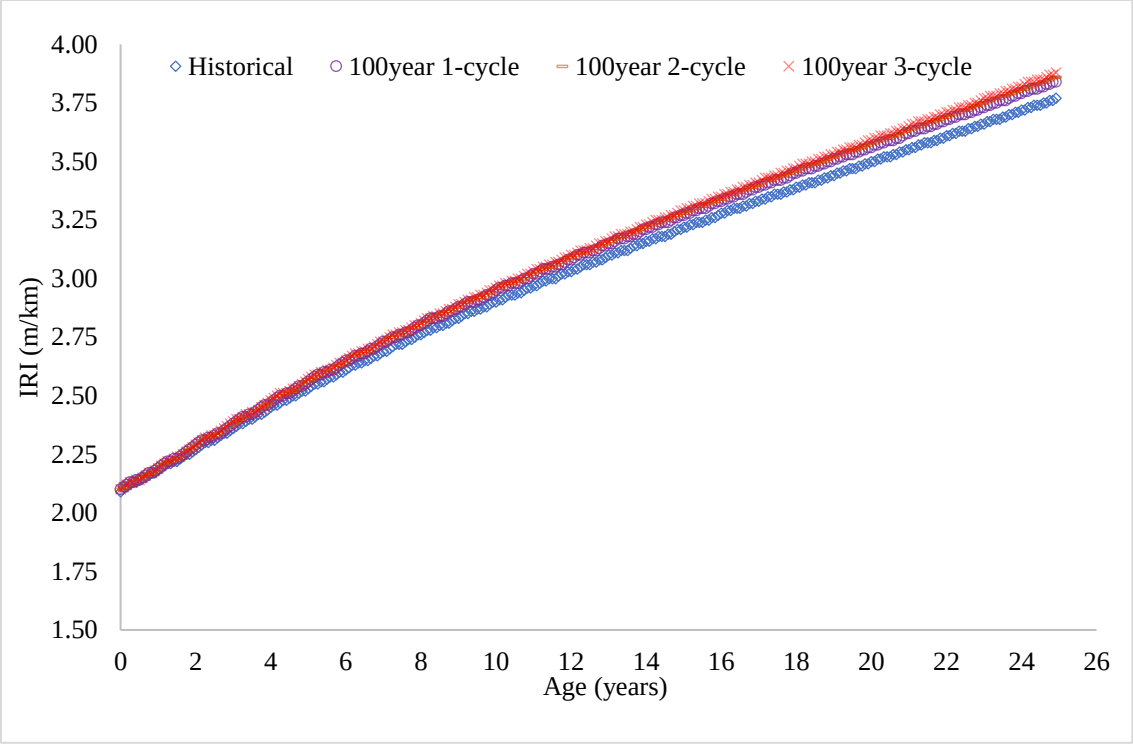

Figure 2-8 100-year Flood Arterial IRI Performance at One, Two, and Three Event Cycles.

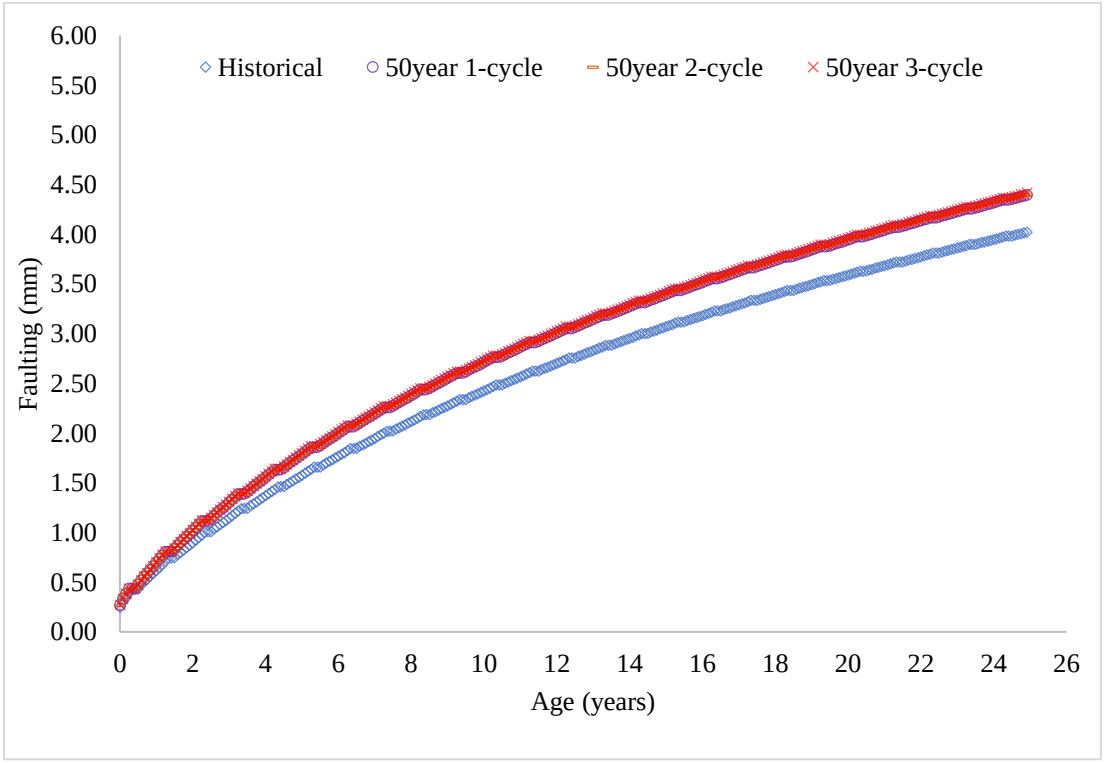

Figure 2-9 50-year Flood Collector Faulting Performance at One, Two, and Three Event Cycles

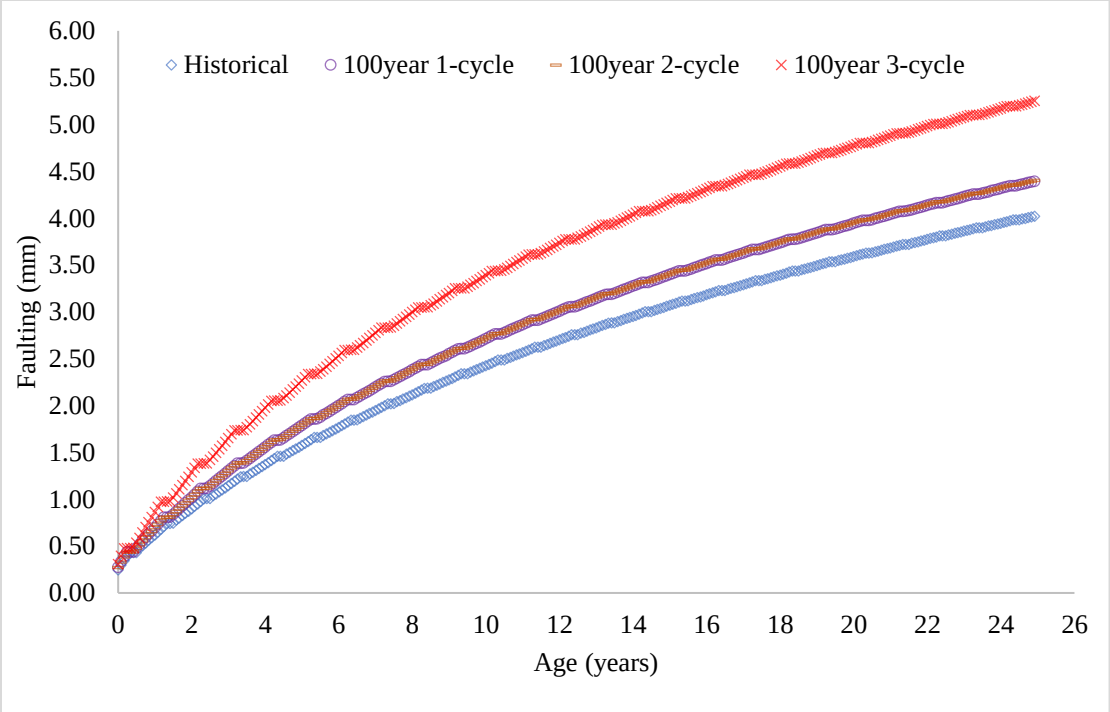

Figure 2-10 100-year Flood Collector Faulting Performance at One, Two, and Three Event Cycles

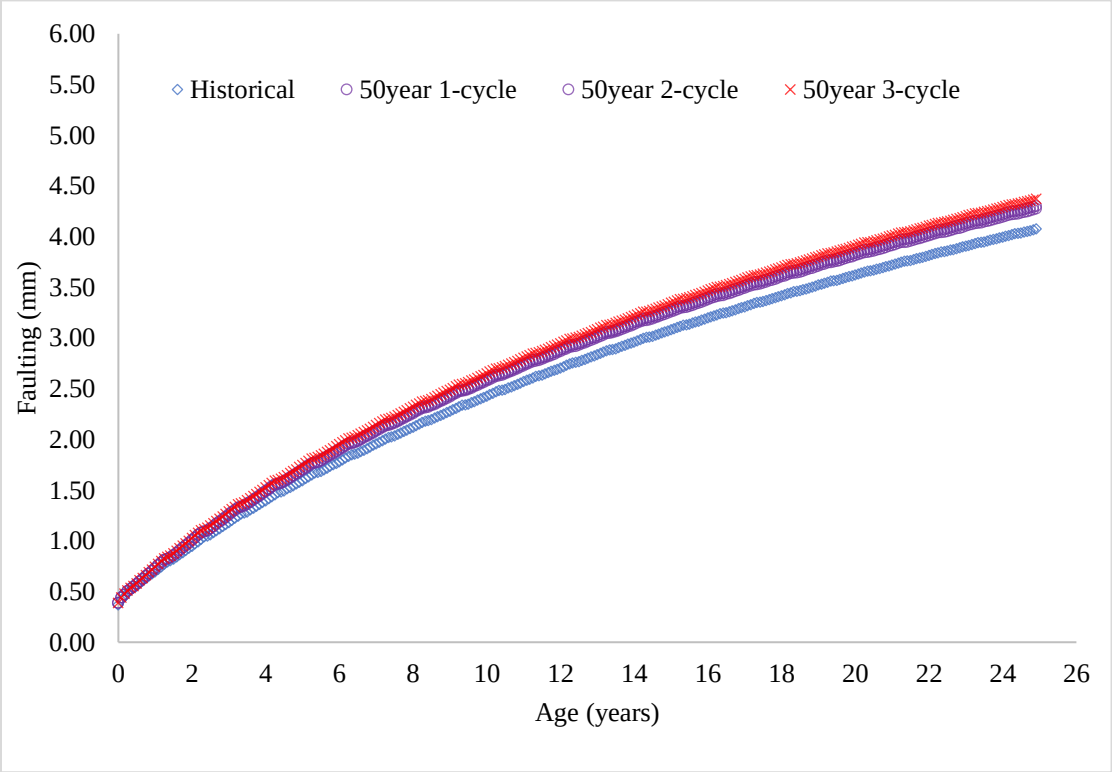

Figure 2-11 50-year Flood Arterial Faulting Performance at One, Two, and Three Event Cycles

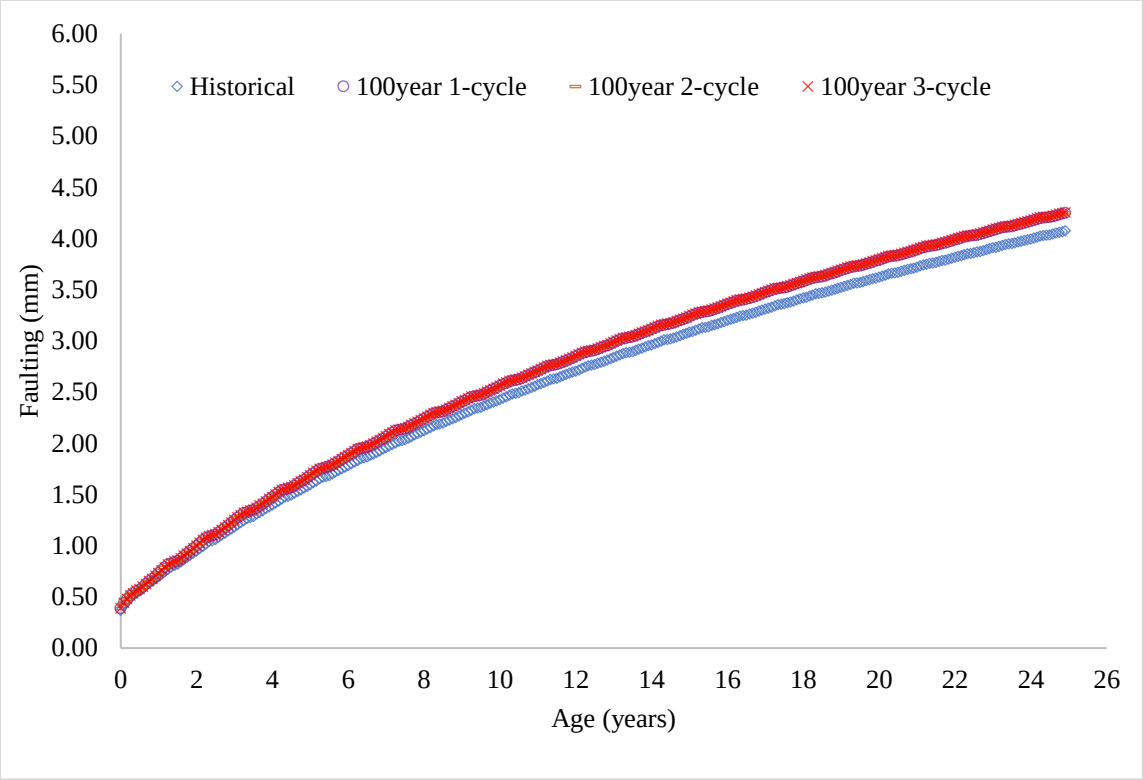

Figure 2-12 100-year Flood Arterial Faulting Performance at One, Two, And Three Event Cycles.

A 7-day extreme event was regarded as one cycle EP event for each 50-year and 100-year return flood under RCP 4.5. This event was further repeated to make second and third cycles. At one event cycle, the same damage was observed across 50 and 100-year return periods in the collector study. This demonstrates the possibility of a higher return period having the same damaging effect as a lower return period at lower cycles of extreme precipitation. The opposite was the case for arterial JPCP as damage ratio increase from 1.06 % to 1.86%. However, damage magnitude in the arterial study was lower to the collector study. The presence of dowels in the arterial pavement must have contributed to its relatively low damage ratios even though it constituted more traffic loading. Same damage pattern exhibited in IRI damage was observed in faulting damages, indicating the influence of faulting change on overall pavement damage. Tables 2-4 and 2-5 present the changes in pavement IRI and faulting respectively.

At two event cycles, damage ratios in collector pavements remained the same as a one-cycle event, no further damage beyond 2.22% was estimated for both 50 and 100-year EP event as observed in

Table 2-4. Increase in cycle event did not cause any increase in damages. Though arterial JPCP experienced a lower damage magnitude compared to collector JPCP, there was an increase in damage across return periods, that is, from 1.59% to 2.39% for 50 and 100 years respectively. With an increase in event cycle from one to two, collector faulting damage increased from 9.20% to 9.70% and remained same across return flood years (50 &100) as shown in Table 2-5.

At three event cycles, an increase in damage ratio was noted across RCP return floods in the collector pavement. From Table 2-4, increase in the number of cycles (two-cycle to three-cycle) resulted in a slight increase under the 50-year flood (from 2.22% to 2.5%) and larger increases under the 100-year EP (2.22% to 5.56%). This sharp augment in damages was due to faulting damages at three-cycle, increasing from 9.70% to 30.60% as presented in Table 2-5. This holistically shows the influence of flooding on faulting failure in non-dowelled JPCP pavements. Also, at three-cycle, arterial pavement damage increased from 1.59% to 2.92% and 2.39% to 2.92% for 50 and 100-year EP event respectively.

Table 2-4 Damage Ratios under RCP 4.5

Damage ratios under RCP 4.5 due to change in IRI			
Pavement Class	Event	50-year return period	100-year return period
Collector	1-cycle	2.22%	2.22%
	2-cycle	2.22%	2.22%
	3-cycle	2.50%	5.56%
Arterial	1-cycle	1.06%	1.86%
	2-cycle	1.59%	2.39%
	3-cycle	2.92%	2.92%

Figures 2-13 and 2-14 shows the flood damage ratio for Ontario collector and arterial pavement respectively under RCP 4.5 future return periods and event cycles. More flood damage was noticed in the collector pavement than the arterial pavement. However, the collector pavement was resilience at first and second cycles of RCP 4.5 50-year and 100-year flood magnitude.

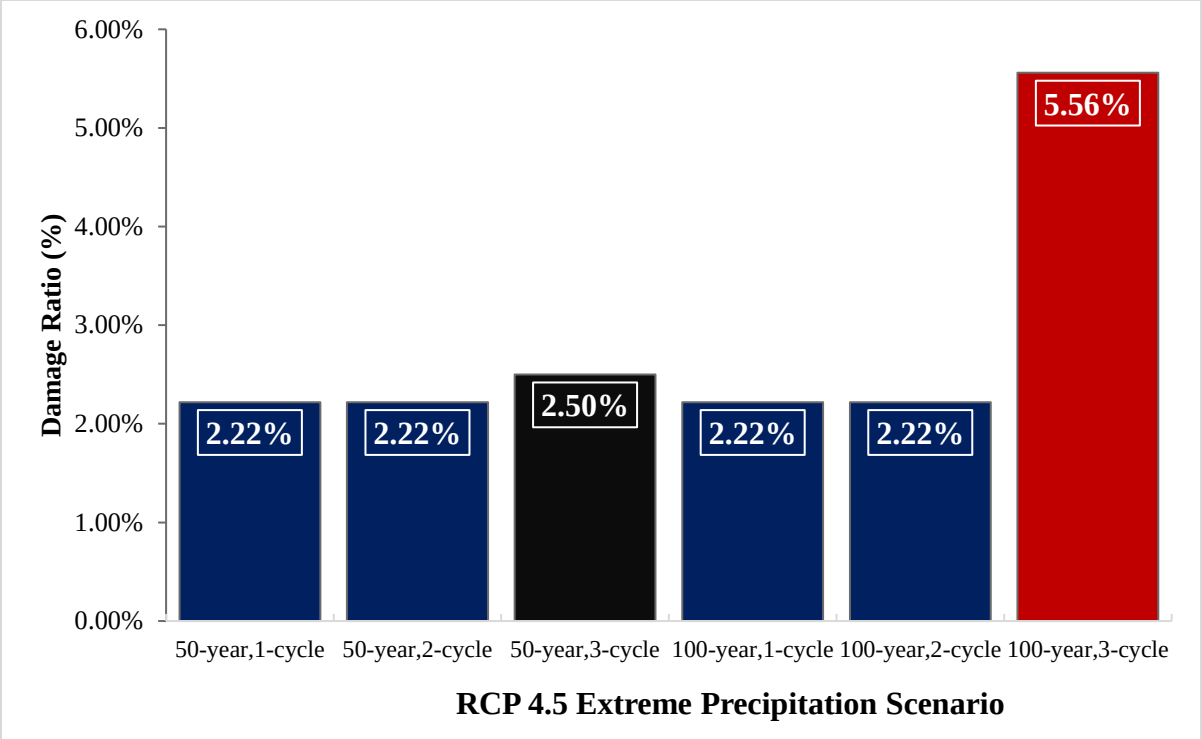

Figure 2-13 Damage Ratio (%) against Return Flood (Years) of JPCP Collector Pavement under RCP 4.5 Climate Change Scenario

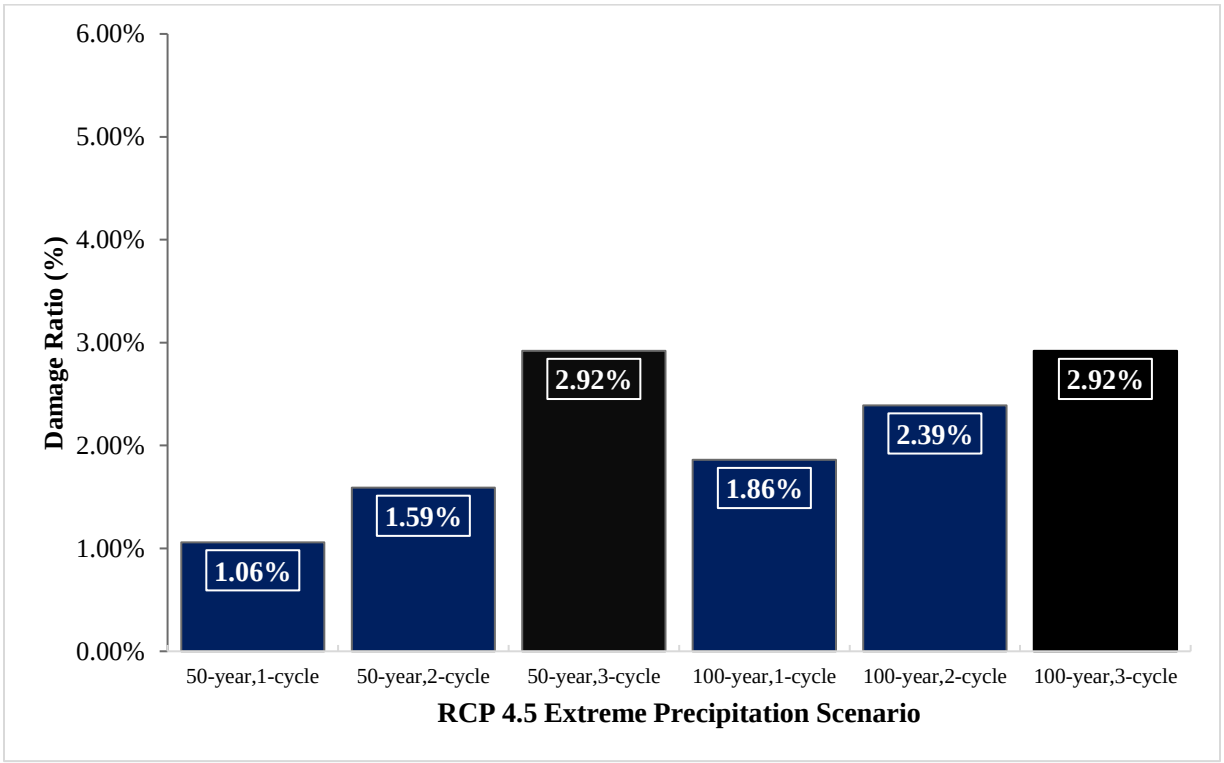

Figure 2-14 Damage Ratio (%) against Return Flood (Years) of JPCP Arterial Pavement under RCP 4.5 Climate Change Scenario

Table 2-5 Faulting Damage or Change under RCP 4.5

Damage ratios due to change in Joint Faulting			
	Event	50 –year return period	100-year return period
Collector	1-cycle	9.20%	9.20%
	2-cycle	9.70%	9.70%
	3-cycle	9.95%	30.60%
Arterial	1-cycle	5.39%	4.17%
	2-cycle	4.90%	4.41%
	3-cycle	7.11%	4.41%

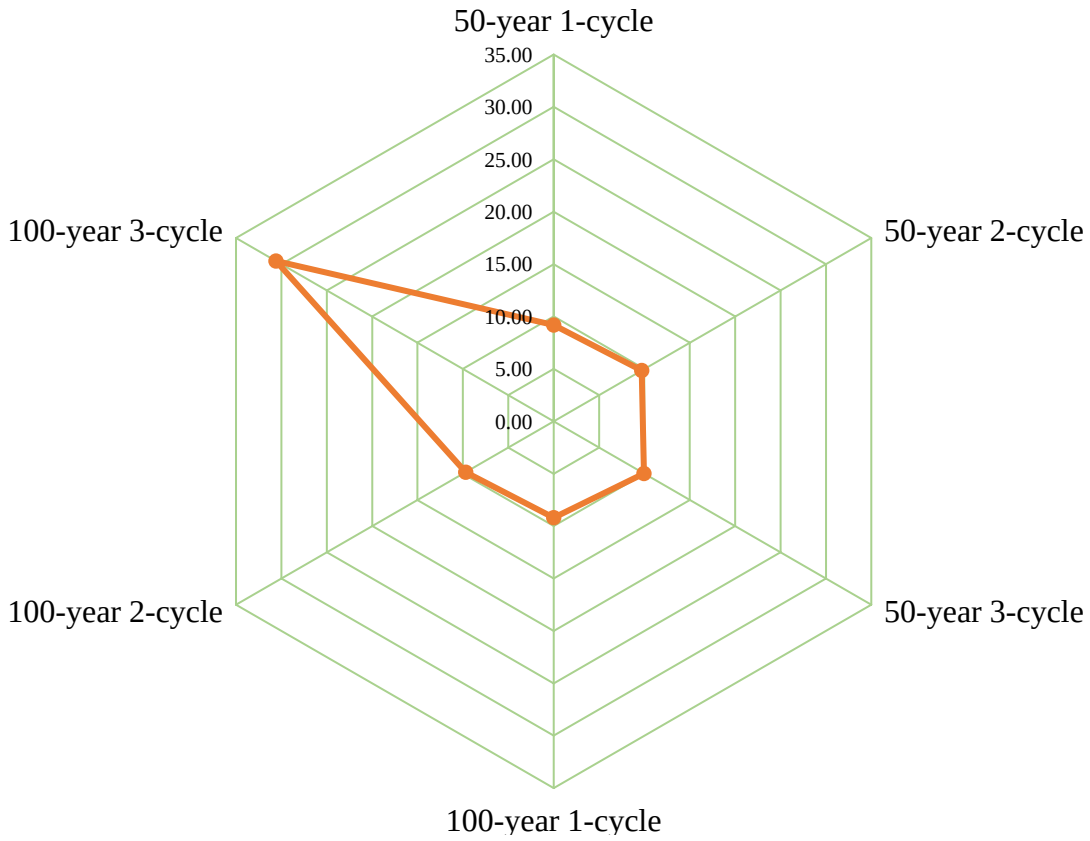

Figure 2-15 Faulting Damage (%) Against Return Flood (Years) of JPCP Collector Pavement under RCP 4.5 Climate Change Scenario.

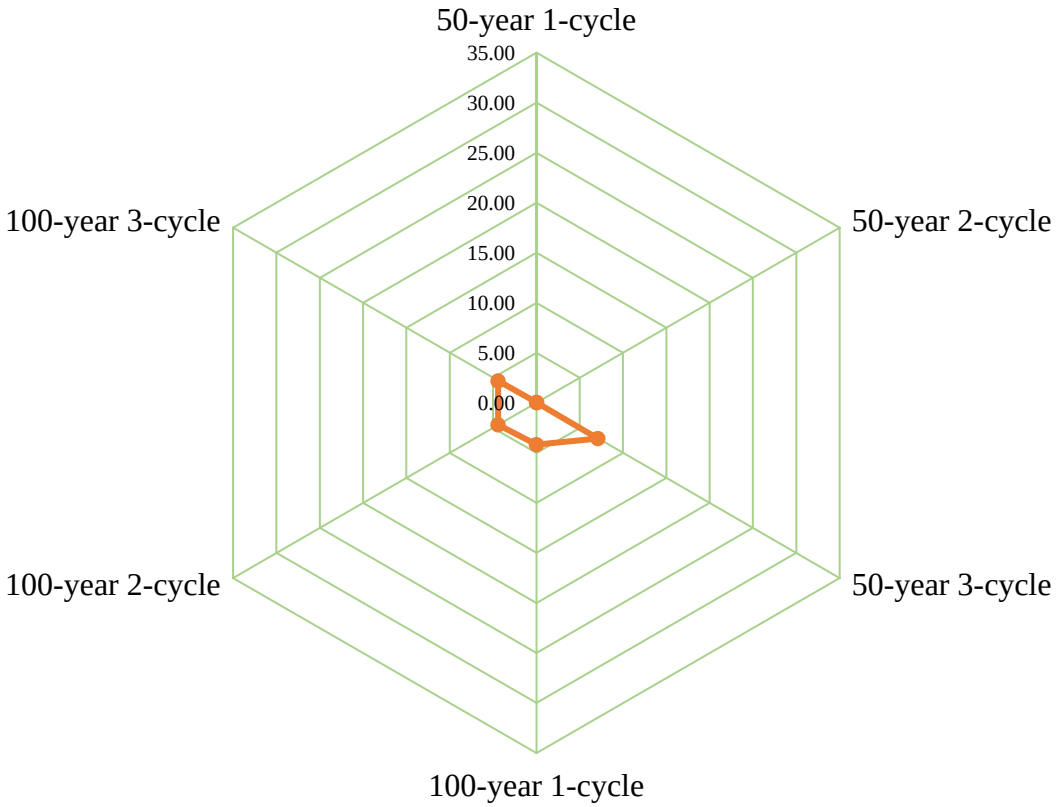

Figure 2-16 Faulting Damage (%) against Return Flood (Years) of JPCP Arterial Pavement under RCP 4.5 Climate Change Scenario

As shown in Table 2-5, arterial faulting damages demonstrated seemingly illogical damage ratios but did not affect progressive IRI or overall damage across event cycles and return floods. This was due to progressive increase in relative cracking change, which contributed more to IRI damage. This further reiterates the intention of using the IRI damage ratio as overall pavement flood damage, being a function of joint faulting and slab cracking along with climate and subgrade factors.

From the observation of damage results, minimum and maximum IRI damage ratio estimated across pavement classes are 1.06% and 5.56% respectively. Comparing these damage ratios to the magnitude of damage recorded two years after the Hurricane Katrina event on highly deteriorated flooded concrete pavements, Ontario typical JPCP would fall in the minimal flood damage category under RCP 4.5 climate scenario. From the Katrina study conducted by Chen and Zhang

(2014), a 23.93% IRI damage ratio estimate was derived and based on this study, hypothetical flood damage categories are proposed in Table 2-6.

Table 2-6 Proposed Damage Ratio Categories for Flooded Concrete Pavements

Damage Ratio (%) - Based on pre-flood and post-flood IRI change.		
Minor Damage	Moderate Damage	Major Damage
0 – 8%	8 – 16%	More than 16%

2.9 Reduction in Pavement Life

In reference to damage sustained by the Ontario JPCP road classes, loss of pavement life was estimated by comparing terminal IRI of the road classes at base-case or no-flood scenario with RCP 4.5 IDF extreme precipitation or flood scenarios. Table 2-7, Figure 2-17 and Figure 2-18 show the pavement life loss in days and percentages. Considering the 25 years design life, pavement life loss is higher in collector compared to arterial pavements, peaking at 507days to 266days respectively after three-cycle extreme precipitation. Generally, increase in the event cycles resulted in more loss of pavement life in the pavement classes.

Table 2-7 Reduction in Design Life under RCP 4.5

(Design life of 25 years)			
JPCP Pavement	Event Cycle	50-year Return Period (days)	100-year Return Period (days)
Collector	1	203	203
	2	203	203
	3	228	507
Arterial	1	97	169
	2	145	218
	3	266	266

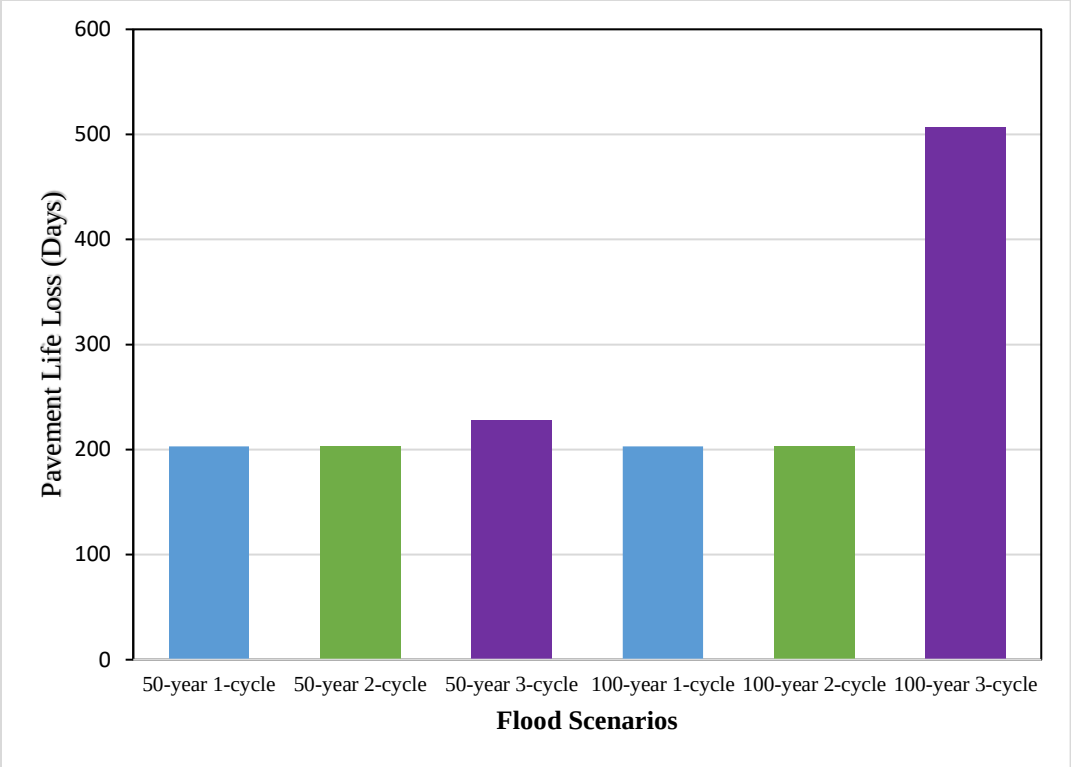

Figure 2-17 Pavement Life Loss (days) in Collector Pavement across Return Periods and Event Cycles under RCP 4.5

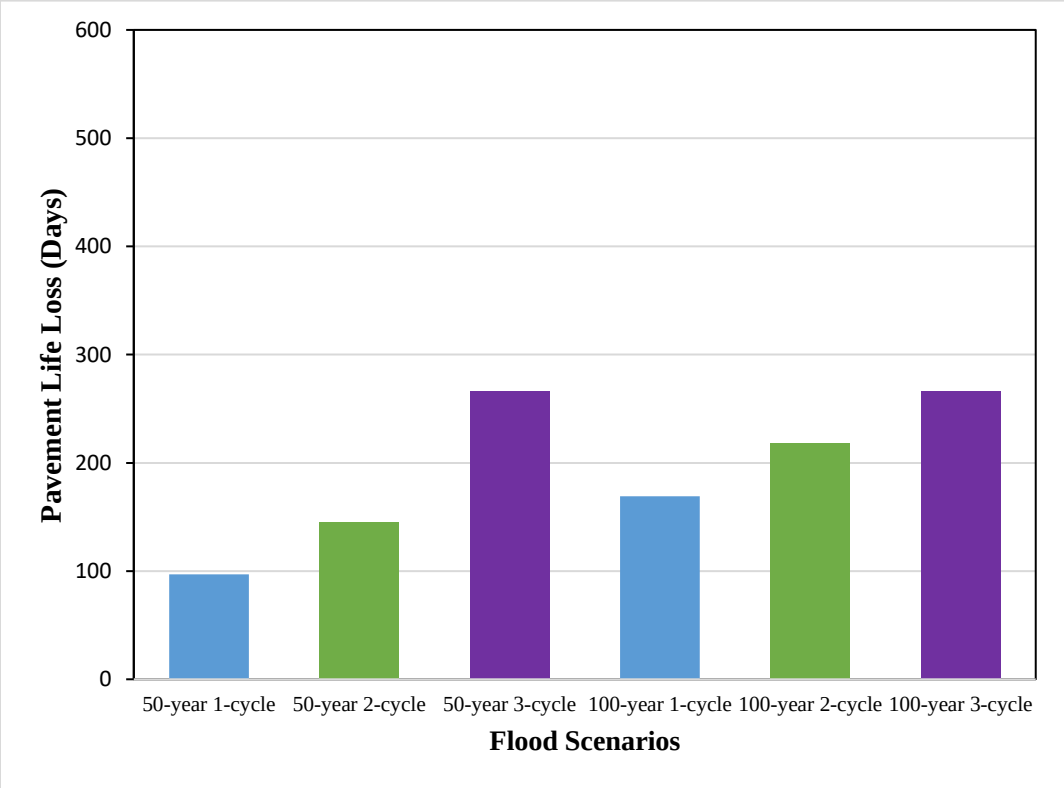

Figure 2-18 Pavement Life Loss (Days) In Arterial Pavement across Return Period and Event Cycles under RCP 4.5

2.10. Conclusion

In this study, review of flood impact on pavement and analysis of flood-induced distresses on JPCP pavements were conducted. The performance of Ontario JPCP concrete pavement classes was then assessed under flooded and no-flooding conditions employing the AASHTOWare Pavement ME Design (PMED) 2.5.3 tool with the use of global calibration coefficients. Extreme precipitation values of predicted Intensity Duration Frequency (IDF) obtained under RCP 4.5 climate change scenarios were used to modify the PMED climate file to evaluate performance under flood conditions, while historical climate data estimated performance under no-flood condition. Extreme precipitation depth, event cycles, and flood duration were variables used in the analysis. PMED representative JPCP collector and arterial pavement designs for Ontario were selected as case studies. Changes in IRI and faulting performance values were utilized to estimate flood damage ratios. Below are the conclusions drawn from this study:

- Minor flood damages were observed across return periods and event cycles under RCP 4.5 in the case studies, which therefore corroborates with existing studies on rigid pavement flood resilience.

- Higher resilience is observed at lower cycles of extreme precipitation in comparison to higher cycles

- Faulting immensely contributed to flood damage as performance change was proportional to IRI or overall damage.

- Increase in extreme precipitation cycles under RCP 4.5 intensified flood damage on non-dowelled JPCP to dowelled JPCP irrespective of traffic conditions. As a consequence, estimated pavement life loss is much greater in non-dowelled (collector) to dowelled (arterial) JPCP pavements in the Ontario study.

Chapter 3

Calibration of AASHTOWare Pavement ME Transverse Cracking Transfer Function for Jointed Plain Concrete Pavement (JPCP) in Ontario

3.1 Overview

The Ministry of Transportation Ontario (MTO) as part of the commitment to implement the use of the Mechanistic Empirical Pavement Design Guide (MEPDG) for current and future design projects, initiated three major research projects aimed to calibrate the AASHTOWare Pavement ME Design (PMED) program for accurate prediction of pavement distresses and performance for Ontario roads under the Highway Infrastructure Innovation Funding Program (HIIFP). This process is important as the globally calibrated transverse cracking prediction model underpredicts observed transverse cracking distresses in the province of Ontario. While the first two research projects focused on flexible pavements, the local calibration of rigid pavements was incorporated in the third research project. A new Automatic Road Analyzer (ARAN 9000) system had been used to collect accurate field measurements of concrete pavement distress as observed across the province. Data from this survey was made available for local calibration of the transverse cracking model for Jointed Plain Concrete Pavement (JPCP) and as a result, calibration coefficients to fit JPCP cracking performance in Ontario were derived.

The transverse cracking model calibration exercise was conducted using a non-linear optimization tool, Statistical Analysis System (SAS). Calibration coefficients were derived for the transverse cracking model using MTO's design inputs and performance data of thirty-two (32) JPCP sections, consisting of freeways and arterials roadways in the province. The calibration process significantly reduced the bias (consistent under-prediction), improved precision and accuracy of the transverse cracking model based on the validation conducted. This improvement is prominent, signifying that the MTO-calibrated transverse cracking model could provide reliable data for consistent and economical concrete pavement designs across the province.

3.2 Introduction

Canadian road agencies were actively involved in the development of the MEPDG implemented under the National Cooperative Highway Research Program (NCHRP Projects 1-37A, and 1-40), and a number of these agencies have concerted effort towards adopting the guide for pavement design and analysis. The guide, packaged in the AASHTOWare Pavement ME Design (PMED) software employs a mechanical approach to simulate pavement responses such as strains, stresses and deflections to traffic and environmental loadings using response models, and further converts these responses into distress prediction through empirical models. Therefore, it employs both mechanistic and empirical approach in predicting pavement performance.

The NCHRP (2004) report advises that the MEPDG prediction models be locally calibrated by state and provincial road agencies before the program is officially implemented for industry use as the influence of material properties, traffic conditions, climate, and maintenance and operational policies relative to certain locations may not be well captured under the globally calibrated models. These could as a consequence limit the program's accurate pavement performance prediction (Ceylan and Gopalakrishnan 2007, Kaya 2013). In consideration of this, three (3) research projects focused on local calibration were implemented by the Ministry of Transportation Ontario (MTO) under her Highway Infrastructure Innovation Funding Program (HIIFP). Under the first project, database development of representative pavement sections, design inputs and performance data in the province were established. Under the second project, local calibration of flexible pavement rutting models was achieved. The third project aimed at calibrating the International Roughness Index (IRI) and cracking models of both flexible and rigid pavements to local conditions using MTO's second-generation Pavement Management System (PMS-2) (Yuan et. al. 2017). The first two (2) projects were conducted by Ryerson University and the third research project was completed by Ryerson University and the University of Waterloo for flexible and rigid pavement local calibration respectively.

The local calibration process minimizes the bias and standard error between the predicted and observed pavement distress values by optimizing the prediction model to predict observed conditions. This results in the derivation of new calibration coefficients that can reliably make predictions of pavement performance and distresses in the local region under scope. Implementation of this exercise does not only provide better performance predictions, but also improves cost effectiveness, timely maintenance and preservation of pavement assets over their service life. For the calibration of rigid pavements, the AASHTO 2010 Guide to Local Calibration of the MEPDG details a stepwise calibration approach. However, engineering judgement should be employed alongside this approach.

To conduct local calibration, it is necessary to verify if MEPDG globally calibrated roughness and distress transfer functions are predictive of Ontario conditions. If this is the case, there will be no need to locally calibrate the models. However, if this is not the case, a local calibration exercise will need to be conducted. For Ontario rigid pavements, the MTO Interim report, currently encourages the use of the globally calibrated International Roughness Index (IRI) and Faulting models for rigid pavement design as they were found to be predictive of Ontario conditions. (MTO 2019). The transverse cracking model, in the current AASHTOWare Pavement ME Build 2.5 and above versions, was however not indicative of Ontario conditions and needed to undergo calibration to reflect transverse cracking performance in Ontario. If AASHTO decides to change any of the distress and performance models through a global recalibration exercise, then local recalibration of all performance and distress models would have to be updated. (MTO 2019). The MEDPG software version used in this study for local calibration is the AASHTOWare Pavement ME Design Build 2.5.3, released in October 2018.

A notable Ontario rigid pavement local calibration study was conducted by Zhong in 2017 who used an earlier version of the PMED program, specifically Version 2.3.1. The local calibration study provided insight on the implications of globally calibrated models on Ontario pavement performance prediction, and certain calibration coefficients for International Roughness Index (IRI), faulting distress and transverse cracking were developed for Ontario conditions.

With improvement in AASHTO Pavement ME versions and upon the discovery of the inability of the rigid pavement transverse cracking to predict locally observed performance trends, the transverse cracking model prediction had to be improved by finding new calibration coefficients that fit Ontario conditions. This paper describes how the new local calibration coefficients were derived to calibrate the transverse cracking transfer function to Ontario conditions.

3.3 Transverse Cracking in Jointed Plain Concrete Pavement (JPCP)

Transverse cracking is a pavement crack propagation on the pavement surface, perpendicular to the centerline of road alignment. This pavement distress can be found both in flexible and rigid pavements. In rigid pavements, it is initiated by tensile forces acting in the concrete due to temperature-induced contraction and expansion under traffic loading. Transverse cracking is generally one of two types, namely, top-down or bottom-up and both are distresses common to asphaltic and concrete pavements.

The transverse cracking prediction model is made up of two other models, the fatigue model which estimates the extent of fatigue damage induced, and the transfer function which converts the estimated fatigue damage into transverse cracking predictions (Kim et al. 2014). The fatigue damage model uses a comprehensive iterative damage accumulation algorithm to estimate the fatigue damage, an indicator of crack initiation. The algorithm accumulates monthly fatigue damages by considering daytime and nighttime hourly thermal gradients, truck axle loadings (four types of axles, lateral distribution, full axle load spectra), and moisture gradients (permanent shrinkage and transitory shrinkage) as developed under NCHRP 1-37A (NCHRP 2003, NCHRP 2004). The fatigue model is a function of the number of load applications (n) and allowable load applications (N) on the PCC pavement at various conditions.

The transverse cracking transfer model seperately predicts the pavement distress performance for top-down and bottom-up transverse cracking. This is because damage accumulation for these two transverse cracking types are estimated differently. Slabs may crack from top-down or bottom-up

but not from both directions. Therefore, PMED is programed to combine both cracking types, excluding the possibility of both modes of cracking occurring on the same slab.

In the fatigue damage model, the allowable number of load applications (N) at various conditions (i, j, k, l, m, n, o) is first estimated to compute the bottom-up and top-down fatigue damage using equation 3-1 and 3-2.

$$\log\left(N_{i,j,k,l,m,n,o}\right) = C_1 \cdot \left[\frac{MR_i}{\sigma_{i,j,k,l,m,n,o}}\right]^{C_2} \quad 3\text{-}1$$

$$DI_{F=} \sum \frac{n_{i,j,k,l,m,n,o}}{N_{i,j,k,l,m,n,o}} \quad 3\text{-}2$$

Where:

MR_i = PCC modulus of rupture at age "i",

$\sigma_{i,j,k,l,m,n,o}$ = Applied stress at condition of i, j, k, l, m, n, o

$n_{i,j,k,l,m,n,o}$= Applied number of load applications at condition i, j, k, l, m, n, o

$N_{i,j,k,l,m,n,o}$= Allowable number of load applications at condition i, j, k, l, m, n, o

DI_F = Fatigue damage (top-down or bottom-up)

i = Age (accounts for change in PCC modulus of rupture and elasticity, slab/base contact friction, deterioration of shoulder LTE)

j = Month (accounts for change in base elastic modulus and effective dynamic modulus of subgrade reaction)

k = Axle type (single, tandem, and tridem for bottom-up cracking; short, medium, and long wheelbase for top-down cracking)

l = Load level (incremental load for each axle type)

m = Equivalent temperature difference between top and bottom PCC surfaces.

n = Traffic offset path

o = Hourly truck traffic fraction

In the cracking prediction model, top-down and bottom-up fatigue damage are converted into top-down and bottom-up cracking values using equation 3-3 and 3-4 respectively. Equation 3-5 is then used to calculate the total transverse cracking.

$$Crack_{Top-down} = \frac{100}{1+ C_4(DI_{FT})^{C_5}} \quad 3\text{-}3$$

$$Crack_{Bottom-up} = \frac{100}{1+ C_4(DI_{FB})^{C_5}} \quad 3\text{-}4$$

$$TCrack = (Crack_{Bottom-up} + Crack_{Top-down} - Crack_{Bottom-up} * Crack_{Top-down}) \quad 3\text{-}3$$

Where:

DI_{FT} = Top-down fatigue damage

DI_{FB} = Top-down fatigue damage

C_1, C_2, C_4, C_5 = calibration coefficients;

$TCrack$ = Total Transverse Cracking

3.3.1 Bottom-up Transverse Cracking

Bottom-up transverse cracking occurs when a critical bending tensile stress develops at the bottom of the slab under wheel load, when axles are closer to the longitudinal edge of the PCC slab. This stress can further increase under positive temperature gradient conditions. A positive temperature gradient implies that the top of the slab is warmer than its bottom and therefore a downward curling of the slab is present. Rigorous loading from heavy axles would permanently lead to fatigue damage along the bottom edge of the slab, further propagating upwards (NCHRP 2018). This distress reduces pavement smoothness properties and could in severe cases cause pavement rapid

deterioration. Figure 3-1 shows a descriptive diagram of the occurrence of bottom-up cracking on JPCP pavements.

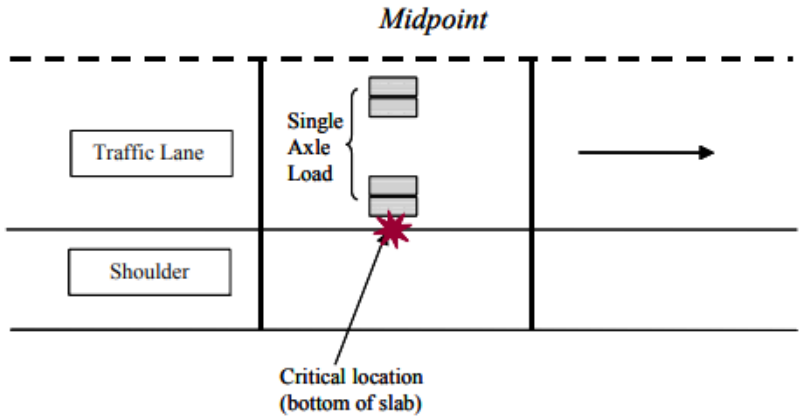

Figure 3-1 JPCP Bottom-up Transverse Cracking (NCHRP 2003)

3.3.2 Top-down Transverse Cracking

Top down cracking occurs when heavy truck axles with certain axle spacing repeatedly load the opposite ends of a PCC slab with high negative temperature gradient. Under negative temperature gradient condition, an upward slab curling occurs and the loading of steering and drive axles loads with short axle spacing simultaneously at slab opposite ends intensifies tensile stresses near the middle of the critical longitudinal edge, inducing fatigue damage at the slab surface.(NCHRP 2018). Therefore, top-down cracking damage accumulation is different from bottom-up cracking as their initiation is subjected to the type of traffic loading, and climatic conditions. Figure 3-2 shows a descriptive diagram of the occurrence of top-down cracking in JPCP pavements.

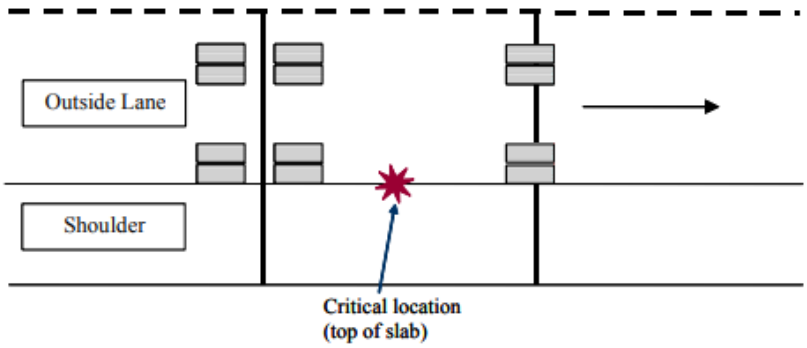

Figure 3-2 Top-down Transverse Cracking (NCHRP 2003)

3.3.3 Other JPCP Distress Transfer Functions in the AASHTOWare Pavement ME Design Program

Other JPCP PMED distress transfer functions apart from transverse cracking include International Roughness Index (IRI) and faulting models. Faulting is the difference in elevation at JPCP joints brought about by soil pumping. The faulting model follows an incremental approach to its appearance as increases from previous months in pavement life is used to determine what the faulting would be for the current month. The IRI model predicts the smoothness or roughness of the pavement over its service life, characterizing the pavement's functional performance. It is derived through a regression function of cracking, spalling, faulting, and site factor in addition to an initial IRI. Table 3-1 summarizes the equations for the models, default calibration coefficients and their values as appeared in the PMED program.

Table 3-1 JPCP Distress Transfer Models

Performance Indicator	Transfer Functions	Coefficients	Global Values
Transverse Cracking	$\log(N_{i,j,k,l,m,n,o}) = C_1 \cdot \left[\frac{MR_i}{\sigma_{i,j,k,l,m,n,o}}\right]^{C_2}$ $Crack = \frac{100}{1+C_4*FD^{C_5}} = \frac{100}{1+C_4*(N_{applied}/N_{allowable})^{C_5}}$ $TCrack = (Crack_{Bottom-up} + Crack_{Top-down} - Crack_{Bottom-up} * Crack_{Top-down})$	C_1 C_2 C_4 C_5	2.00 1.22 0.52 -2.17
Mean Faulting	$Fault_m = \sum_{i=1}^{m} \Delta Fault_i$ $\Delta Fault_i = C_{34} * (FAULTMAX_{i-1} - Fault_{i-1})^2 * DE_i$ $FAULTMAX_i = FAULTMAX_{i-1} + (C_7/10^6) \sum_{j=1}^{m} DE_j * \log(1 + C_5 * 5^{ERO}$ $FAULTMAX_0 = C_{12} * \delta_{curling} * [\log(1 + C_5 * 5^{EROD}) * \log(\frac{P_{200}*Wet\ Days}{p_s})$ $C_{12} = C_1 + C_2 * FR^{0.25}$ $C_{34} = C_3 + C_4 * FR^{0.25}$	C_1 C_2 C_3 C_4 C_5 C_6 C_7	0.595 1.638 0.00217 0.00444 250 0.47 7.3

		C_8	400
International Roughness Index	$IRI = IRIini + C1 \times CRK + C2 \times SPALL + C3 \times TFAULT + C4 \times SF$	C1 C2 C3 C4	0.8203 0.4417 16.145 56.944

Where faulting parameters are:

$Fault_m$ = Mean joint faulting at the end of month m, mm;

$\Delta Fault_i$= Incremental change (monthly) in mean transverse joint faulting during month i,mm;

$FaultMax_i$= Maximum mean transverse joint faulting for month i, mm;

$FaultMax_o$= Initial maximum mean transverse joint faulting, mm;

EROD = Base/subbase erodibility factor;

DE_i = Differential density of energy of subgrade deformation accumulated during month i;

$\delta_{curling}$= Maximum mean monthly slab corner upward deflection PCC due to

P_s = Overburden on subgrade, kg;

P_{200} = Percent subgrade material passing #200 sieve;

WetDays = Average annual number of wet days with a rainfall of more than 2.54 mm;

$C_{1, 2,3,4,5,6,7,12,34}$ = Calibration coefficients;

FR = Base freezing index defined as the percentage of time the top base temperature is below freezing (0°C) temperature.

And International Roughness Index (IRI) parameters are:

IRI = Predicted IRI, mm/km;

IRI_{ini}= Initial smoothness measured as IRI, mm/km;

CRK = Percent slabs with transverse cracks (all severities);

SPALL = Percentage of joints with spalling (medium and high severities);

Fault = Total cumulative joint faulting, cm;

SF = Site factor;

$C_{1,2,3,4}$ = Calibration coefficients.

4.3.4 Transverse Cracking Model Calibration Coefficients

From Table 3-1, four calibration coefficients (C_1, C_2, C_4 and C_5) are used to predict JPCP transverse cracking distress. The values of the calibration factors were developed based on model calibration to the Federal Highway Authority's Long Term Pavement Performance (LTPP) data, and are also results of model recalibrations conducted in 2011/2012 and 2012/2013 under the NCHRP 20-07 Task 288 and Task 327 projects. However, through the several software upgrades and model recalibrations by AASHTO, C_1 and C_2 globally calibrated values have been constant as they were derived based on substantial field and laboratory testing for allowable number of load applications to failure. (NCHRP 2018) A significant pavement design parameter that could influence C_1 and C_2 change is pavement joint spacing.

Generally the maximum JPCP joint spacing is 15fts (4.6m) in the LTPP data and current practice, C_1 and C_2 globally calibrated values should be sufficient in estimating Allowable Number of Load Applications ($N_{i,j,k,l,m,n,o}$). However, states with higher joint spacing may be required to locally calibrate C_1 and C_2 values to ensure better cracking prediction. Louisiana for instance was required

to calibrate the Allowable Load Application ($N_{i,j,k,l,m,n,o}$) or, in broader term, the fatigue model, as its JPCP sections have larger joint spacing of approximately 20ft (6.1m) (NCHRP 2018).

Generally, the NCHRP Project 20-07 report and AASHTO recommends no change in the globally calibrated C_1 and C_2 transverse cracking values and a consistent use of globally calibrated C_1 and C_2 values have been successfully employed by most State Department of Transportations (DOTs) that have undergone local transverse cracking calibration (NCHRP 2018, AASHTO 2008, Pierce and Mcgovern 2014, Haider et al. 2017). Table 3-2 identifies some of the states using the globally calibrated C_1 and C_2 values:

Table 3-2 Local Calibrated Coefficients used by some State DOTs

	Calibration Coefficients			
States	C_1	C_2	C_4	C_5
Nationally Calibrated	2	1.22	1	-1.98
Arizona	2	1.22	0.19	-2.067
Colorado	2	1.22	0.6	-2.05
Missouri	2	1.22	1	-1.98
Washington	2	1.22	0.139	-2.115
Minnesota	2	1.22	0.9	-2.64
Ohio	2	1.22	1	-1.98

Local calibration of the transverse cracking model is mostly domiciled in the (prediction) model or transfer function, hence warrants a change to the C_4 and C_5 model coefficients to predict local conditions. C_4 and C_5 values influences the slope and magnitude of the transverse cracking prediction. The C_4 tends to direct cracking predictions in the horizontal direction and C_5 affects the slope (rate or magnitude) of cracking prediction (Haider et al. 2017). Also, C_4 and C_5 coefficients affects the bias and precision of the cracking model respectively with C4 noted as the most sensitive coefficient in the transfer function (Zhong 2017).

It is noteworthy to mention that the rigid pavement models in the PMED program were recalibrated in 2015 with specific changes made to the transverse cracking model. As C_1 and C_2 remained constant, C_4 and C_5 values changed from 1 and -1.98 to 0.52 and -2.17 respectively following the recalibration exercise (Sachs et al. 2016, Mallela et al. 2015). The calibration coefficients C4 and C5 are regression coefficients for the top-down fatigue damage and bottom-up fatigue damage explanatory variables, and are used to obtain top-down and bottom-up transverse cracking respectively.

3.4 Local Calibration Methodology

As earlier stated, the globally calibrated IRI and faulting models with the exception of transverse cracking model in the AASHTOWare Pavement ME Design version 2.5 were found to give better prediction of performance in Ontario. As a result, model accuracy and precision of transverse cracking model would need to be improved by deriving new calibration coefficients that improves local prediction accuracy and precision. The primary objective of model calibration is to significantly reduce overall model bias. When a model is biased, it could either result in an overdesigned or under-designed pavement, thereby having a relative impact on cost. The second objective is to increase precision in order to gain consistency in model predictions. To achieve this, predicted distresses are compared to measured distresses and reasonable calibration coefficients are determined to eliminate significant bias and improve model precision (AASHTO 2015). The NCHRP Project 1-40B provides a general procedure and best practices for completing local calibration (AASHTO 2010).

3.4.1 Local Calibration Procedure

The AASHTO 2010 local calibration guide has been summarized into the following steps:

- Select PCC sections with detailed information relating to traffic, climate and materials conditions.

- Obtain measured or observed values on the selected sections from local Pavement Management System (PMS) and process values to comparable units with Pavement ME performance results

- Using global calibration coefficients, conduct Pavement ME runs to obtain the predictions and compare with observed values to determine the model prediction accuracy.

- If the accuracy of model is found adequate, accept the use of global coefficients for local conditions.

- If accuracy of model is not adequate, calibrate the model by conducting an optimization (linear or non-linear) operation to limit residuals between measured and predicted values and propose calibration coefficients

- Evaluate the adequacy of local calibration coefficients by conducting validation and accuracy evaluations.

- Recommend reasonable local coefficients with the least error in prediction

When preparing and comparing calibration data, the PMED cracking prediction values should be at 50% reliability and the corresponding measured values should be a mean or average measurement of the respective section. It is also important to note the age of the pavement when distress measurement was conducted, as this should correspond to the PMED predicted cracking. If this is not well considered, local calibration coefficients derived through the calibration exercise would erroneously over or under predict pavement distress and performance over design life.

3.4.2 Rigid Pavement Sections Used for Local Calibration

Table 3-3 presents the rigid pavements sections selected for Ontario local calibration of transverse cracking.

The major characteristics of the rigid pavement sections are listed below:

- Average Annual Daily Truck Traffic (AADTT) ranged from 1,160 to 25,300 with a mean of 5921

- The age of the sections ranged from 1 to 26 years having an average of 10 years approximately.

- All rigid pavement sections were Jointed Plain Concrete Pavement (JPCP) and totaled thirty-two (32) sections.

The AASHTO 2010 Guide for MEPDG Local Calibration recommends a minimum of thirty (30) pavement segments selected for the calibration and validation process in order to statistically obtain reasonable transverse cracking calibration coefficients. For this exercise, a total of thirty-two (32) sections were considered to meet up with this requirement. Although a larger data set would have been desired, rigid pavements are unfortunately fewer in Ontario compared to flexible pavements. A split-sample approach was followed for the calibration exercise as 90% sections were separated for calibration and the remaining 10% for model validation. The validation process further used 90% and 100% sections to test the accuracy of the locally developed coefficients.

The MTO provided measured cracking data on the selected rigid sections from its Pavement Management System-2 as well as predicted Pavement ME cracking data using global calibration coefficients. This data was used to initiate an optimization process to determine local calibration coefficients that fits the transverse cracking model to Ontario conditions.

Table 3-3 Selected Pavement Sections used for Calibration

HWY	Age (Yr.)	District
401(412E)	7	Chatham
401(412W)	7	Chatham
401(716E)	6	Chatham
401(716W)	6	Chatham
401(991E)	9	Chatham
401(991W)	9	Chatham
401(1025E)	8	Chatham

401(1025W)	8	Chatham
401(1047E)	9	Chatham
401(1047W)	9	Chatham
401(389W)	5	Chatham
401(389E)	5	Chatham
401(389C2)	5	Chatham
401(389C)	5	Chatham
No3	15	Chatham
No3-1	5	Chatham
No3-2	7	Chatham
No3-3	7	Chatham
N404(5.4N)	1	Toronto
N404(5.4S)	1	Toronto
N404(68N)	1	Toronto
N404(68S)	1	Toronto
No417	13	Ottawa
No417-1	11	Ottawa
N115	24	Bancroft
N115-1	24	Bancroft
N115-2	25	Bancroft
N115-3	25	Bancroft
N115-4	26	Bancroft
N115-5	26	Bancroft
N402	8	Chatham
N402-1	8	Chatham

3.4.3 Non-linear Optimization - Statistical Analysis Software (SAS) Programming

A non-linear optimization operation was initiated to minimize the Sum of Squared Error (SSE) between the predicted and measured cracking values. This is intended to reduce or completely eliminate transverse cracking model bias (under prediction or over prediction). As the cracking transfer model was found to have a non-linear relationship, a non-linear optimization was required to determine new C_4 and C_5 calibration coefficients for the model. To carry out this operation, several optimization and statistical techniques are available. Examples of these techniques are the

Generalized Reduced Gradient (GRG) and Evolutionary algorithm in Microsoft Excel Solver, Levenberg–Marquardt optimization technique and Gauss-Newton algorithm. To estimate local calibration coefficients for the transverse cracking model, the Gauss-Newton algorithm for non-linear optimization is initiated in the Statistical Analysis System (SAS). The transverse cracking model, top-down fatigue damage, bottom-up fatigue damage, default C_4 and C_5 calibration coefficients, observed cracking values and predicted cracking data for the 90% calibration sections were programmed using SAS coding. A SAS procedure is run to initiate the Gauss-Newton optimization algorithm which reduces the Sum of Squared Error (SSE) between the observed and predicted cracking values by changing the calibration coefficients values through an iterative process.

In addition, a total of five constrained iterative phases were separately introduced alongside the SAS iteration to further minimize the SSE and derive reasonable calibration coefficients. Engineering judgment was then employed to select reasonable coefficients which minimized the SSE across the five (5) constrained iterative phases. The selected coefficients were proposed and tested through statistical tests to confirm their ability to accurately predict local cracking performance in Ontario.

3.4.4 Accuracy Evaluation

Locally predicted values were statistically compared to PMS measured values to determine the suitability of the calibration coefficients for prediction accuracy and precision. A line of equality at 45 degrees angle between the locally predicted cracking and measured cracking values was plotted and fit statistics such as Sum of Square Error (SSE), Bias, Standard Error of Estimate (Se) and paired t-test were conducted to ascertain model accuracy and coefficient suitability.

$$Sum\ of\ Squared\ Error\ (SSE) = \sum_{i=1}^{n}(Observed_i - Predicted_i)^2 \qquad 3\text{-}4$$

$$Standard\ Error\ of\ Estimate\ (S_e) = \sqrt{\frac{\sum_{i=1}^{n}(Observed_i - Predicted_i)^2}{n}} \qquad 3\text{-}5$$

$$Bias = \frac{\sum_{i=1}^{n}(Observed_i - Predicted_i)}{n} \quad 3\text{-}6$$

Paired t-test; H_0: There is no statistical significant difference between Measured and Predicted (Measured cracking values = Predicted cracking values) indicating a P-value greater than 0.05 with 95% confidence.

H_1: There is a significant difference between Measured and Predicted (Measured cracking values ≠ Predicted cracking values) indicating a P-value less than 0.05 with 95% confidence.

S_e = Standard Error of Estimate

SSE = Sum of Squared Error

n = number of data points in each distress comparison.

$Observed_i$ = Measured cracking data points

$Predicted_i$ = Predicted cracking data points

3.5 Calibration and Validation

3.5.1 Calibration of Transverse Cracking Model

As earlier stated, 90% of the calibration data set was used as calibration dataset and the remaining 10% for validation. Optimized C_4 and C_5 values with reduced SSE were selected from the constrained and unconstrained iterative phases as shown in Table 3-4 and these coefficients were used to predict cracking for the validation sections. The predicted cracking is statistically compared to its corresponding measured cracking values.

Table 3-4 Proposed Local Calibration Coefficients

No	C_4	C_5	Sum of Squares Errors (SSE)	Remarks
Global	0.52	-2.17	0.00316	Default or Global
1	12.8612	-0.3073	0.00236	Local 1

2	15.135	-0.266	0.00239	Local 2
3	7.43	-0.4	0.00244	Local 3
4	3.2393	-0.4801	0.00255	Local 4
5	0.8378	-0.6934	0.00257	Local 5
6	0.52	-0.78	0.00258	Local 6

3.5.2 Validation of Transverse Cracking Model

Validation is the process of applying the model to the data that was not used in the calibration process. After this is conducted, validation and calibration data are recombined to optimize the local calibration coefficients using the entire data set in order to confirm the robustness of the model.

The proposed calibration coefficients were used to predict cracking performance of the 10% validation sections and compared to its corresponding measured performance using statistical analysis. A paired t-test was performed to test if the null hypothesis (Ho) was to be accepted or rejected. Description of hypothesis testing is shown below:

H_0: There is no statistical significant difference between Measured and Predicted (Measured cracking values = Predicted cracking values) indicating a P-value greater than 0.05($p=>0.05$) at 95% confidence level.

H_1: There is a significant difference between Measured and Predicted (Measured cracking values ≠ Predicted cracking values) indicating a P-value less than 0.05 with 95% confidence level.

An ideal situation for a better model coefficient would suggest an acceptance of the null hypothesis, indicating no significant difference between the local calibration predictions and measured field values.

Table 3-5 Results of Statistical Analysis using Validation data set (10% of sections).

Calibration Set	C_4	C_5	Bias (%)	Avg. Predict (%)	P-value	P > 0.05	Remarks
Global	0.52	-2.17	0.97	1.3E-09	0.03334	Significant Difference	Reject Ho
Local 1	12.86	-0.307	0.69	0.28	0.063	No Significant Difference	Accept Ho
Local 2	15.135	-0.266	0.56	0.41	0.087	No Significant Difference	Accept Ho
Local 3	7.43	-0.4	0.82	0.15	0.047	Significant Difference	Reject Ho
Local 4	3.2393	-0.4801	0.84	0.13	0.044	Significant Difference	Reject Ho
Local 5	0.8378	-0.6934	0.94	0.04	0.036	Significant Difference	Reject Ho
Local 6	0.52	-0.78	0.95	0.02	0.035	Significant Difference	Reject Ho
Mean Measured Value (%)	*******	*******	*******	0.97	******	*********	*******

From Table 3-5, there exists a significant difference between the predictions from Local 3, Local 4, Local 5 and Local 6 calibration sets of C_4 and C_5. Though the bias of the validation set was somewhat minimized especially in Local 3 and Local 4. The paired t-test suggests a rejection of the null hypothesis as the p-value of these calibration sets were less than 0.05. This suggests lack of 95% confidence in calibration set predictions.

Local 1 and Local 2 predictions against measured values showed no significant difference when the paired t-test was performed, suggesting more reasonableness in their ability to predict local conditions in Ontario. Local 1 and Local 2 had a P-value of 0.087 and 0.063 respectively which was greater than 0.05 at 95% level of confidence.

A reduction in bias from 0.97% to 0.56% in Local 2 was noticeable, and average cracking predictions in Local 1 and Local 2 also showed better improvement compared to other calibration sets. Therefore, Local 1 and Local 2 calibration sets were selected and considered in the 90% calibration sections validation and statistical analysis conducted.

Table 3-6 Results of Statistical Analysis using 90% of the calibration sections.

Calibration Set	C_4	C_5	Bias (%)	Se (%)	Avg. Cracking Prediction (%)	P Value	P > 0.05	Remarks
Global	0.52	-2.17	0.66	0.82	0.000015	0.000092	Significant Difference	Reject Ho
Local 1	12.86	-0.307	0.22	0.89	0.44	0.118	No significant difference	Accept Ho
Local 2	15.135	-0.266	0.10	0.92	0.56	0.295	No significant difference	Accept Ho
Mean Measured Value (%)	***	***	***	***	0.66	***	***	***

From Table 3-6, Local 1 and Local 2 calibration sets resulted in good predictions using 90% calibration sections for validation as there was no significant difference between its predicted values and measured values. The p-values 0.118 and 0.295 for Local 1 and Local 2 respectively, are both greater than 0.05, reflecting no significant difference in their predicted and measured

values at 95% confidence. Local 1 and Local 2 calibration sets also improved the cracking model predictions compared to the global calibration sets as mean predictions improved from a globally calibrated value of 0.0000146% to 0.43% and 0.55% respectively, giving close values to the mean measured value of 0.66%. With the mean measured value of 0.66%, and mean prediction under global coefficients predicting a mean value of 0.0000146%, a bias (under prediction) obviously exists using the global calibration set.

Changes in the Standard Error of Estimate (Se) was negligible, increasing only by 0.09% with a significant reduction in bias from 0.66% to 0.10%, indicating an approximate 84% bias reduction under Local 2 calibration set. There was also a considerable reduction from 0.66% to 0.22% in Local 1, with no significant change in the Se

Furthermore, validation was conducted using 100% sections to examine the accuracy and capacity of the Local 1 and Local 2 calibration set in predicting observed cracking trends in Ontario. Paired t-test, bias and Standard Error of Estimate (Se) for the model were conducted to evaluate the accuracy of the model in predicting measured or field transverse performance. Results of the statistical analysis is presented in Table 3-7.

Table 3-7 Validation of Calibration Coefficients using 100% of Sections

Calibration	C_4	C_5	Bias (%)	Se	SSE	Avg. Predict (%)	P-value	P > 0.05	Remarks
Global	0.52	-2.17	0.69	0.80	0.0035	1.33E-05	0.000015	Significant Difference	Reject Ho
Local 1	12.86	-0.307	0.26	0.89	0.0025	0.42	0.047	Significant Difference	Reject Ho
Local 2	15.135	-0.266	0.15	0.89	0.0025	0.54	0.178	No Significant Difference	Accept Ho

Mean Measured Value (%)	***	***	***	***	***	0.69	***	***	***

From Table 3-7, Local 2 predictions showed no significant difference with measured values and it was recommended as the best calibration coefficients for predicting Ontario's conditions. The paired t-test results of the three calibration sets are shown below:

- P-value of test showed a significant difference in the values predicted by the Global calibration coefficients and measured field cracking values. $P = 0.000015 < 0.05$ at 95% level of confidence.

- P-value of test showed a significant difference in the values predicted by the Local 1 calibration coefficients and measured field cracking values. $P = 0.047 < 0.05$ at 95% level of confidence.

- P-value of test reported showed no significant difference in the values predicted by the Local 2 calibration coefficients and measured field cracking values. $P = 0.1787326 > 0.05$ at 95% level of confidence.

The best calibration set derived was Local 2, which had a mean predicted value of 0.54%, reducing the bias of the cracking transfer model from 0.69% to 0.15% and Sum of Squared Errors (SSE) reduced from 0.0035 to 0.0025.

3.5.3 Model Bias of Local Transverse Cracking Model

Figure 3-3 shows the distribution of residual errors for the local and global cracking models. A non-biased model should have a balance of negative and positive residual errors with the average around zero, providing better distribution of residual errors. (Smith and Nair 2015) As observed in Figure 3-3, residuals from the global calibration set were all positive thus demonstrating extreme under-prediction of cracking to measured or observed dataset. A model with a positive bias would

result in under prediction while a negative bias signifies over prediction of the distress parameter. The global coefficients inaccurate predictions could be linked to the exemption of Ontario rigid pavement sections in the LTPP data used to globally calibrate the PMED transverse cracking model. Difference in climate conditions, maintenance and preservation policies could have also contributed to the bias in the model prediction.

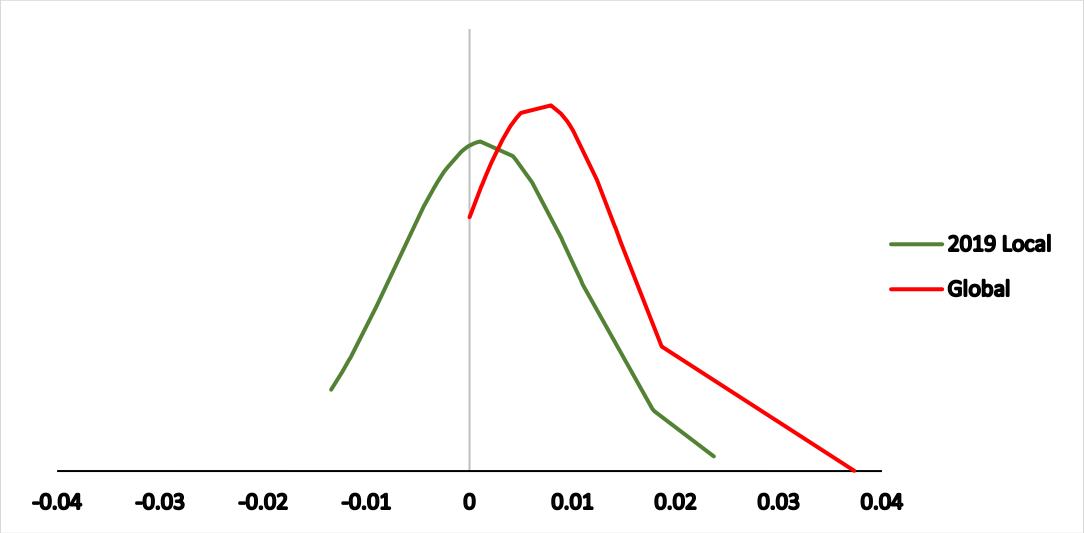

Figure 3-3 Distribution of Residual Errors for Globally and Local Calibration Models

Underprediction refers to the underestimation of distress prediction and therefore less conservative design which could result in an inaccurate prediction of performance and early transverse cracking development in the new pavements designed using these calibrations coefficients. If the global cracking calibration factors are used for pavement project design, cracking propagation suggesting longer service life would be erroneously predicted. Potentially increasing maintenance and rehabilitation cost, as cracking distresses would be observed earlier in the pavement design life than anticipated.

The underestimated transverse cracking predictions from global calibration coefficients however moved closer to the line of equality when newly derived local calibration coefficients were used. Local calibration values improved the accuracy of the model by minimizing the bias and provided a relative balance in the positive and negative residual errors, moving the overall bias closer to zero and establishing better prediction of observed local conditions in Ontario. In

summary, no significant bias was recorded at a 0.05 (5%) significance level for Local 2 based on the statistical tests performed. Figures 3-4 and Figure 3-5 below show the equality plot of measured and predicted cracking values using global and local calibration sets respectively.

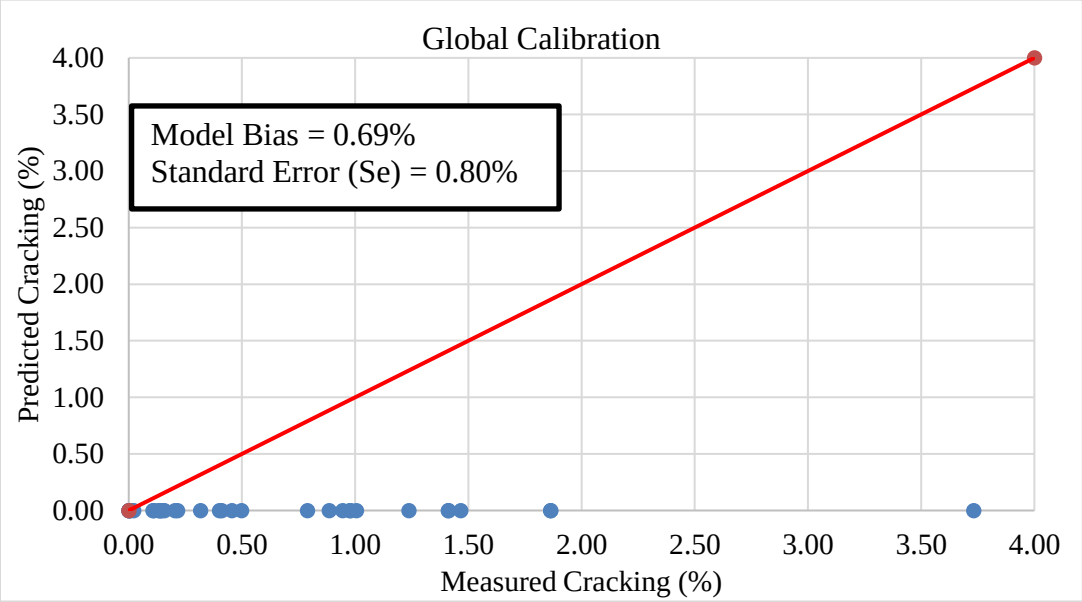

Figure 3-4 Equality Plot of Predicted versus Measured Cracking using Global Calibration Coefficients

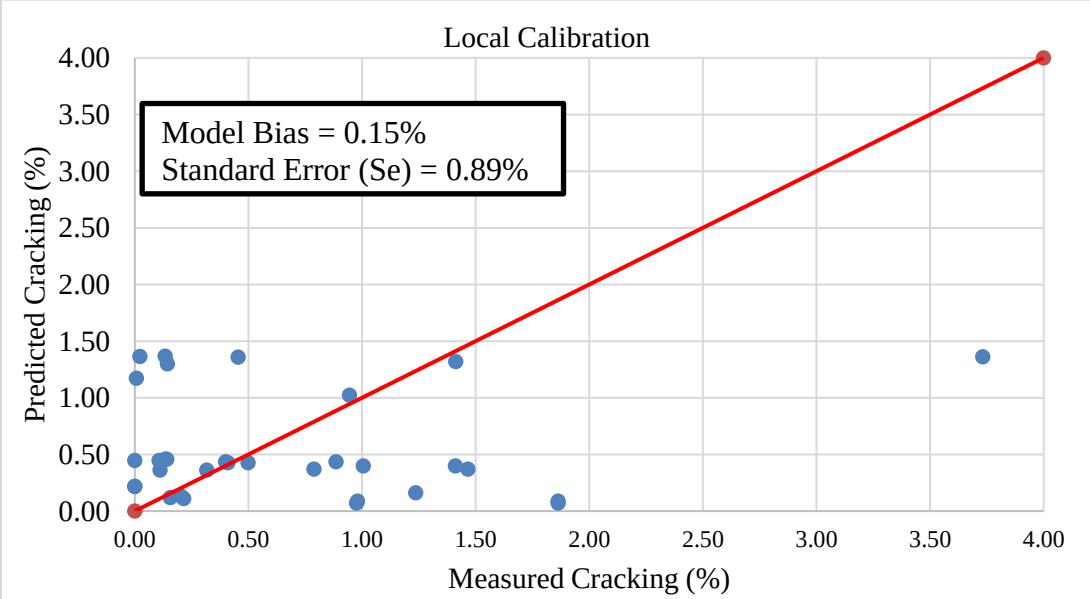

Figure 3-5 Equality Plot of Predicted versus Measured Cracking using Local 2 Calibration Coefficients

3.5.4 Standard Deviation or Error (Se) of Local Transverse Cracking Model

Two approaches were taken in the evaluation of the Standard Error of Estimate (Se) of the newly calibrated model based on AASHTO 2010 local calibration guide.

The first was to statistically determine if there was a significant difference between Se generated from global and local calibration factors using the selected Ontario rigid pavements.

The second was to statistically determine if there was a significant difference between Se generated from the original global calibration using LTPP sections, and Se generated by local calibration using the selected Ontario rigid pavements considered in this study.

In the first approach, the null hypothesis (Ho) is that no significant differences exists between the global and local calibration standard errors at a 95% level of confidence (Se of Predicted = Se of Measured). If this null hypothesis is accepted, the local calibration factors can be recommended for use. If the null hypothesis is rejected, it is recommended to recalibrate the cracking model in an attempt to lower the standard error. The road agency, can however, decide to just accept the higher standard error or default standard error determined from the original calibration process using LTPP sections.

The Standard Error of Estimate (Se) of the local and global calibrations are 0.80% and 0.89% respectively. To statistically test for significant difference between the two, an F-test for variance was conducted on the residual errors computed from local and global calibration factors at a 95% level of confidence. F-test result is shown in Table 3-8.

Table 3-8 F-Test for Variance between Residual Errors Generated by Local and Global Calibration Factors

F-Test	Measured Cracking	Predicted Cracking
Observations	32	32
Mean	0.001471	0.006882
Variance	7.93E-05	6.36E-05
F	1.248	
P-value	0.27	
F Critical	1.822	

From Table 3-8, the p-value of 0.27 > 0.05 implies that the null hypothesis can be accepted, indicating no significant difference between the Standard Error of Estimate (Se) of the global and locally calibrated models. The F value was also lower than F-critical (1.248 < 1.822) at 95% level of confidence, further reaffirming no statistically significant difference between both standard error terms.

In the second approach, the null hypothesis (Ho) is that no significant difference between the standard error for the local and global calibration efforts from the LTPP original calibration. If the null hypothesis is accepted, the local calibration factors are recommended for use. The local calibration coefficients are also recommended for use if it has a lower standard error than the global standard error from LTPP calibration. The null hypothesis is rejected when the local calibration has a higher standard error than global calibration standard error. Table 3-9 shows comparison between local and global LTPP standard error and tolerable bias for JPCP.

Table 3-9 Tolerable Bias and Standard Error from Global Calibration Exercise NCHRP 20-07 (327) compared to Ontario Local Calibration (Mallela et.al 2016, Sachs et al. 2015)

Pavement Distress	Calibration	Number of Sections (N)	C4	C5	Tolerable Bias	Standard Error of Estimate, Se (%)
JPCP Transverse Cracking	Global	1676	0.52	-2.17	7.20%	4.58%
	Local	32	15.135	-0.266	0.15%	0.89%

From Table 3-9, the local calibration standard error was very low compared to global calibration (0.89% < 4.58%), therefore the null hypothesis can be accepted and local calibration coefficients recommended. This low calibration standard error, however, could affect design reliability predictions if the Se equation in the PMED program is changed to fit 0.89%. This is because observed cracking of selected Ontario sections had low cracking values, and the number of calibration sections were much lower compared to LTPP sections used for global calibrations (32sections versus 1676 sections).

The global Standard Error of Estimate (Se) or Standard Deviation equation suggest a more realistic influence of design reliability on cracking performance prediction as it was calibrated using many sections across North America. As more data is recorded on the Ontario calibration sections and more concrete pavement constructed, MTO should periodically validate the local transverse cracking coefficients and its standard error (Se). Using the global Se equation for low local calibration standard error was also recommended to the State of Wyoming DOT by the developers of the PMED program, Applied Research Associates (ARA, 2015).

In summary, the global standard deviation equation is sufficient for cracking distress prediction at various reliability and there is no need to develop a new standard deviation model for the Ontario transverse cracking local calibration coefficients. The standard deviation equation as reported in NCHRP 20-07(327) and observed in the PMED program is shown below:

$$CRK_R\ (Design\ Relaibility) = CRK_{50}\ (50\%\ Reliability) + STDEV * Z(Design\ Relaiability)$$

$$Standard\ Deviation\ (CRK_{50}) = 3.5522 * (CRK_{50})^{0.3415} + 0.75$$

Where:

$$CRK = Predicted\ Transverse\ Cracking\ at\ Design\ Reliability$$

$$Z = Standard\ Normal\ Deviate\ for\ Design\ Reliability$$

$$CRK_{50} = \ Predicted\ Transverse\ Cracking\ at\ 50\%\ Reliability$$

By employing the derived calibration factors, reasonable predictions of transverse cracking for new and existing JPCP at various reliability under Ontario conditions is achieved.

3.6 Acceptance of Ontario Transverse Cracking Calibration Factors

The Ministry of Transportation Ontario (MTO) validated the calibration factors using actual designs of several representative concrete pavement projects and was recommended to achieve the lowest Sum of Squared Error (SSE) and Bias, as it also produced acceptable results for 28-year design life. As a result, calibration values have been published in the Revised 2019 Ontario's Default Parameters for AASHTOWare Pavement ME Design Interim Report for industry use (MTO 2019). A summary of the transverse cracking global and Ontario local calibration coefficients for JPCP transverse cracking is shown in Table 3-10.

Table 3-10 Transverse Cracking Calibration Coefficients for Global, and 2019 Ontario Local Calibration for Jointed Plain Concrete Pavement (JPCP)

Rigid Pavement Model	Model Coefficients	Global Calibration Coefficients	Local Calibration Coefficients
JPCP Transverse Cracking Transfer Function	C_1	2	2
	C_2	1.22	1.22
	C_4	0.52	15.135
	C_5	-2.17	-0.266

3.7 Conclusions

Although the AASHTOWare Pavement ME Design (PMED) program is by default globally calibrated with the use of Long Term Pavement Performance (LTPP) data, it is recommended that road agencies validate the suitability of these global models for accurate predictions of observed performance and distress trends in their various states or provinces. Currently, globally calibrated IRI performance and faulting prediction models are found adequate for JPCP performance prediction in Ontario. However, the transverse cracking prediction model underpredicts JPCP performance and it was deemed necessary to calibrate the transverse cracking model. The Pavement ME transverse cracking model consists of two (2) different models, and has four (4) calibration coefficients denoted as C_1, C_2, C_4 and C_5. C_1 and C_2 coefficients are part of the fatigue damage model, while C_4 and C_5 are coefficients of the prediction model or transfer function. Global calibration values for C_1 and C_2 coefficients were recommended for local use, while C_4 and C_5 values were derived through non-linear optimization. These coefficients were then validated to determine prediction accuracy and reliability through statistical analysis. They were also incorporated into the design of several representative Ontario concrete pavement projects by

the MTO, and were found to provide better prediction of cracking distress performance. Following this process, C_4 (15.135) and C_5 (-0.266) coefficients were proposed as JPCP transverse cracking local calibration coefficients for Ontario. The calibration coefficients have also been included in the published '2019 Ontario's Default Parameters for AASHTOWare Pavement ME Design Interim Report' for JPCP design, analysis, and forensic investigations in Ontario, by the Ministry of Transportation Ontario (MTO).

Chapter 4

Towards a Flood Resilient Pavement System in Canada - A Rigid Pavement Design Approach – Case Study of Ontario and Manitoba

4.1 Overview

As climate change continues to threaten pavement infrastructural performance across the world, the need for sustainable solutions for pavement adaptation cannot be overstated. In Canada, flooding is a prominent climate hazard common to most Canadian provinces and adaptation of pavements to this hazard is desired. Based on previous investigations, concrete pavements are recorded as sustainable, resilient to flood hazards, and proposed to be a good pre-flood strategy. However, design properties need to be given utmost consideration to provide required resilience. This paper takes a design approach to examine the resilience of Jointed Plain Concrete Pavement (JPCP) to flood by modelling the performance of matrices of typical PCC pavement designs in Canada under a Representative Concentration Pathway (RCP) of 4.5 W/m^2 future precipitation scenario. The AASHTOWare Pavement ME Design (PMED) program is used to simulate and predict performance changes under flood scenarios taking the Provinces of Ontario and Manitoba as case studies. In the Ontario study, mean flood damage peaked at 5.99% and 2.39% for collector and arterial JPCP pavement. In the Manitoba study, a total of 27 pavement classes was developed based on typical traffic, slab thickness and subgrade parameters common to the province. From the analysis of all pavement design classes, minimum and maximum damage observed was 0.31% and 3.03% respectively. The performance of the pavement design classes in terms of flood resilience, service life and cost feasibility were analyzed with respect to traffic and subgrade conditions. Generally, results provided insight into the resilience and adaptive capacity of rigid pavements to climate flood hazards under Canadian climate condition (Oyediji et al 2019).

4.2 Introduction

Climate change is increasing the occurrence of climate hazards across Canada. Flooding is the most common climate hazard of high recurrence in all Canadian provinces. Based on a report published by Public Safety Canada, flooding is reported to have occurred 241 times more than

other climate hazards between 1900 to 2005 (Sandink et al. 2010) and the frequency of an event has been on the rise. Some instances include the notable flood events that have occurred between 2005 and 2018 in Ontario, Manitoba, New Brunswick, Quebec and Alberta. The likelihood of the occurrence of flood events such as storm surge, flash floods, extreme precipitation in almost all of Canada's provinces during the spring season have remained high over the past two decades and future projections from climate change reports show increases in the frequency of this climate hazard in major parts of the country (Gaus et al 2018). In the wake of these extreme events, two major infrastructure systems, water and transportation are reported most vulnerable to the impact of flood hazards. This is of particular interest as they are pivotal to the sustainability of socioeconomic activities such as agriculture, natural resources, fisheries, tourism, insurance and health; which all depend on a safe and reliable transportation network (Warren and Lemmen 2014). In 2011, Transport Canada reported that the transport services contribute up to 4.2% of Canada's Gross Domestic Product (GDP) total over a $100 billion in that year. Therefore it is of national interest to ensure assets are preserved and continue to provide required service even in the wake of unforgivable climate events. The main components of these services in Canada are air, marine, rail and roads systems. Out of these four, road transportation is noted as the most important asset for passenger and freight transportation, local (intra-city) and intercity transportation, intra-provincial transportation activities, and trade between Canada and the United States (in terms of value transported) (Transport Canada 2011). Road pavements, an operational and functional component of any road infrastructure, is not inexorable to climate hazards (Schweikert et al. 2014). The underlying reason for this vulnerability can be traced to the design and engineering behind pavement assets as considerations were only given climate conditions at the time of construction. As a consequence, changes in climate conditions coupled with the frequent occurrence of climate hazards predominantly flooding as respective to Canada limits the infrastructural capacity to withstand extreme conditions beyond acceptable thresholds, relatively reducing infrastructure service life. This, in most cases, potentially results in increased maintenance and rehabilitation costs in a bid to sustain structural integrity (Prowse et al., 2009). Therefore, given its importance, potential climate change impacts on pavement need to be addressed (Tighe 2015).

To properly address the influence of climate-induced flood hazards on the pavement, a number of studies have been conducted by various researchers in the pavement community to understand the interaction between flood hazards and pavement infrastructure from a performance perspective. Chen and Zhang 2014 investigated the functional performance of pavements submerged in the 200 - 250mm of flooding induced by the 2005 Hurricane Katrina event. The researchers observed considerable increase in the IRI of flexible pavements to rigid pavements due to the influence of debris carrying trucks deployed immediately after the flood event. The trucks are removing debris that could be detrimental to human and environmental wellbeing. In the same vein, Gaspard et al 2006 evaluated structural performance of the submerged pavements affected by hurricane Katrina using parameters such as pavement Deflection at the plate (D1), Effective Structural Number (SNeff) and subgrade Resilient Modulus (Mr) of inundated pavements determined from Falling Weight Deflectometer (FWD) testing. Their study observed diminutive loss of SNeff and subgrade resilient modulus of the concrete pavement when compared to asphalt concrete pavement. An Australian study analyzed functional performance data before and after the 2011 Queensland flood event which had a mean rainfall magnitude of 210mm. The authors of the study concluded that the high strength rigid pavements provided the highest resilience to flood damage, thus proposed the use of rigid pavements as a pre-flood adaptation strategy. (Khan *et al.* 2017). Based on these studies, rigid pavements can be proposed as a better alternative for roads in flood plain areas due to their resilience to flood damage than flexible pavement. However, the extent of damage may be respective to rigid pavement type.

The performance of a Continuously Reinforced Concrete Pavement (CRCP) and Jointed Plain Concrete Pavement (JPCP) under flood conditions may be different. A study was carried out on CRCP following the 1270 mm flood during the 2017 Hurricane Harvey in Texas. No major maintenance was needed to be carried out on the CRCP sections as it provided a good resilience to both traffic and extreme weather conditions without premature deterioration. Aswell, the CRCP structure was overlying a heavily stabilized base which may have provided waterproof properties for the underlying layers, allowing adequate drainage and enhancing soil stiffness (Powell 2018,

Lukefahr 2018). In Canada, JPCP is the dominant rigid pavement type but there is no intrinsic investigation into the structural and functional performance of inundated JPCP pavements in the Canadian climate. The use of modelling techniques to gain insight is therefore encouraged. A program which could be employed for this approach is the AASHTOWare Pavement ME Design (PMED) program as it properly incorporates important climate parameters in its simulation of pavement performance (Tighe *et al.* 2008, Mills *et al.* 2007; Meagher *et al.* 2012 Lu *et al*. 2018). The main objective of this study is to investigate the flood resilience of Jointed Plain Concrete Pavement (JPCP) from a design perspective, by modelling the performance of matrices of typical PCC pavement designs in Canada under Representative Concentration Pathways RCP of 4.5 W/m^2 future precipitation scenarios.

4.3 Flood Impact Modelling Methodology

To model the effect of flooding on concrete pavements in the Canadian climate, pavement design practice of two Canadian provinces were evaluated, Ontario and Manitoba. Available data and pavement structural information published by road agencies of the two provinces served as representative design inputs. The Mechanistic Empirical Pavement Design Guide (MEPDG) (ARA 2004, 2011) currently referred to as the AASHTOWare Pavement ME Design (PMED) program, is employed as a design tool to simulate the performance of typical pavement structures identical to the two provinces considering a no-flood and flood scenario. A no-flood scenario or base case scenario is the performance prediction using historical precipitation data while flood scenario is the performance prediction under climate-induced extreme precipitation values. These extreme values were obtained in form of Intensity Duration Frequency data considering a future climate period of (2018 to 2100) using the Intensity Duration Frequency Climate Change Tool (IDF_CC Tool 3.0). The IDF_CC tool is an open source information which estimates precipitation accumulation depths for a variety of return periods (2, 5, 10, 25, 50 and 100 years) and durations (5, 10, 15 and 30 minutes and 1, 2, 6, 12 and 24 hours) for the Canadian environment. The tool engages 24 Global Circulation Models (GCMs) and 9 downscaled GCMs using rigorous downscaling method such as spatial and temporal downscaling, statistical analysis and

optimization to update pre-estimated IDF from historical precipitation data to IDF under Representative Concentration Pathway (RCP 2.6, 4.5 and 8.5W/m2) climate change scenarios (Simonovic *et al.* 2016).

Out of the RCP scenarios, RCP 4.5, an intermediate emission scenario was chosen based on an extensive analysis of the uncertainty of future flood occurrences under various RCP scenarios across Canada. RCP 4.5 is reported to have the least uncertainty in projected increase or decrease in flood frequencies across Canada compared to other RCP scenarios. Northwest Territories, Yukon Territory, Nunavut, and southwestern Ontario are projected to experience higher flood frequencies in the future as a 100-year historical flood could reduce to a frequency of 10–60 years by the end of the 21st century. In contrast, return flood in northern prairies and north-central Ontario could experience lower flood frequencies, with a return period of 100-year historical floods becoming 160–200 years return period in the future (Gaur *et al* 2018). As a consequence, extreme precipitation values for 50 and 100 years return period with repeated cycles of flood events under RCP 4.5 were generated for modelling the Ontario case study, and a RCP 4.5 100 year flood event in the Manitoba case study using an ensemble of climate prediction models. To establish a baseline scenario, historical climate data available through the National Centers for Environmental Prediction (NCEP) North American Regional Reanalysis (NARR) program is obtained via the AASTHO M-E design open source database. Table 4-1 shows the mean values of extreme precipitation under RCP 4.5 scenario at case study locations.

Table 4-1 Ontario and Manitoba Future Return Period under RCP 4.5

Location (Lat, Long)	Duration	RCP 4.5 50-year	RCP 4.5 100-year
Toronto, Ontario (43.81174, -79.41639)	24hr	151.94mm	168.84mm

Winnipeg, Manitoba (43.86200 -79.37000)	24hr	127.35mm

Considering no-flood and flood scenario, pavement structural configuration, and various traffic levels of representative pavement designs, pavement performance over design life was simulated for the two case studies using the Pavement ME. Of utmost interest was the performance response of JPCP under climate conditions considering no-flood and flood cases, as well as the comparative analysis of percentage changes or relative due to flood impacts. PMED default or global calibration coefficients were harnessed in the design of the province's respective JPCP road class as no document regarding local calibration of the JPCP transfer functions in the PMED was published at the time of writing.

There are limitations to the simulations using the PMED program as some of the secondary damages caused by flood and inundation cannot be evaluated using this program. Secondary damages as inferred in this study refers to the creation of sinkholes, road cuts, washouts, road collapse propagated by the impact of flood velocity and flood debris during a flood event. Other limitation is its inability to explore the influence of flood contaminants on pavement material integrity. Flood hazards could potentially deposit chemical contaminants on the surface of the pavement which may result in short term aging or rapid deterioration. For instance, the inundation and flooding of fertilized soils could lead to the deposition of ammonium sulfate and nitrates on concrete pavement surface leading to severe scaling and disintegration of the rigid pavement surface. With regards to representing floods events, the Pavement ME can only harness flood depth and flood duration parameters in its simulation and prediction of pavement performance.

4.4 JPCP Performance Indicators

The PMED program can provide insight into the structural and functional performance of JPCP. Performance indicators such as faulting, spalling, and transverse slab cracking could depict the pavement’s structural performance while the International Roughness Index (IRI) represents the functional performance of the road in terms of predicted roughness or smoothness through

regression analysis of faulting, cracking, spalling, and site factor. PMED distress prediction models and transfer functions are used to estimate mean values of performance indicators over the pavement design life and at specified reliability levels.

4.5 JPCP Performance Results

Based on the flexibility of having to visualize the influence of design inputs on pavement performance trends over pavement design life, the impact of flood hazards on the pavement deterioration was evaluated. Possible extreme precipitation events under climate change scenario were modelled and relative impact on pavement performance assessed. Relative change in performance between the no-flood and flood scenario under RCP 4.5 is then calculated and regarded as the percentage flood damage. As IRI is a function of joint faulting and slab cracking along with climate (frost) and subgrade factors (AASHTO 2008) it could give a holistic look into the overall performance of the pavement. Therefore, IRI was the main performance parameter used to estimate flood damage. However, consideration was given to faulting performance in the Ontario study. This is because JPCP faulting performance had a proportional relationship to IRI in the study. Whereas, in the Manitoba case study, damage was only noted under the IRI performance of all pavement classes considered.

4.6 Case Studies

4.6.1 Case Study of JPCP Design in Ontario

Typical arterial and collector JPCP road designs and PMED inputs common to Ontario were obtained from the Ontario Pavement Structural Design Matrix for Municipal Roadways document prepared by Applied Research Associates (ARA 2011a, ARA 2011b). Figure 4-1 shows the cross-section of the pavement road types and Table 4-2 shows the JPCP design inputs. To avoid overloading or under-loading of the pavement structure and accurately represent traffic information in the M-E design simulation, a commercial vehicle distribution or Truck Traffic distribution was included to properly define traffic orientation for the respective pavement road types. Truck traffic Classification of Class 4 to Class 13 trucks as described in the provincial

PMED document was used to define traffic conditions for the typical Ontario collector and arterial pavement structures.

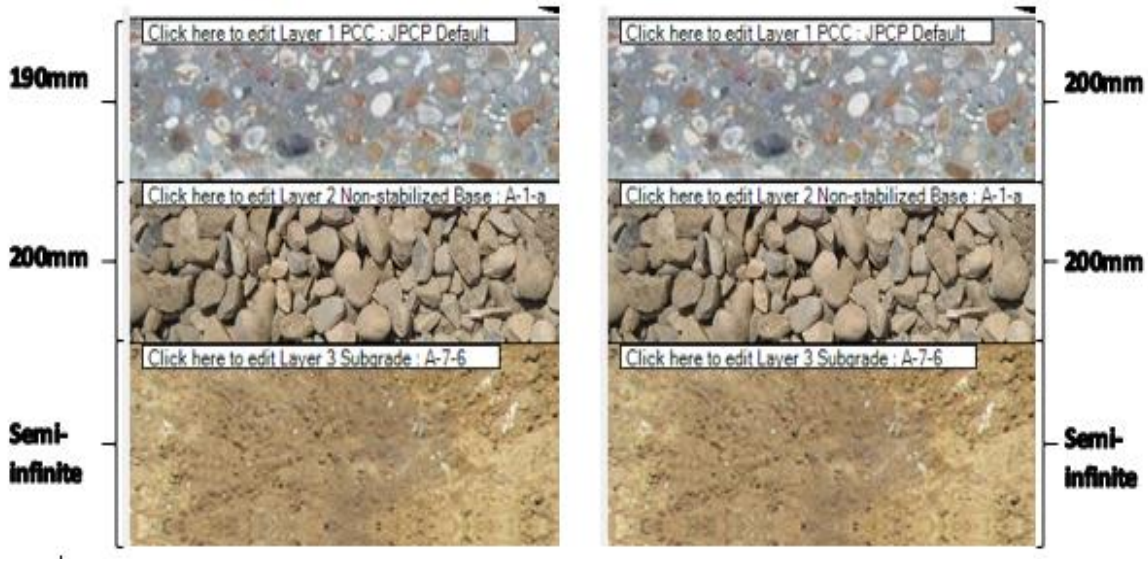

a) Collector (non-dowelled) b) Arterial (dowelled)

Figure 4-1 Pavement Structure for a Collector and Arterial Typical Ontario Pavement

Table 4-2 Ontario PMED Typical Design Inputs.

	Design Parameters	Collector	Arterial
Traffic inputs	Two-way AADTT	500	5000
	Truck traffic in design lane	100%	90%
	No. of lanes in design direction	1	2
	% of trucks in design direction	50%	50%
	Reliability	75%	90%
Concrete slab properties	Dowel diameter(mm)	**No Dowel**	**Dowelled** (32mm)
	Slab length	4.0m	4.5m
	Tied shoulder/curb	Tied	Tied
	Load transfer efficiency	70%	70%

Performance trigger values	International Roughness Index (IRI)	2.70m/km	2.70m/km
	Mean joint faulting	3.00mm	3.00mm
	JPCP transverse cracking	20%	10%
	Design life	25years	25years

Future extreme precipitation for 50-year and 100-year flood from one to three cycles under RCP 4.5 scenario was then modelled and performance results evaluated for comparison with pavement performance under the historical or no-flood scenario. The relative IRI damage in every month of the pavement life is estimated and plotted against pavement age for each return flood period and flood event cycles. Mean and standard deviation values of monthly IRI damage was calculated to estimate the minimum, mean, and maximum damage ratio at return flood period and event cycles. Estimation of the loss of pavement service life was also conducted based on the damage results. Equations 4-1 to 4-10 were used for the analysis.

$$\delta_{ave}\ (\%)\ =\ \frac{\sum_{i=0}^{m}\left(\frac{IRI_{fi}\ -\ IRI_{nfi}}{IRI_{nfi}}*100\%\right)}{m} \quad 4\text{-}1$$

$$\sigma_d\ (\%) = \sqrt{\frac{\sum_{i=0}^{m}((\frac{IRI_{fi}\ -\ IRI_{nfi}}{IRI_{nfi}}*100\%)-\ \delta_{avg}))^2}{m}} \quad 4\text{-}2$$

$$LS_{ave}\ (days) =\ 365 * n * \left[\left(\frac{\delta_{ave}}{100}\right)\right] \quad 4\text{-}3$$

$$\Delta_{LS}\ (\text{days}) = 365 * n * \left[\left(\frac{\sigma_d}{100}\right)\right] \quad 4\text{-}4$$

$$\Delta_{fault}\ (\%)\ =\ \frac{\sum_{i=0}^{m}\left(\frac{F_{fi}\ -\ F_{nfi}}{F_{nfi}}*100\%\right)}{m} \quad 4\text{-}5$$

$$\Delta_{Tcrack}\ (\%) = \frac{TC_{ft}\ -\ TC_{nft}}{TC_{nft}} *\ 100\% \quad 4\text{-}6$$

$$\delta_{min}\,(\%) = \ \delta_{ave} - \sigma_d \quad (4\text{-}7)$$

$$\delta_{max}\,(\%) = \ \delta_{ave} + \sigma_d \quad (4\text{-}8)$$

$$LS_{min} = \ LS_{ave} - \Delta_{LS} \quad (4\text{-}9)$$

$$LS_{max} = \ LS_{ave} + \Delta_{LS} \quad (4\text{-}10)$$

Where:

i = month

δ_{ave} = Mean flood damage (%)

δ_{min} = Minimum flood damage (%)

δ_{max} = Maximum flood damage (%)

m = Pavement design life in months

n = Pavement design life in years

IRI_{fi} = International Roughness Index of JPCP for Month i under flood conditions (m/km)

IRI_{nfi} = International Roughness Index of JPCP for Month i under no-flood conditions (m/km)

σ_d = Standard Deviation of flood damage (%)

Δ_{fault} = Mean change in faulting (%)

F_{fi} = Faulting for Month i under flood conditions (mm)

F_{nfi} = Faulting for Month i under no-flood conditions (mm)

TC_{ft} = Terminal Transverse cracking under flood conditions (%)

TC_{nft} = Terminal Transverse cracking under no-flood conditions (%)

LS_{ave} = Mean Loss of pavement service life (days)

LS_{min} = Minimum loss of pavement service life (days)

LS_{max} = Maximum loss of pavement service life (days)

4.6.2 Case Study of JPCP Design in Manitoba

As concrete pavements are more common in Manitoba than in other Canadian provinces, an assessment of flood impact on various configurations of representative JPCP designs typical of the province's pavement practice was conducted. Available provincial PMED inputs as contained in published agency documents was used (Ahammed *et al.* 2013, Oberez *et al.* 2015). Following this, a matrix of road design classes were developed based on these documents using slab thickness, subgrade and traffic information as design parameters. Each of the three parameters was further divided into three groups as shown in the Table 4-3 to Table 4-5. Figure 4-2 shows a typical pavement design structure in the province. The PCC slab is underlain with 100mm of Granular A crushed stone (A-1-a) base layer and 200mm of Granular C (A-1-b) sub-base layer which sits on the subgrade and their properties are presented in Table 4-6. (Ahammed et al. 2013).

Table 4-3 Matrix Design Parameter - Slab Thickness

PCC Slab Thickness (ST)	
Type	Thickness (mm)
Thin	225mm
Average	250mm
Thick	275mm

Table 4-4 Matrix Design Parameter - Subgrade

Subgrade			
Type	Subgrade (Mpa)	Moisture Content	AASHTO Soil Class
Weak	35	23.80%	A-7-6
Medium	73.1	13%	A-6
Strong	66.6	8.50%	A-4

Table 4-5 Matrix Design Parameter – Traffic

Traffic		
Type	Two-Way AADTT	Design Lane
Low	500	250
Moderate	1000	500
High	2000	1000

Table 4-6 Base and Sub-base Properties

Base and Sub-base Course	Granular A	Granular C
Thickness	100mm	200mm
OMC	9%	6.40%
Unit Weight (kg/m^3)	2170	2200

Table 4-7 Truck Traffic Classification

Truck Class	250AADTT	500 AADTT	1000 AADTT
Class 4	0%	0%	0%
Class 5	8%	6%	7%
Class 6	10%	7%	8%
Class 7	2%	1.5%	1%
Class 8	6%	3%	6%
Class 9	26%	23%	55%
Class 10	25%	33%	11%
Class 11	4%	1%	1%
Class 12	1%	0.5%	6%
Class 13	18%	25%	5%

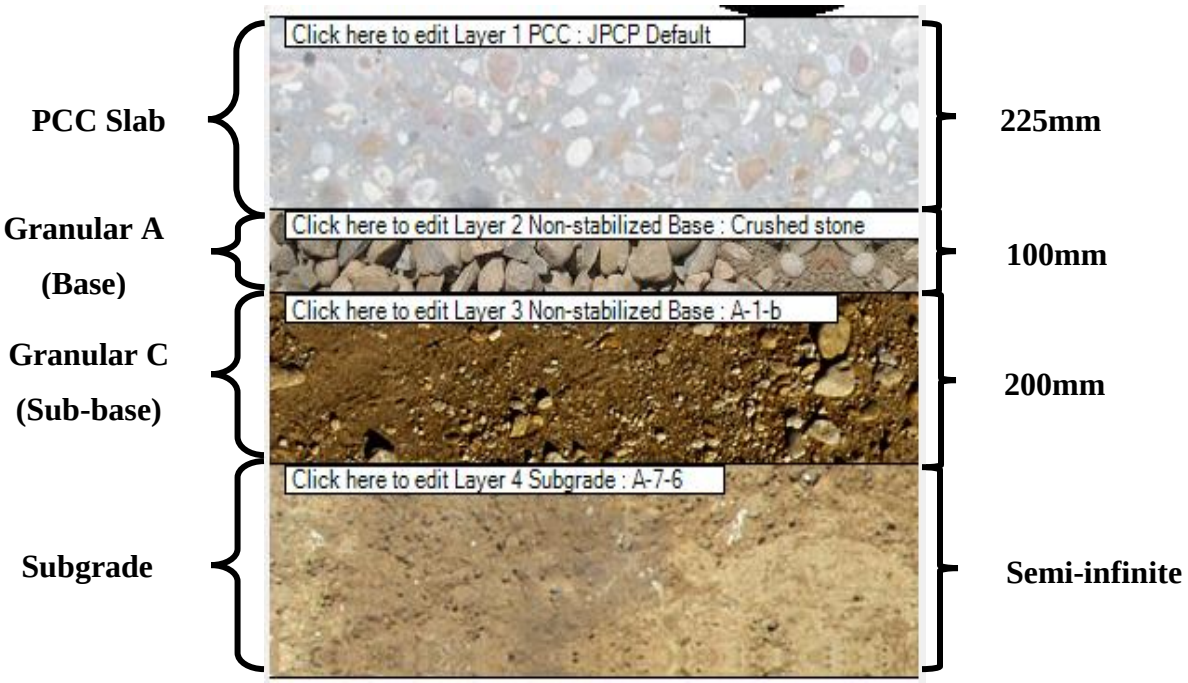

Figure 4-2 Typical Manitoba JPCP Pavement Structure (instance of Class C1)

A more detailed configuration of traffic which includes Truck Traffic Classification (TTC) collected from the Manitoba Highway Traffic Information System (Grande G. et al 2018) was however incorporated in the design, representing a MEPDG level one input traffic category for the three groups of the volume of Average Annual Daily Truck Traffic (AADTT). Truck classifications for MEPDG TTC 9, PTH 2; 5.2 km West of PR 332 (Starbuck), and PTH 75; 1.1 km North of PR 247, were selected for low, moderate and high traffic sub-classes respectively as shown in Table 4-7. Default MEPDG values were employed for hourly and monthly truck distribution and axle per truck configuration. Further, material and soil information such as Maximum Dry Density of soil and optimum moisture content of base and subbase layers were also incorporated to represent local conditions in the province. (Oberez et al. 2015). Subgrade soil groups were representative of soil deposits in the province, sandy silt (A-4) in central & southern Manitoba, sandy clay (A-6) in western Manitoba, and high plastic clay (A-7-6) in Red River Valley (Soliman & Shalaby 2010).

In total, twenty-seven (27) JPCP road classes were developed as shown in Table 4-8. Class C1 to C9 represents nine (9) different combinations of subgrade and slab thicknesses groups under low traffic conditions, Class A1 to A9 represents nine (9) different combinations of subgrade and slab thicknesses groups under moderate traffic conditions, and Class A10 to A18 represents nine (9) different combinations of subgrade and slab thickness groups under high traffic conditions. Extreme precipitation under RCP 4.5 scenario for the Winnipeg location is modelled on the pavement classes with flood event assumed to occur in the month of May for a duration of seven (7) days.

Table 4-8 Matrix of JPCP road classes

Classes	Traffic Volume (AADTT)	Slab Thickness (ST)	Subgrade
C1	Low	Thin	Weak
C2	Low	Thin	Average
C3	Low	Thin	Strong
C4	Low	Medium	Weak
C5	Low	Medium	Average
C6	Low	Medium	Strong
C7	Low	Thick	Weak
C8	Low	Thick	Average
C9	Low	Thick	Strong
A1	Medium	Thin	Weak
A2	Medium	Thin	Average
A3	Medium	Thin	Strong
A4	Medium	Medium	Strong
A5	Medium	Medium	Average
A6	Medium	Medium	Weak
A7	Medium	Thick	Weak
A8	Medium	Thick	Average
A9	Medium	Thick	Strong
A10	High	Thin	Strong
A11	High	Thin	Average
A12	High	Thin	Weak
A13	High	Medium	Weak
A14	High	Medium	Average

A15	High	Medium	Strong
A16	High	Thick	Weak
A17	High	Thick	Average
A18	High	Thick	Strong

4.7 Discussion

4.7.1 Flood Impact on Ontario JPCP Designs for Ontario

In the Ontario collector pavement study, the highest damage was induced at the first cycle of flood event with an estimated mean damage of 2.52%. An increase in flood cycle of 50-year return period only resulted in 0.1% additional damage, augmenting the initial damage to 2.62% from 2.52%. At the third event cycle, mean damage increased from 2.62% to 2.71% by 0.09% which indicative of third event cycle having an approximate damaging impact as a second event cycle ($0.1\% \approx 0.09\%$) under RCP 4.5 50-year flood scenario.

After increasing the return flood period from 50-year to a 100-year flood event, the same values of mean damage were observed as a 50-year return period for the first and second event cycle of 100-year flood. The first and second event cycle of 50-year and 100-year return period both had a magnitude of 2.52% and 2.62% respectively. One could argue JPCP possesses the resilience capacity to withstand higher return periods without sustaining additional damage.

However, this could be the case if JPCP is inundated within acceptable limits and possibly under lower event cycles. Reason being the collector JPCP experienced a damage increase that doubled its second event cycle damage, increasing from 2.62% to 5.99% after the third event cycle. This same trend was noted in the relative faulting change, which thus apparently explains the direct relationship between IRI and faulting performance when the pavement is inundated as shown in Table 4-9. The only difference in the magnitude of damage and percentage faulting change between the 50-year and 100-year flood event was the sudden increase in damage at the third cycle of a 100-year event. It should be noted that the pavement is non-dowelled and this might have contributed to the observed changes.

Table 4-9 Flood Damage (%), Loss of Pavement Service Life (days), and Relative Faulting Change (%) of JPCP Collector Pavement at Respective Return Periods and Event Cycles under RCP 4.5 Scenario

Flood Scenarios	δ_{ave} (σ_d)	LS_{ave} (Δ_{LS})	Δ_{fault}
50-year 1-cycle	2.52(±0.55)%	230(±50) days	10.92%
50-year 2-cycle	2.62(±0.57)%	239(±52) days	11.23%
50-year 3-cycle	2.71(±0.59)%	248(±54) days	11.50%
100-year 1-cycle	2.52(±0.55)%	230(±50) days	10.92%
100-year 2-cycle	2.62(±0.57)%	239 (±52) days	11.23%
100-year 3-cycle	5.99(±1.65)%	546 (±151) days	29.44%

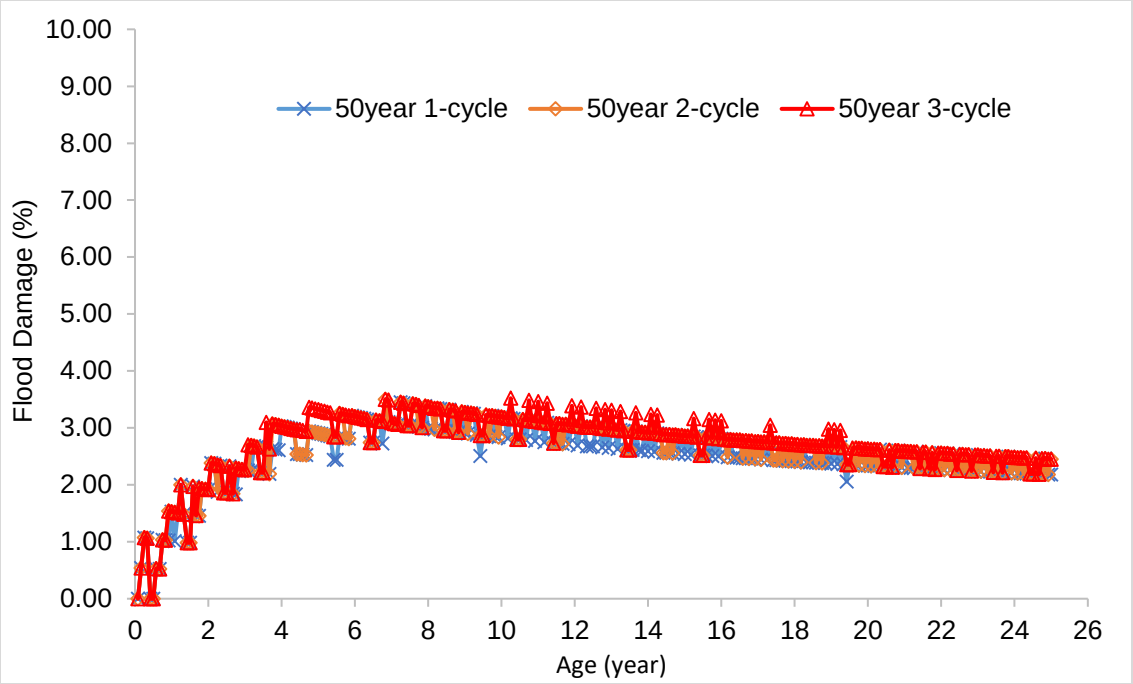

Figure 4-3 Flood Damage Progression in Collector Pavement at 50-year Return Period and Event Cycles under RCP 4.5

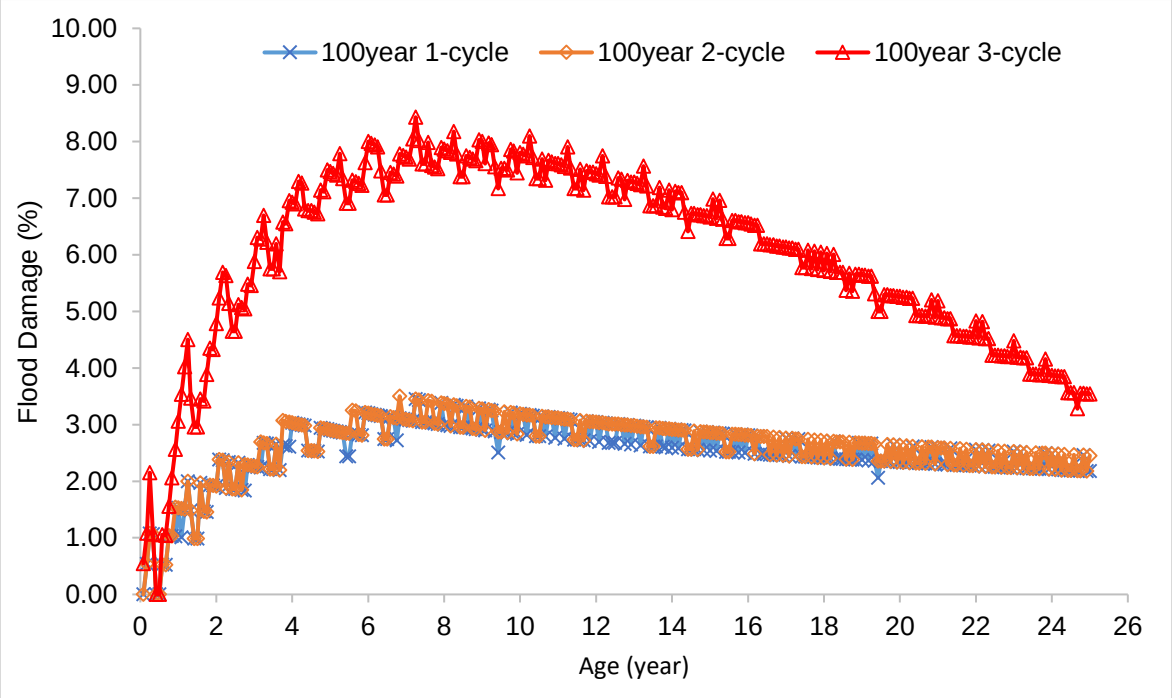

Figure 4-4 Flood Damage Progression in Collector Pavement at 100-year Return Period and Event Cycles under RCP 4.5

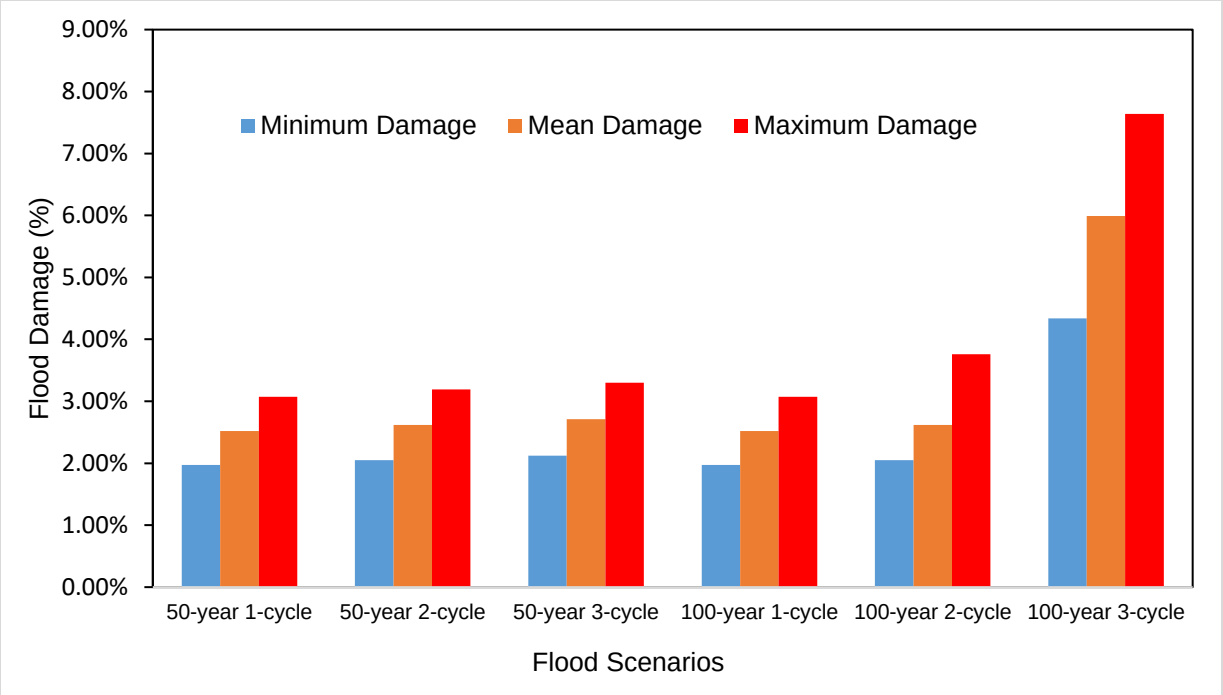

Figure 4-5 Minimum, Mean and Maximum Flood Damage for Collector Pavement at Return Periods and Event Cycles under RCP 4.5

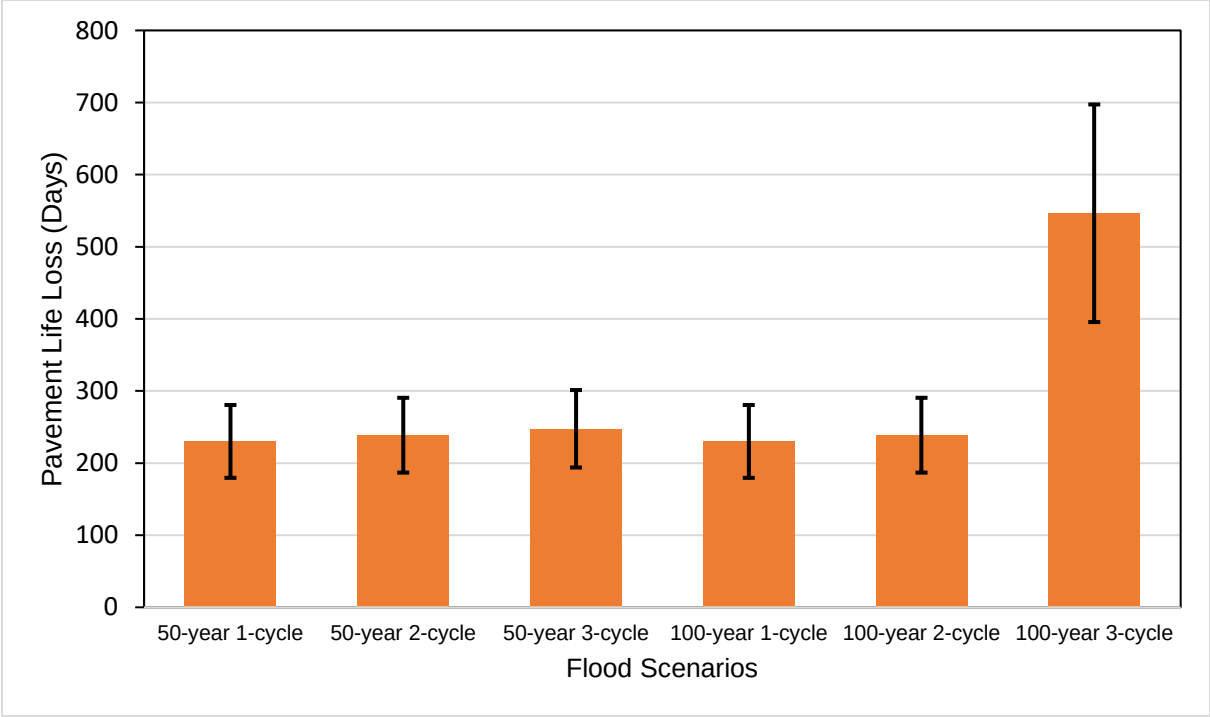

Figure 4-6 Loss of Pavement Service life in Collector pavement for Return Periods and Event Cycles under RCP 4.5

Loss of service life was further estimated with respect to the damage induced by 50-year and 100-year flood cycles. Loss of collector service life peaked after the third cycle of a 100-year flood, reducing pavement life by 546 days. A minimum loss of 230 days was recorded on average after one cycle of 50-year and 100-year event. As shown in Figure 4-6, the same service life loss was observed after the first and second cycle of 50-year and 100-year flood events.

In arterial pavements, estimated damage increased from one to three event cycles but was of lesser magnitude compared to collector pavement flood damage. IRI damage or relative IRI change was noted to have increased from a 50-year to 100-year return period for the first and second flood event cycles shown in Table 4-10. However, after three cycles of flood event, comparative damage induced by a 50-year flood was a little higher than that induced by a 100-year flood and the same trend was observed in the faulting change. This happened as a result of a positive change in the transverse cracking pavement performance between the second and third event cycle 100-year scenario under heavy traffic arterial road. Cracking change is shown in Table 4-10.

Table 4-10 Flood Damage (%), Loss of Pavement Service Life (days), Relative Faulting Change (%) and Relative Cracking Change (%) of JPCP Arterial Pavement at RCP 4.5 Flood Scenarios

Scenarios	δ_{ave} (σ_d)	LS_{ave} (Δ_{LS})	Δ_{fault}	Δ_{Tcrack}
50-year 1-cycle	1.06(±0.3)%	96(±27)	6.20(±0.73)%	-2.44%
50-year 2-cycle	1.33(±0.38)%	122(±35)	5.60(±0.69)%	-3.25%
50-year 3-cycle	2.39(±0.73)%	218(±66)	8.30(±1.00)%	-0.63%
100-year 1-cycle	1.50(±0.49)%	137(±44)	4.90(±0.57)%	-9.39%
100-year 2-cycle	1.78(±0.60)%	162(±55)	5.20(±0.54)%	-3.07%
100-year 3-cycle	2.00(±0.72)%	182(±66)	5.10(±0.55)%	5.33%

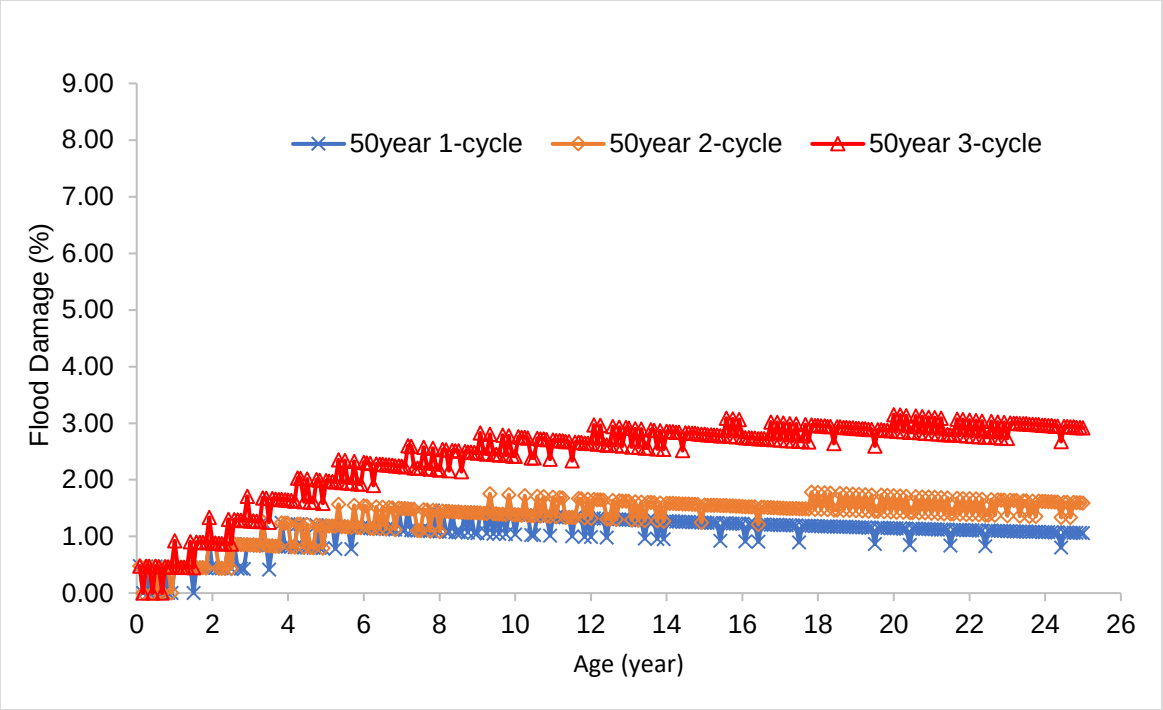

Figure 4-7 Flood Damage Progression in Arterial Pavement at 50-year Return Period and Event Cycles under RCP 4.5

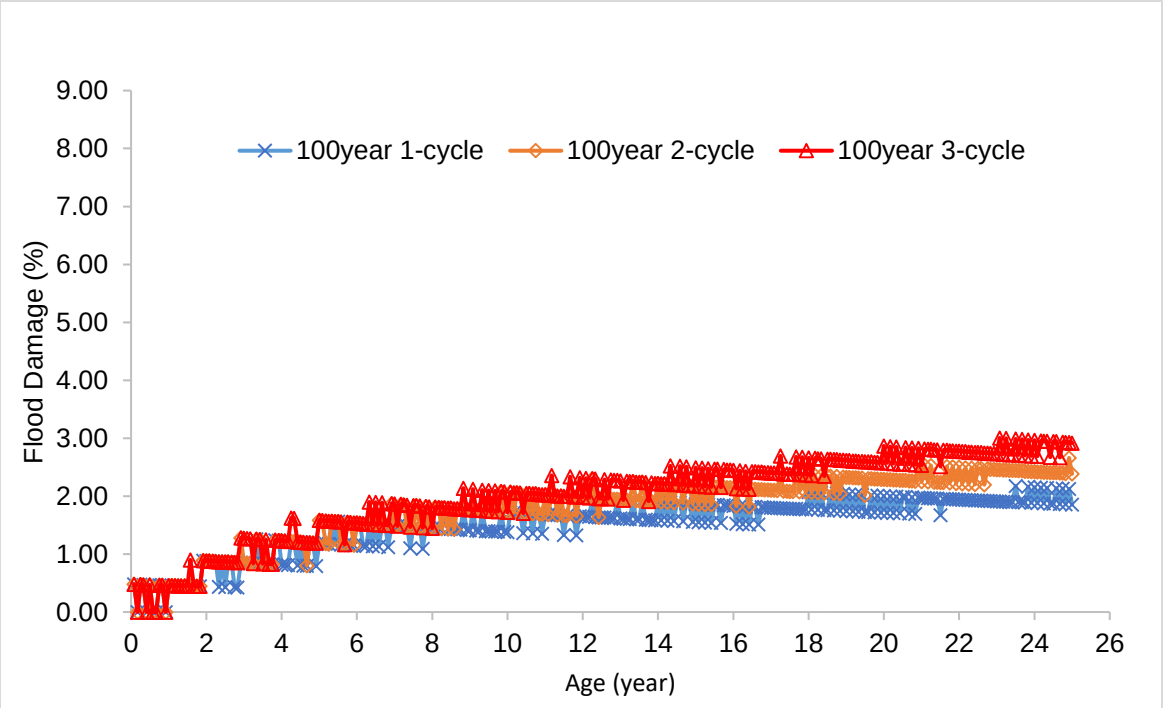

Figure 4-8 Flood Damage Progression in Arterial Pavement at 100-year Return Period and Event Cycles under RCP 4.5

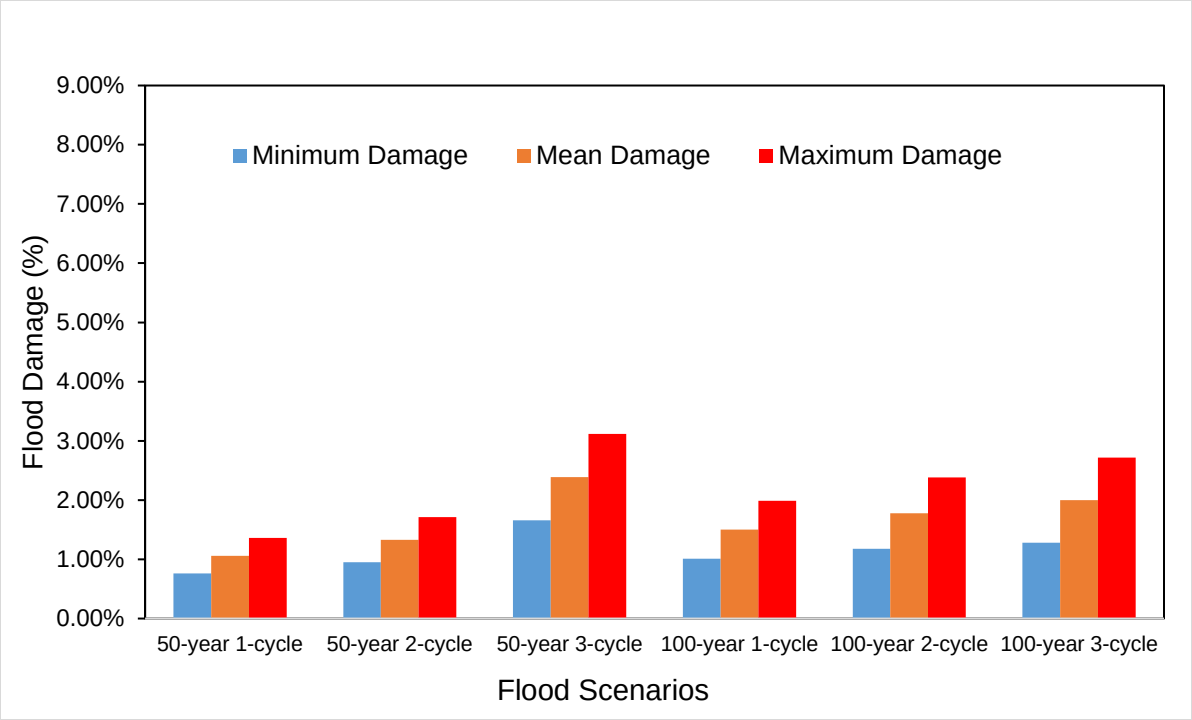

Figure 4-9 Minimum, Mean and Maximum Flood Damage for Arterial Pavement at Return Periods and Event Cycles under RCP 4.5

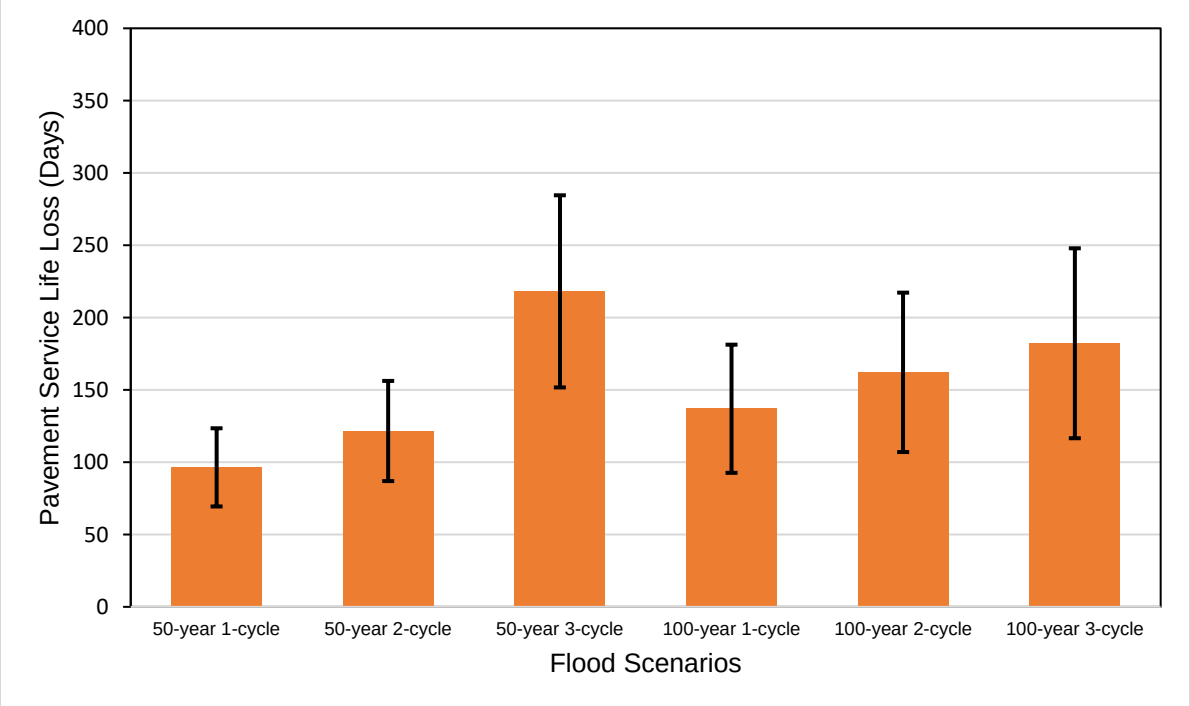

Figure 4-10 Loss of Pavement Service Life in Arterial Pavement for Return Periods and Event Cycles under RCP 4.5

4.7.2 Flood Impact on Manitoba JPCP Classes – Resilience, Cost Implications and Service Life

4.7.2.1 Impact under Low Traffic Conditions

The pavement classes were grouped by of traffic volume - low, moderate and high. Each level of traffic had a total of nine (9) pavement class. Class C1 -C9 represents various combinations of thickness and subgrade under the low traffic and results of extreme precipitation under RCP 4.5 on these pavement classes is shown in Figure 4-11.

From Figure 4-11 and Figure 4-12, flood damage had a minimal influence of pavement Classes C2 and C3 and maximum impact on Class C7. In terms of service life, Class C9 possessed better service life than all other pavement class but sustained an approximate average damage. However, Class C9 comprises of a 275mm thick slab and a strong subgrade and would be considered an overdesign which is not economically feasible for a low level of traffic, 500 AADTT. Low traffic should realistically be provided with a lower slab thickness. Therefore, thin to medium slab thicknesses (Classes C1-C6) and intensity of damage should be considered for recommendation of pavement design classes of less damage, better service life, and better cost feasibility. Considering these three constraints, Classes C2 and C3 would be preferred depending on the existing subgrade material.

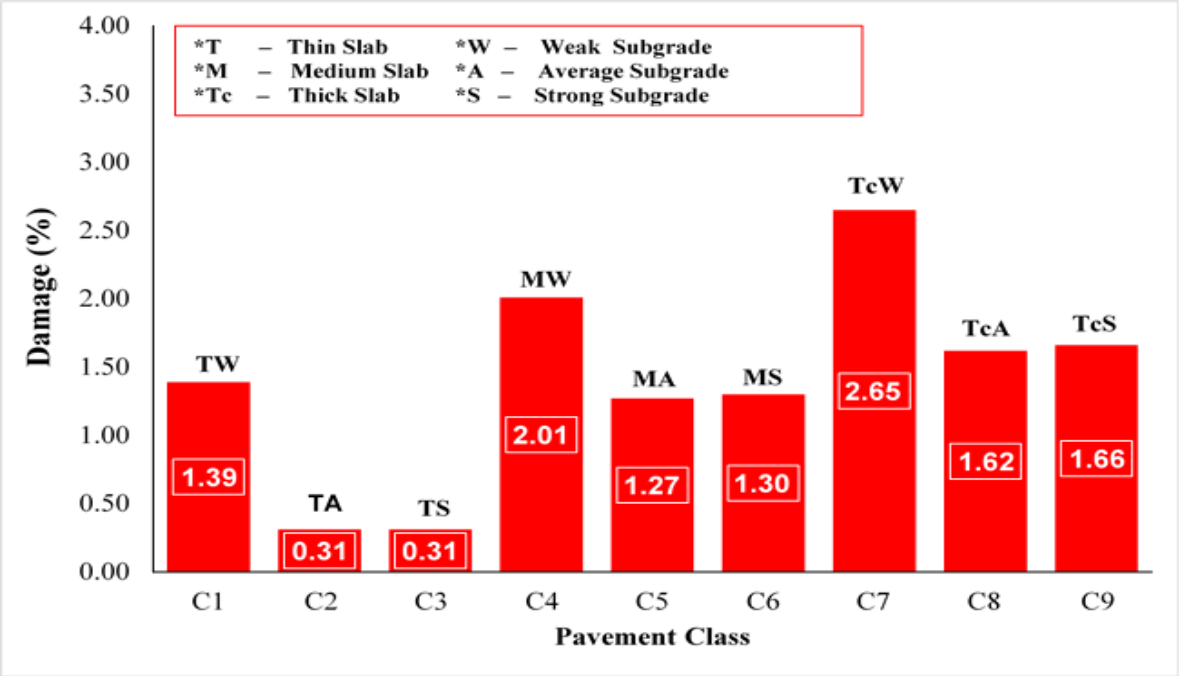

Figure 4-11 Flood Damage (%) of Pavement Classes (C1 - C9) under Low Traffic Condition

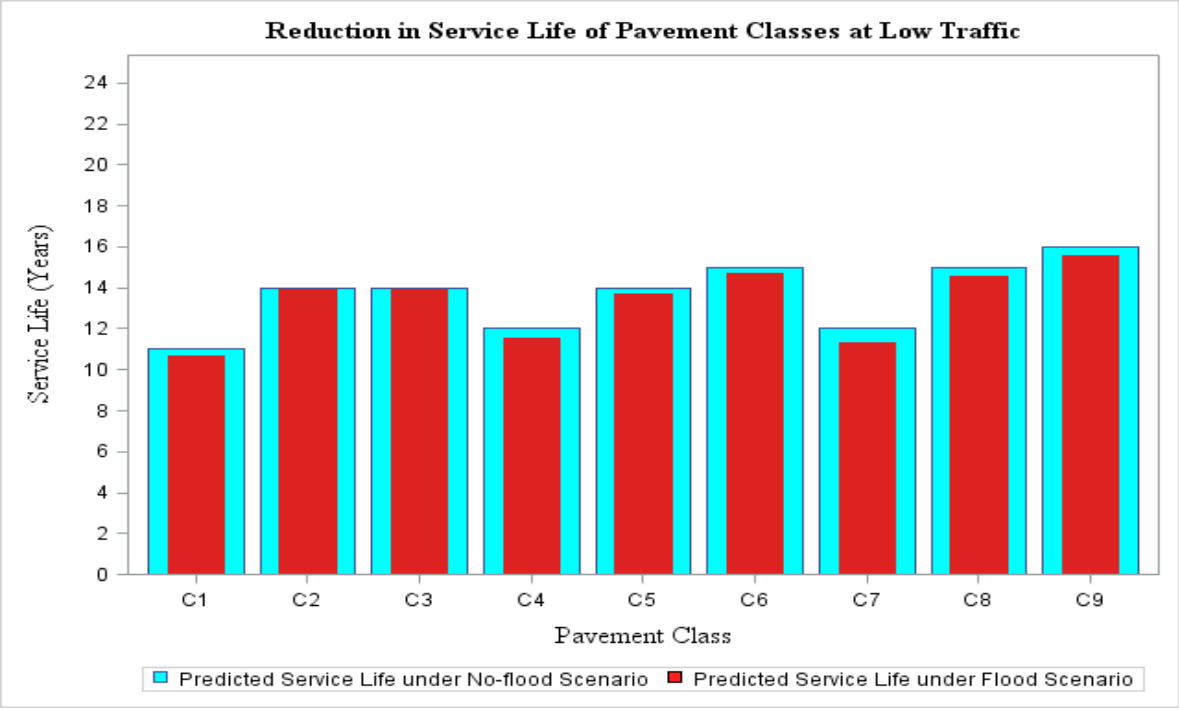

Figure 4-12 Estimated Service Life of Pavement Classes (C1 - C9) under Low Traffic Condition

4.7.2.2 Impact under Moderate Traffic Conditions

For pavement classes under moderate traffic and weak subgrade conditions, increases in slab thickness did not contribute to the predicted service life both before and after flood event as observed in Classes A1, A6 and A7 and shown in Figure 4-13 and Figure 4-14. The performance of a thin pavement was commensurate to that of medium and thick pavement owing to the existing soil condition and magnitude of flood damage similar across classes. Classes A1, A6 and A7 had estimated flood damage of 3.02%, 3.03% and 3.03% respectively. Class A1 would be considered a more economically viable option for locations of under this soil condition and traffic group.

Classes A2, A5 and A8 represent pavements with average subgrade, moderate traffic conditions, and varied slab thicknesses. Percentage of flood damage in Class A5 and A8 had a magnitude of 2.69%, less than A2 of 3.02% damage. Initially, the predicted service life of these classes before flood impact was the same. However, after the 100-year event, A5 and A8 had better service life compared to A2. Therefore, considerations would be given to A5 and A8 based on its service life. In terms of economic feasibility, Class A5 has more leverage as its slab is of a medium thickness. This 250mm slab thickness is also typically preferred for moderate traffic volume in Manitoba.

Classes A3, A4 and A9 represent pavements with strong subgrade, moderate traffic, and varied slab thicknesses. Estimated damage for Classes A3, A4 and A9 are 2.73%, 2.74% and 3.74% respectively. Class A3 had a better service life compared to other road classes even after flood event. Classes A3, A4 and A9 had the same predicted service life before flood impact but after flood impact, Classes A3 and A4 outperformed Class A9 in terms of service life. The reduced cost of having a thin pavement perform better than a medium or thick pavement is a viable option as this holistically reduce the cost implications.

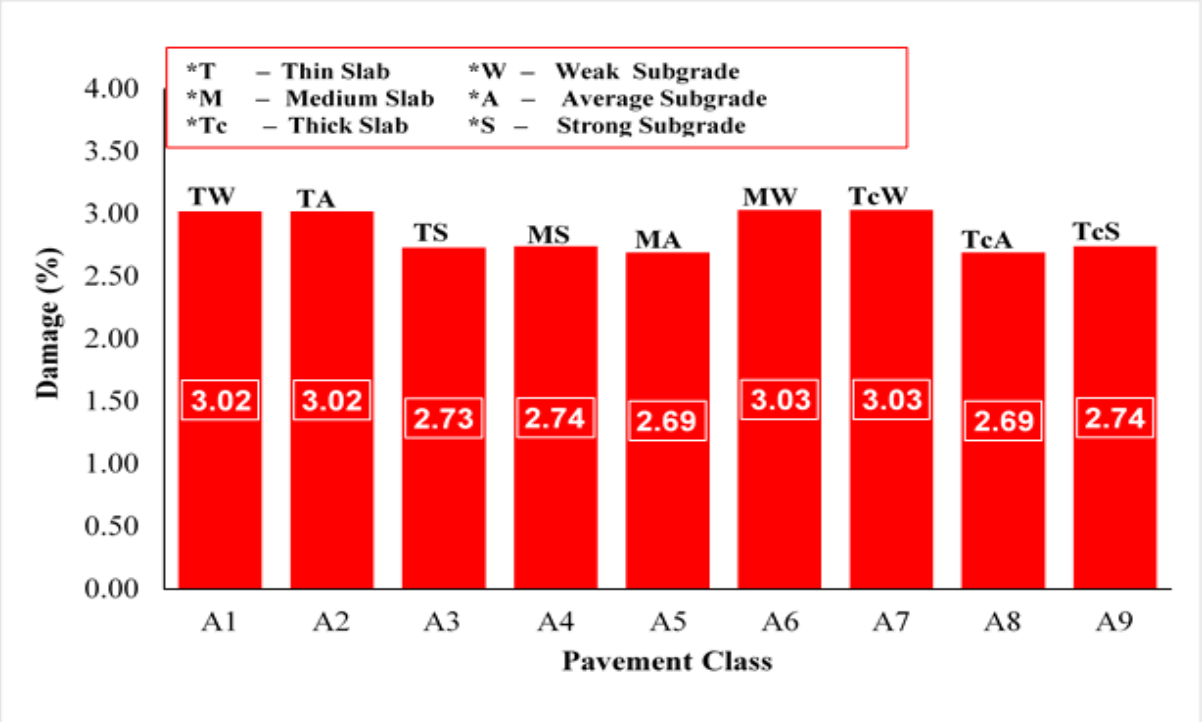

Figure 4-13 Flood Damage (%) of Pavement Classes (A1 - A9) under Moderate Traffic Conditions

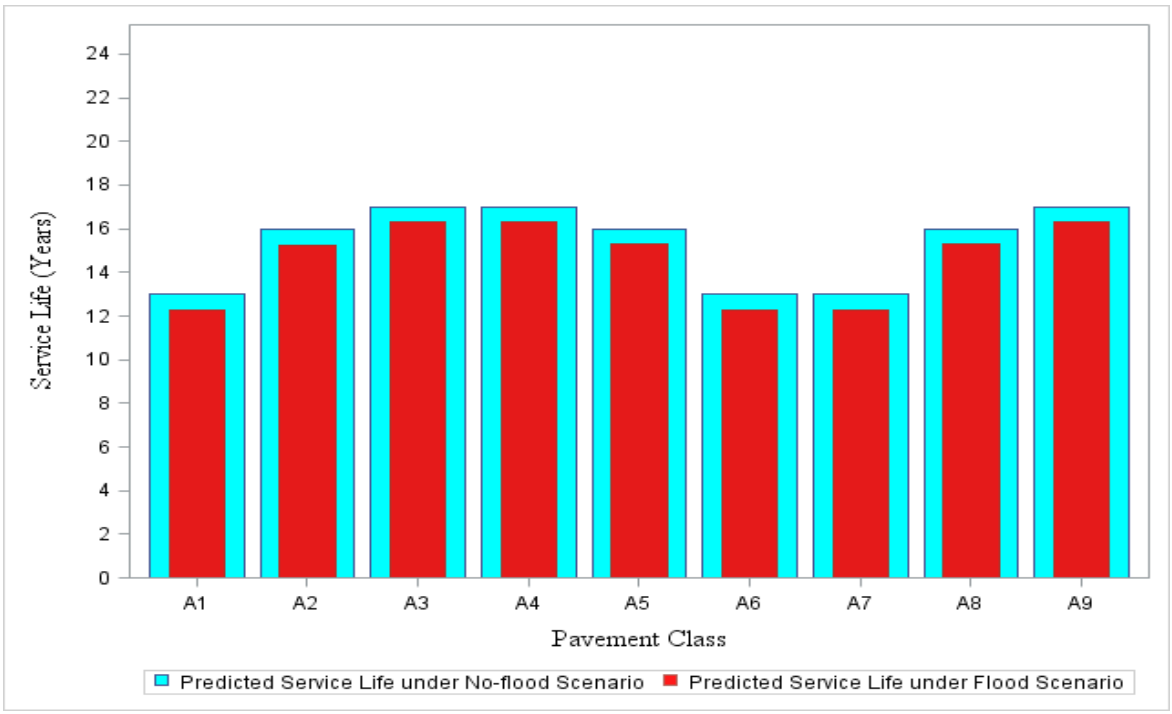

Figure 4-14 Estimated Service Life of Pavement Classes (A1-A9) under Moderate Traffic Conditions

4.7.2.3 Impact under High Traffic Condition

Classes A12, A13 and A16 represent pavement of low subgrade and high traffic condition having thin, medium and thick slab thicknesses respectively. Class A16 experienced the lowest damage magnitude, having a value of 0.31% compared to Classes A12 and A13 which had flood damage of 3.00% and 3.02% as shown in Figure 4-15. Class A16 has a thick slab thickness while Classes A12 and A13 have thin and medium slab thickness respectively. Figure 4-16 shows that the three pavement classes had the same predicted performance before the influence of flood. However, after flood impact, the pavement reduction in service life was more pronounced in the Class A12 and A13 compared to A16. Class A16 shows more sustainability and resilience to both high traffic conditions and flood-induced damage. Generally, pavement with thick slabs such as we have in A16 is often required under high traffic loading conditions, especially when the subgrade is made up of weak soils. Supposing a road agency decides to use Class A13 and A12 based on their equivalent performance and lower cost implication under historical climate conditions, the performance of these pavement classes could significantly reduce if relatively compared to Class A16 performance in the wake of a major flood event.

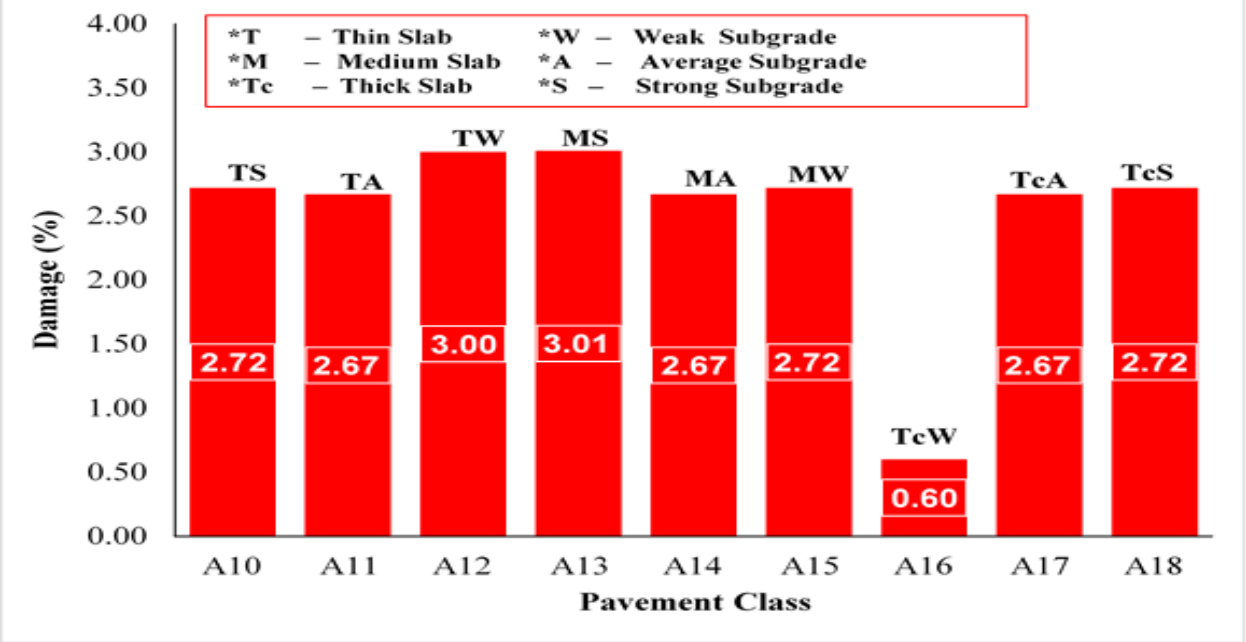

Figure 4-15 Flood Damage (%) of Pavement Classes (A10 - A18) under High Traffic Conditions

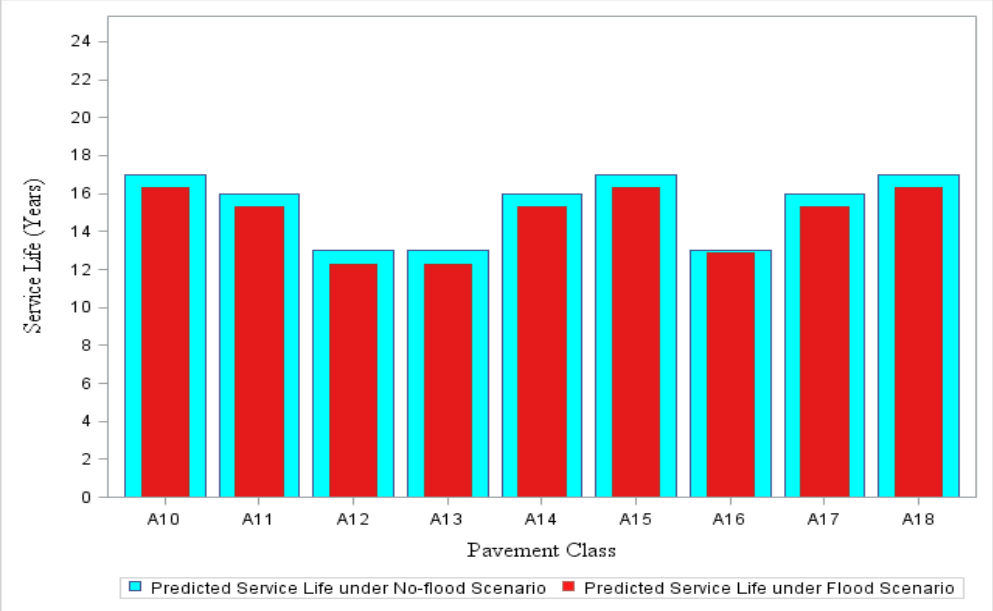

Figure 4-16 Estimated Service Life of Pavement Classes (A10-A18) under High Traffic Conditions

Class A11, Class A14 and Class A17 represent pavements with average subgrade and high traffic volume with respective slab thicknesses. These classes all had the same damage ratio (2.67%) irrespective of slab thickness and the same predicted service life before and after extreme precipitation or flood hazard as shown in Figure 4-15 and Figure 4-16. This relatively implies that cost and performance under extreme climate events could be optimized in Manitoba when the underlying soil is an average subgrade as indexed in this study.

Classes A10, A15 and A18 represent pavements with strong subgrade, high traffic volume and varied slab thicknesses. The same damage magnitude was observed across the three classes (2.72%). This further reinstates the ability of the subgrade soil to contribute to pavement overall performance both under flood or no-flood conditions. A good subgrade could invariably optimize the performance, service life and cost of the pavement structure as it allows more flexibility in selecting JPCP slab thicknesses both under flood and no-flood scenarios.

4.8 Conclusion

In this study, an investigation of flood impact on rigid pavements in Canada was conducted. To understand the impact of flooding on rigid pavements in the Canadian climate, typical JPCP

pavement designs common to the provinces of Ontario and Manitoba were chosen as case studies. The performance of JPCP concrete pavement was assessed under no-flood and flood conditions using the AASHTOWare Pavement ME Design (PMED) build 2.5.3 program. Extreme precipitation values of predicted Intensity Duration Frequency (IDF) obtained under RCP 4.5 climate change scenarios were used to modify the PMED climate file to evaluate performance under flood condition, while historical climate data estimated performance for no-flood conditions.

In the Ontario study, damage induced by locally predicted 50-years and 100-years flood under climate change is evaluated on typical arterial and collector pavement types common to the province. Results indicate a slight reduction in pavement performance across pavement types and percentage damage was estimated using the International Roughness Index (IRI) prediction values. There was also an increase in flood damage as flood event cycles increased. The damage was however more pronounced in collector pavements as they were non-dowelled compared to arterial pavements which are dowelled. The major distress indicator which contributed to damage was faulting being that it increased across event cycles irrespective of return periods. In this study, mean damage peaked at 5.99% and 2.39% for the typical collector and arterial pavement respectively.

In the Manitoba study, a matrix of 27 pavement classes was developed based on traffic, subgrade and slab thickness to adequately represent possible pavement classes as the province owns a lot of rigid pavement asset. A 100-year flood or extreme precipitation event is then modelled on each pavement class and damage estimated. Analysis of the response of various pavement classes was conducted to determine the pavement classes which performed well in terms of flood resilience, service life and cost feasibility. The maximum and minimum flood damage observed across the 27 pavement classes is 3.03% and 0.31% respectively. These low damage ratio further reiterates the resilience and adaptive capacity of the JPCP to withstand extreme precipitation. In all of the pavement classes considered in this study, there was no positive change or damage to faulting and fatigue cracking after extreme precipitation events. The IRI parameter was influenced by inundation, therefore indicates that pavement classes may actually be experiencing moisture-

induced warping. In this case, results show IRI increase in the rigid pavement, thus accounted for in the PMED as moisture effects.

Chapter 5
Conclusions and Recommendations for Future Work

5.1 Conclusions

The research presented herein provides a comprehensive study on the resilience of concrete pavement to flood hazards by observing performance changes under flood and no-flood scenarios in terms of performance change properties of JPCP. Based on the pavement performance modelling and existing studies, the performance of representative JPCP designs of varying traffic and structural configuration under various flood scenarios for two Canadian provinces have been investigated. Two manuscripts have been developed to document findings on concrete pavement flood impact and one other manuscript to document the local calibration of the AASHTOWare Pavement ME Design (PMED) JPCP transverse cracking model to Ontario conditions. The local calibration of the PMED program led to an improvement in JPCP performance modelling in the province of Ontario. Conclusions from this research study are the following:

1) In the Ontario case study, an increase in extreme precipitation cycles under RCP 4.5 intensified flood damage on collector (non-dowelled) JPCP to arterial (dowelled) JPCP irrespective of traffic conditions. As a consequence, estimated pavement life loss was greater in non-dowelled to dowelled JPCP pavements. The major distress indicator which contributed to flood damage was faulting, being that it increased across event cycles irrespective of return periods. No flood damage impact was observed on the cracking performance. In this study, mean flood damage peaked at 5.99% and 2.39% for the typical collector and arterial pavement respectively

2) As the Pavement ME JPCP global cracking prediction model was found to underpredict conditions in Ontario, a local calibration of the model was conducted with the support of the Ministry of Transportation (Ontario). Calibration factors derived would be of help in modelling JPCP cracking performance under flood and no-flood conditions in the future.

3) In the Manitoba case study, flood impact had no major impact on pavement performance as the maximum and minimum flood damage observed across the 27 pavement classes developed for the provinces is 3.03% and 0.31%. No damage or change in faulting and cracking performance was observed on all pavement class even with increases in event cycles. The only change in performance parameter was observed in the IRI indicating the possible presence of a permanent moisture-induced warp due to flood impacts.

5.2 Recommendations for Future Work

The AASHTOWare Pavement ME Design program has been used in this thesis to evaluate pavement performance under flood conditions. However, there are some limitations to the use of the program, and opportunities for improvement in the future. Specific recommendations for future research work are the following:

1. The current Enhanced Integrated Climate Model (EICM) in the AASHTOWare Pavement ME uses a surrogate model known as Thornthwaite Moisture Index (TMI) model to estimate the influence of precipitation on equilibrium suction and stiffness properties in pavement underlying layers. The model is a surrogate for the inactive EICM infiltration and drainage model which should simulate precipitation infiltration. Therefore, the enhancement or development of a new infiltration and drainage model which predicts water infiltration from the pavement surface due to precipitation will be resourceful in estimating further, the flood resilience capabilities of concrete pavements under traffic loading. .

2. Apart from using a modelling approach to gain insight into flood impact, field investigations could be conducted in the wake of flood events and data collected to better monitor pavement performance. This will validate pavement performance under flooding, and could be resourceful in developing programs that model high flood velocity, runoffs and flood debris impact on pavement, as the impact of these stressors could be more catastrophic than the ones considered in this study

3. Future work could develop new prediction calibration coefficients under flood conditions once flooded pavement field investigations provides validation of PMED predictions. State DOTs could use the calibration factors to accurately predict pavement flood performance, and develop pavement deterioration curves under flood conditions. This may aid the proactive implementation of maintenance and preservation policies geared towards climate change adaptation.

4. Intentions to upgrade from the use of the North America Regional Reanalysis (NARR) to Modern-Era Retrospective Analysis for Research and Applications (MERRA) historical climate data for rigid pavement analysis could as well be expedited by the developers of the AASHTOWare Pavement ME. This achievement could result in a more accurate estimation of climate impact on concrete pavement performance.

5. Although temperature curling in PCC slab has been of major interest to the pavement engineering community, a good understanding of slab moisture-induced warping under repeated inundated conditions need also to be prioritized due to increases in flood events. This will be resourceful in measuring and modelling the extent of JPCP slab's resilience to frequent flood hazards, which may further promote its use as a flood adaptation measure

6. More so, investigative studies on the interaction of moisture gradient, drying and autogenous shrinkage, self-desiccation, shrinkage and concrete water absorption on concrete pavement on short and long term pavement performance is encouraged. This would definitely help to accurately model concrete and water interactions under traffic and extreme flood events conditions.

7. As more data is collected and more JPCP sections constructed, there may arise a need to locally recalibrate the pavement ME prediction models. Calibration is a continuous exercise!

References

AASHTO. (2008). “Mechanistic-Empirical Pavement Design Guide: A Manual of Practice Interim Edition. [Viewed 16 January 2019] https://fenix.tecnico.ulisboa.pt/downloadFile/563568428712666/AASHTO08.pdf

AASHTO. (2010). Guide for the Local Calibration of the Mechanistic-Empirical Pavement Design Guide, American Association of State Highway and Transportation Officials, Washington, D.C.

AASHTOWare Pavement ME Design Climatic Data [online]. AASHTO. Available from: www.me-design.com/MEDesign/ClimaticData.html [Accessed 5 Oct 2018]

ACPA. (2018) “Concrete Pavement Joint Sealing/Filling”. ACPA Technical Bulletin TB010. [Viewed 1 April 2019] http://www.acpa.org/wp-content/uploads/2019/04/Jointing-Sealing-Tech-Bulletin-TB010-2018.pdf

Ahammed, M. A., Kass, S., & Hilderman, S. (2013). Implementing the AASHTOWare Pavement ME Design guide: Manitoba issues and proposed approaches. [Viewed 12 March 2019] https://www.scopus.com/inward/record.uri?eid=2-s2.0-84896642865&partnerID=40&md5=84054c27916c6f4de89b5290a3c3f49e

American Concrete Pavement Association ACPA. (2010). Perviouspave: background, purpose, assumptions and equations [online]. Available from: http://1204075.sites.myregisteredsite.com/perviouspave/About%20PerviousPave.pdf [Accessed 12 June 2018].

Applied Research Associates ARA Inc. (2004a). Guide for mechanistic-empirical design of new and rehabilitated pavement structures. NCRHP Project 1-37A, National Cooperative Highway Research Program Washington, D.C: ERES Consultants Division,

Applied Research Associates ARA Inc. (2015a). Methodology for the development of equivalent pavement structural design matrix for municipal roadways- Ontario [online]. Available from: http://www.rediscoverconcrete.ca/assets/files/Typical-Ontario-Pavement-Designs-Final-Report_012115.pdf [Accessed 12 Sept 2018].

Applied Research Associates ARA Inc. (2015b). Methodology for the development of equivalent pavement structural design matrix for municipal roadways: including maintenance and rehabilitation schedules and life cycle cost analysis. Toronto, Ontario: ARA

Applied Research Associates ARA Inc. (2018). AASTHO Pavement ME Design Build 2.5.0 Release Notes [online]. Available from: http://www.me-design.com/MEDesign/data/AASHTOWare%20Pavement%20ME%20Design%20Build%202.5%20Release%20Notes.pdf [Accessed 20 Sept 2018].

Applied Research Associates ARA Inc., (2004). Guide for Mechanistic-Empirical Design of New and Rehabilitated Pavement Structures. NCRHP Project 1-37A, National Cooperative Highway Research Program Washington, D.C: ERES Consultants Division

Applied Research Associates ARA Inc., (2011a). Methodology for the Development of Equivalent Pavement Structural Design Matrix for Municipal Roadways- Ontario [online]. [Viewed 12 Sept 2018]. http://www.rediscoverconcrete.ca/assets/files/Typical-Ontario-Pavement-Designs-Final-Report_012115.pdf

Applied Research Associates, ARA Inc. (2004b). Transverse joint faulting model. In: ARA. Guide for Mechanistic-Empirical Design of New and Rehabilitated Pavement Structures. Washington, D.C: Appendix JJ.

ARA (2015). Implementation and Local Calibration of the MEPDG Transfer Functions in Wyoming. Wyoming, USA. Final Report, FHWA-WY-16/02F.

Bjørnæs, Christian. (2013). A guide to Representative Concentration Pathways is92 second assessment report 2000 SRES-special report on emissions and scenarios third and four assessment report 2009 RCP-Representative Concentration Pathways Fifth Assessment Report [online]. Max planck institute for meteorology. Available from: https://www.mpimet.mpg.de/fileadmin/communication/Im_Fokus/IPCC_2013/uk_ipcc_A_guide_to_RCPs.pdf [Accessed 15 Sept 2018].

Brown, S.F., M.R. Thompson, and E.J. Barenberg,(2006) Research Results Digest 307, in ResearchResults Digest, National Cooperative Highway Research Program..

Ceylan, H., Gopalakrishnan, K., (2007). Neural Networks Based Models for Mechanistic-Empirical Design of Rubblized Concrete Pavements. Denver, CO. New Peaks in Geotechnics.

Chen, X. and Zhang, Z. (2014). Effects of hurricanes Katrina and Rita flooding on Louisiana pavement performance. pavement materials, structures and performances. In: Geo-Shanghai 2014 Conference, 26-28 May, 2014 Shanghai, China: ASCE, 212-221.

Clean Air Partnership, CAP, (2006). A Scan of Climate Change Impacts on Toronto [online]. Available from: http://www.cleanairpartnership.org/pdf/climate_change_scan.pdf [Accessed 16 Sept 2018].

Daniel, J. S., et al., (2014). Impact of climate change on pavement performance: preliminary lessons learned through the infrastructure and climate network (ICNet). In: International Symposium of Climatic Effects on Pavement and Geotechnical Infrastructure 2013, 4-7 August 2013 Fairbanks, Alaska. ASCE

Environment Canada, (2014a). Canada's top ten weather stories of 2013 [online]. Available from: http://www.ec.gc.ca/meteo-weather/default.asp?lang=En&n=5BA5EAFC-1&offset=3&toc=show. [Accessed 10 Sept 2018].

FHWA TECHBRIEF. (2015). Curl and warp analysis of the LTPP SPS-2 site in Arizona [online]. Available from: http://www.cproadmap.org/publications/MAPbriefApril2015.pdf [Accessed 15 Sept 2018].

Gaspard, K., et al., (2006). Impact of Hurricane Katrina on Roadways in the New Orleans Area." Technical Assistance Rep. No. 07-2TA [online], Louisiana Dept. of Transportation and Development, Hammond, LA. [Viewed 2 December 2018] https://www.ltrc.lsu.edu/pdf/2007/07_2ta.pdf

Gaur, A., Gaur, A., and Simonovic, S. P. (2018). "Future Changes in Flood Hazards across Canada under a Changing Climate". Water (Switzerland), 10(10) [online]. [Viewed 2 March 2018] https://doi.org/10.3390/w10101441

Grande G. et al (2018). Traffic on Manitoba Highways, University of Manitoba Transport Information Group, University of Manitoba. [Viewed 2 Feb 2018] http://umtig.eng.umanitoba.ca/reports/2017 MHTIS Traffic Report.pdf

Gudipudi, P. P., et al., (2017). Impact of climate change on pavement structural performance in the United States. Transportation Research Part D: Transport and Environment [online], 57 (172-184). Available from: https://doi.org/10.1016/j.trd.2017.09.022 [Accessed 18 Aug 2018].

Haider W. H., Brink W. C., and Buch N. (2017) Local calibration of rigid pavement performance models using resampling methods, International Journal of Pavement Engineering, 18:7, 645-657, DOI: 10.1080/10298436.2015.1121777

IPCC, 2013. Climate Change 2013: The physical science basis working group i contribution to the fifth assessment report of the Intergovernmental Panel on Climate Change (IPCC) summary for policymakers [online], Available from: http://www.climatechange2013.org [Accessed 2 Sept 2018].

Karamihas, S. M. and K. Senn. (2012). Curl and warp analysis of the LTPP SPS-2 site in Arizona. McLean, VA: Turner-fairbank highway research center, Federal Highway Administration., FHWA-HRT-12-068. Available from: https://www.fhwa.dot.gov/publications/research/infrastructure/pavements/ltpp/12068/12068.pdf [Accessed 20 Sept 2018].

Kaya, O, (2015).Investigation of AASHTOWare Pavement ME Design/Darwin-ME Performance Prediction Models for Iowa Pavement Analysis and Design. Iowa State University.

Khan, M. U., et al., (2014). Development of road deterioration models incorporating flooding for optimum maintenance and rehabilitation strategies. Road and Transport Research, 23 (1), 3–24.

Khan, M. U., et al., (2017). A case study on pavement performance due to extreme moisture intrusion at untreated layers. International Journal of Pavement Engineering [online],

Available from: https://doi.org/10.1080/10298436.2017.1408272 [Accessed 15 Oct 2018].

Khan, M. U., et al., (2017). Estimating pavement's flood resilience. Journal of Transportation Engineering, Part B: Pavements [online], 143(1), 1–8. Available from: https://doi.org/10.1061/JPEODX.0000007 [Accessed 12 May 2018].

Kim, S., Ceylan, H., Ma, D., and Gopalakrishnan, K. (2014)."Calibration of Pavement ME Design and Mechanistic-Empirical Pavement Design Guide Performance Prediction Models for Iowa Pavement Systems," ASCE Journal of Transportation Engineering, Vol. 21, Issue 10.

Lu, D., et al., (2018a). Pavement risk assessment for future extreme precipitation events under climate change. Journal of the Transportation Research Record [online]. Available from: https://doi.org/10.1177/0361198118781657 [Accessed 20 Jul 2018].

Lu, D., et al., (2018b). Impact of flood hazards on pavement performance. International Journal of Pavement Engineering [online]. Available from: https://doi.org/10.1080/10298436.2018.1508844 [Accessed 20 Aug 2018].

Lukefahr E. L. (2018). Continuously Reinforced Concrete Pavement Resiliency – A Case Study. In ACPA 55th Annual Meeting 2018 New Orleans Marriot, United States. Available from: http://www.acpa.org/wp-content/uploads/2018/12/Lukefahr-ACPA-2018-CRCP-Resilience.pdf

Mack J., (2017). Impact of flooding and inundation on the performance of concrete pavements [online]. Available from: https://rns.trb.org/details/dproject.aspx?n=41362 [Accessed 15 Feb 2018].

Mallela, J., Titus-Glover, L., Bhattacharya, B. B., Gotlif, A., and Darter, M. I. (2015). Recalibration of the JPCP Cracking and joint faulting Models in the AASHTO ME Design Procedure. In Transportation Research Board 94th Annual Meeting (No. 15-5222).

Meagher, W., et al., (2012). Method for evaluating implications of climate change for design and performance of flexible pavements. Journal of the Transportation Research Board [online], Available from: https://doi.org/10.3141/2305-12 [Accessed 2 Nov 2018].

Meinshausen, M., et al., (2011). The RCP greenhouse gas concentrations and their extensions from 1765 to 2300: Climatic Change, 109: 213. Available from: https://doi.org/10.1007/s10584-011-0156-z [Accessed 9 Oct 2018].

Mills B., et al., (2007). The road well-traveled: implications of climate change for pavement infrastructure in Southern Canada, report prepared for Government of Canada climate change impacts and adaptation program. Available from: http://www.bv.transports.gouv.qc.ca/mono/0970582.pdf [Accessed 5 Sept 2018]

Ministry of Transportation Ontario, MTO (2019). Ontario's Default Parameters for AASHTOWare Pavement ME Design Interim Report – 2019. Toronto: Ministry of Transportation, Ontario.

NCHRP Project 1-40B, (2009). Local calibration guidance for the recommended guide for mechanistic-empirical pavement design of new and rehabilitated pavement structures. Washington, DC: Final NCHRP Report.

NCHRP. (2003). APPENDIX KK: Transverse Cracking of JPCP, Guide for Mechanistic-Empirical Design of New and Rehabilitated Pavement Structures. National Cooperative Highway Research Program 1-37A. Washington, DC: Transportation Research Board, National Research Council.

NCHRP. (2004). Guide for Mechanistic-Empirical Design of New and Rehabilitated Pavement Structures. National Cooperative Highway Research Program 1-37A. Washington, DC: Transportation Research Board, National Research Council.

NCHRP. (2018). User Review of the AASHTO 'Guide for the Local Calibration of the Mechanistic-Empirical Pavement Design Guide'. National Cooperative Highway Research Program Project 20-07/Task 422 Report, Washington, DC: Transportation Research Board, The National Academies of Sciences, Engineering, and Medicine

Nirupama N., Adhikari I., and Sheybanib A., (2014). Natural hazards in Ontario, Canada: an analysis for resilience building: Procedia Economics and Finance [online]. Available from: https://doi.org/10.1016/S2212-5671(14)00913-7 [Accessed 13 Oct 2018].

Oberez, M. E., Kass, S., Hilderman, S., & Ahammed, M. A., (2015). "Estimating Base Layers and Subgrade Moduli for ME Pavement Design in Manitoba." In National Transportation Association of Canada TAC Conference, 27-30 September 2015 Charlottetown. PEI: Transportation Association of Canada.

Oyediji, O., Lu, D. and Tighe, S., (2019) "Impact of Flooding on Concrete Pavement Performance," in 2019 CSCE Annual Conference, Proceedings of Case Studies in Natural Hazards Risk Assessment of Civil Engineering Systems. CSCE 2019 Laval Annual Conference. Laval, QC, Canada.

Pacific Climate Impacts Consortium (PCIC), 2013. Statistically downscaled climate scenarios, https://pacificclimate.org/data/statistically-downscaled-climate-scenarios [Accessed 5 Apr, 2019].

Pierce, L.M., and McGovern, G., (2014). Implementation of the AASHTO mechanistic-empirical pavement design guide and software. Washington, DC Transportation Research Board.

Powell J., (2018). CRCP roadways proved resilient after hurricane Harvey [online]. Available from: https://goo.gl/hQe1Do [Accessed 7 Nov 2018].

Prowse, T.D., Furgal, C., Chouinard, R., Melling, H., Milburn, D., and Smith, S.L. (2009). "Implications of Climate Change for Economic Development in Northern Canada: Energy, Resource, and Transportation Sectors." A Journal of the Human Environment, v. 38, no. 5, p. 272-281.

Public Safety Canada PSC, (2014). The Canadian disaster database. Ottawa, Canada: Public Safety Canada.

Qiao, Y., (2015). Flexible pavements and climate change: impact of climate change on the performance, maintenance, and life-cycle costs of flexible pavements. Thesis (PHD). University of Nottingham.

Sachs, S., J. Vandenbossche, M. Snyder, (2014) Developing Recalibrated Concrete Pavement Performance Models for the Mechanistic-Empirical Pavement Design Guide, NCHRP Project 20-07, Task 327, Transportation Research Board

Sandink, D., et al. (2010). Making Flood Insurable for Canadian Homeowners: A Discussion Paper. Toronto: Institute for Catastrophic Loss Reduction & Swiss Reinsurance Company Ltd.

Schweikert, A., et al., (2014). Road infrastructure and climate change: impacts and adaptations for South Africa. Journal of Infrastructure Systems [online]. Available from: https://doi.org/10.1061/(ASCE)IS.1943-555X.0000235 [Accessed 5 Nov 2018].

Simonovic, S.P., et al., (2016) A web-based tool for the development of intensity duration frequency curves under changing climate. Journal of Environmental Modelling & Software [online]. Available from: https://doi.org/10.1016/j.envsoft.2016.03.016 [Accessed 18 Oct 2018].

Smith, B., and Nair, H. (2015). Development of Local Calibration Factors and Design Criteria Values for Mechanistic-Empirical Pavement Design. Virginia Center for Transportation Innovation and Research (VCTIR 16-R1)

Soliman, H., and Shalaby, A. (2010). "Sensitivity of Subgrade Resilient Modulus to Moisture Variation." In Proceedings from 2010 Annual Conference of the Transportation Association of Canada. Halifax, Nova Scotia, 1–11.

Tighe, S. L., (2015). Vulnerabilities and design considerations for pavement infrastructure in light of climate change. In: National Transportation Association of Canada TAC Conference, 27-30 September 2015 Charlottetown. PEI: Transportation Association of Canada.

Tighe, S. L., et al., (2008). Evaluating Climate Change Impacts on Low Volume Roads in Southern Canada. In: 7th International Conference on Managing Pavement Assets, June 23-28, 2008 Calgary. Alberta: Transportation Research Board.

Transport Canada (2011). Transportation in Canada 2011: Comprehensive Report; Minister of Public Works and Government Services, Canada. [Viewed 10 March 2019] https://www.tc.gc.ca/eng/policy/report-aca-anre2011-index-3010.htm

Transportation Association of Canada, TAC (2016). Canadian Guide: Default Parameters for AASHTOWare Pavement ME Design (DRAFT). Pavement ME Design User Group.

Transportation Research Board TRB, (2018). Research in Progress: The Impact of Hurricane Harvey on Pavement Structures in the South East Texas and South West Louisiana [online]. Available from: https://rip.trb.org/view/1505460 [Accessed 20 Oct 2018].

van de Lindt, J., Taggart Mason, (2009). Fragility analysis methodology for performance-based analysis of wood-frame buildings for flood. Natural Hazards Review, 10 (3), 113–123.

Warren, F.J. and Lemmen, D.S., (editors) (2014). "Canada in a Changing Climate: Sector Perspectives on Impacts and Adaptation." Government of Canada, Ottawa, ON, 286p.

Yuan, D., and Nazarian, S., (2008). Variation in moduli of base and subgrade with moisture. In: GeoCongress 2008, 9-12 March 2008 Louisiana, United States: ASCE. Available from: https://doi.org/10.1061/40971(310)71

Yuan, X., Lee, W., and Li, N. (2017). Ontario's Local Calibration of the MEPDG Distress and Perfromance Models for Flexible Roads: A Summary. Proceedings of Innovations in Pavement, Management, Engineering and Technology Session. In the 2017 Conference of the Transportation Association of Canada St. John's, NL

Yue, E., and Bulut, R. (2014). Equilibrium Matric Suctions in Subgrade Soils in Oklahoma Based on Thornthwaite Moisture Index (TMI). In: Advances in Transportation Geotechnics and Materials for Sustainable Infrastructure, (May), 17–24 2014. Available from: https://doi.org/10.1061/9780784478509.003 [Accessed 3 Mar 2019].

Zareie A., et al., (2016). Thornthwaite Moisture Index Modeling to Estimate the Implication of Climate Change on Pavement Deterioration. Journal of Transportation Engineering [online]. Available from: https://doi.org/10.1061/(ASCE)TE.1943-5436.0000840 [Accessed 5 Apr 2019].

Zhang, Z., et al., (2008). Pavement structures damage caused by Hurricane Katrina flooding. Journal of Geotechnical and Geoenvironmental Engineering, 134 (5), 633–643.

Zhong J. (2017).Rigid Pavement: Ontario Calibration of the Mechanistic-Empirical Pavement Design Guide Prediction models. University of Waterloo.

APPENDIX A - Designs

Towards a Flood Resilient Pavement System in Canada - A Rigid Pavement Design Approach – Manitoba Case Study

Class C1:

Low Traffic ≤ 500 Two-way AADTT

Thin Pavement ≤ 225mm

Weak Subgrade ≤ 35Mpa/23.80% OMC High Plastic Clay Soil (A-7-6)

Class C2:

Low Traffic ≤ 500 Two-way AADTT

Thin Pavement ≤ 225mm

Average Subgrade ≤ 73.1Mpa/13% OMC Sandy Clay Soil (A-6)

Class C3:

Low Traffic = 500 Two-way AADTT

Thin Pavement = 225mm

Strong Subgrade = 66.6Mpa/8.50% OMC Sandy Silt Soil (A-4)

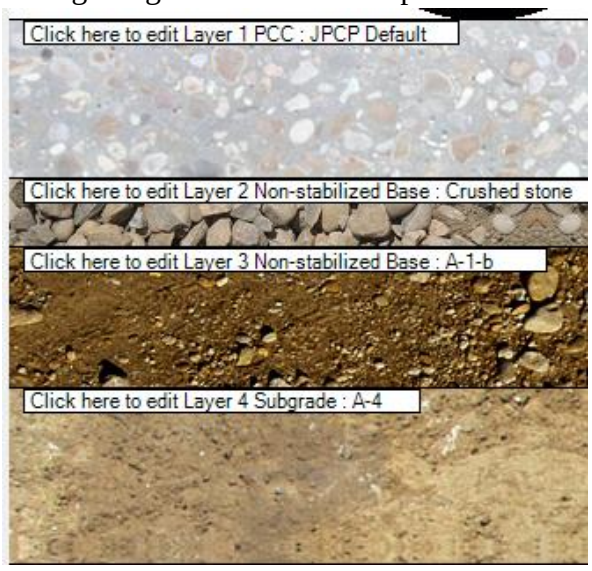

Class C4:

Low Traffic = 500 Two-way AADTT

Average Pavement = 250mm

Weak Subgrade = 35Mpa/23.80% OMC High Plastic Clay Soil (A-7-6)

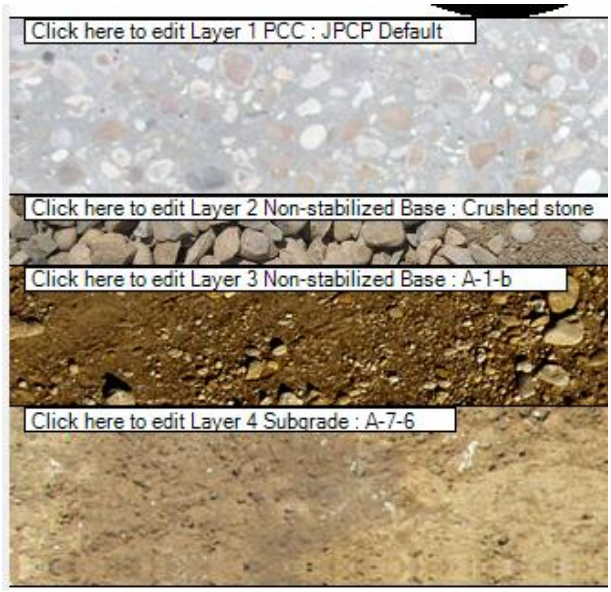

Class C5:

Low Traffic = 500 Two-way AADTT

Medium Pavement = 250mm

Average Subgrade = 73.1Mpa/13% OMC Sandy Clay Soil (A-6)

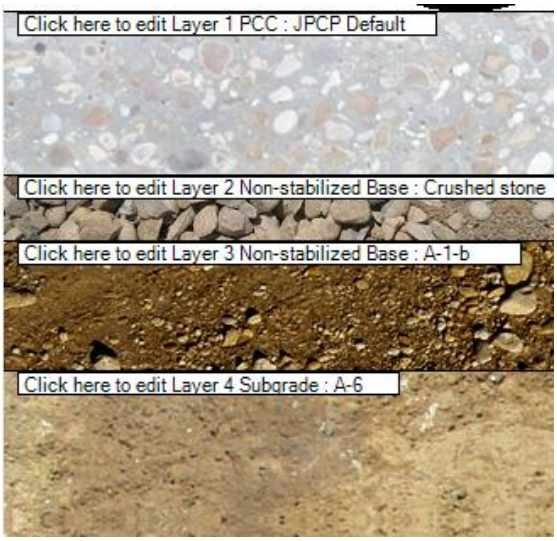

Class C6:

Low Traffic = 500 Two-way AADTT

Medium Pavement = 250mm

Strong Subgrade = 66.6Mpa/8.50% OMC Sandy Silt Soil (A-4)

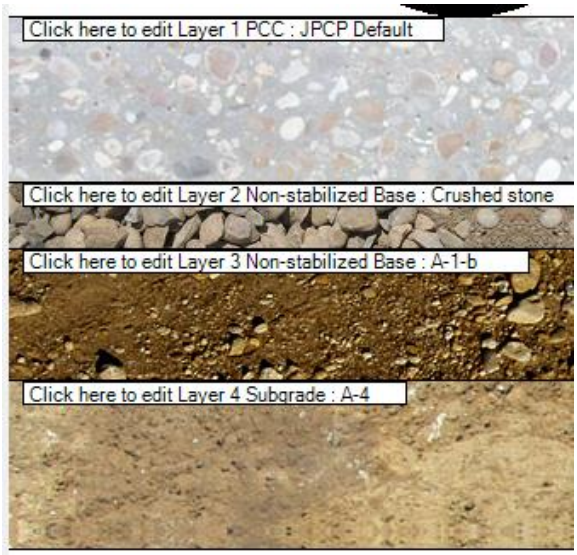

Class C7:

Low Traffic = 500 Two-way AADTT

Thick Pavement = 275mm

Weak Subgrade = 35Mpa/23.80% OMC High Plastic Clay Soil (A-7-6)

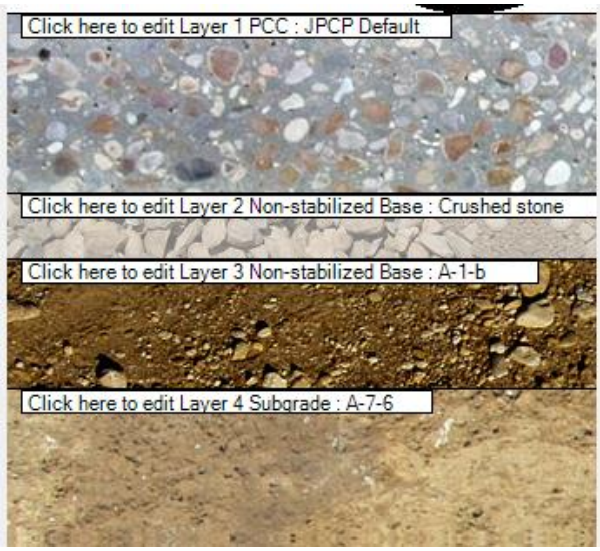

Class C8:

Low Traffic = 500 Two-way AADTT

Thick Pavement = 275mm

Average Subgrade = 73.1Mpa/13% OMC Sandy Clay Soil (A-6)

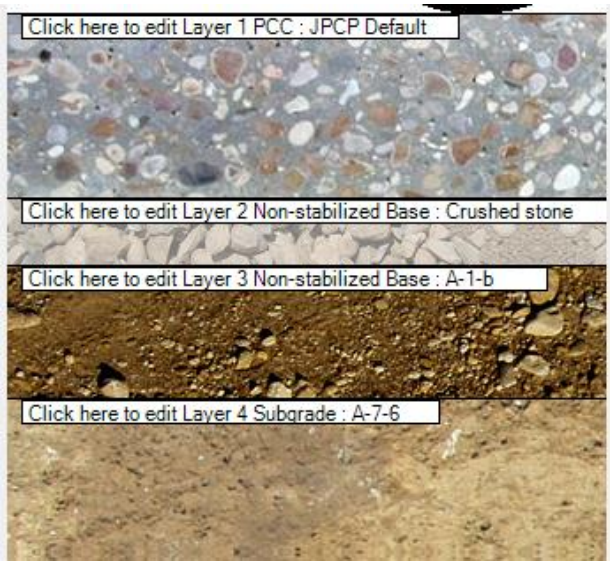

Class C9:

Low Traffic = 500 Two-way AADTT

Thick Pavement = 275mm

Average Subgrade = 66.6Mpa/8.50% OMC Sandy Silt Soil (A-4)

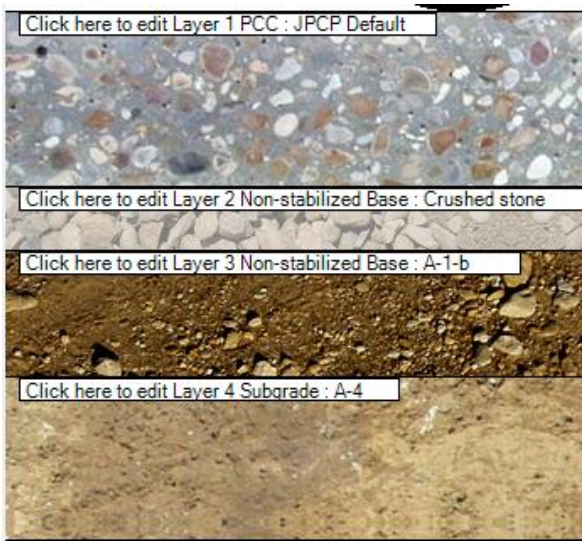

Class A1:

Moderate Traffic ≤ 1000 Two-way AADTT

Thin Pavement ≤ 225mm

Weak Subgrade ≤ 35Mpa/23.80% OMC High Plastic Clay Soil (A-7-6)

Class A2:

Moderate Traffic ≤ 1000 Two-way AADTT

Thin Pavement ≤ 225mm

Average Subgrade ≤ 73.1Mpa/13% OMC Sandy Clay Soil (A-6)

Class A3:

Moderate Traffic ≤ 1000 Two-way AADTT

Thin Pavement = 225mm

Strong Subgrade = 66.6Mpa/8.50% OMC Sandy Silt Soil (A-4)

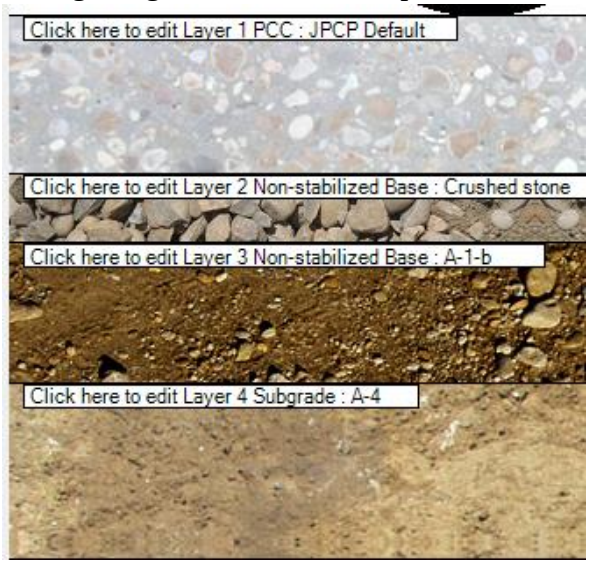

Class A4:

Moderate Traffic ≤ 1000 Two-way AADTT

Medium Pavement = 250mm

Strong Subgrade = 66.6Mpa/8.50% OMC Sandy Silt Soil (A-4)

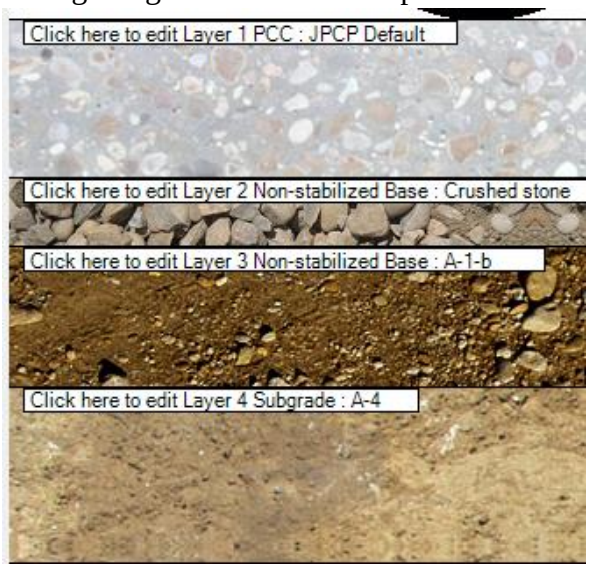

Class A5:

Moderate Traffic ≤ 1000 Two-way AADTT

Medium Pavement = 250mm

Average Subgrade = 73.1Mpa/13% OMC Sandy Clay Soil (A-6)

Class A6:

Moderate Traffic = 1000 Two-way AADTT

Medium Pavement = 250mm

Average Subgrade = 35Mpa/23.80% OMC High Plastic Clay Soil (A-7-6)

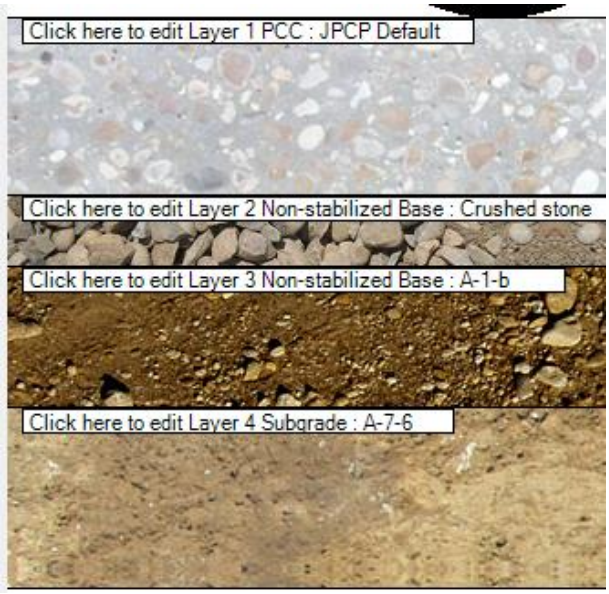

Class A7:

Moderate Traffic = 1000 Two-way AADTT

Thick Pavement = 275mm

Weak Subgrade = 35Mpa/23.80% OMC High Plastic Clay Soil (A-7-6)

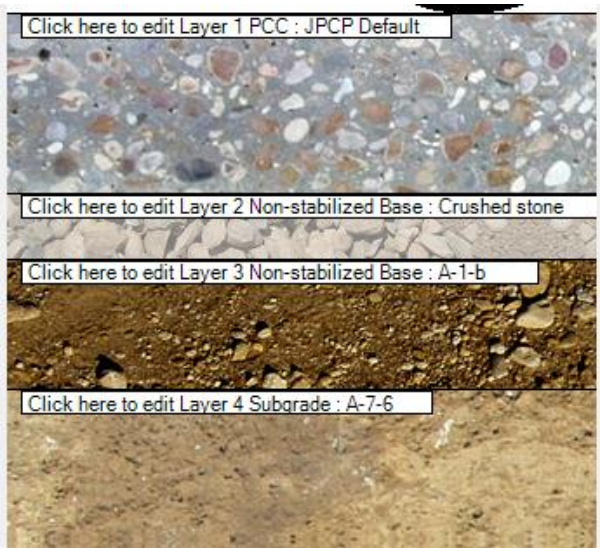

Class A8:

Moderate Traffic = 1000 Two-way AADTT

Thick Pavement = 275mm

Average Subgrade = 73.1Mpa/13% OMC Sandy Clay Soil (A-6)

Class A9:

Moderate Traffic = 1000 Two-way AADTT

Thick Pavement = 275mm

Average Subgrade = 66.6Mpa/8.50% OMC Sandy Silt Soil (A-4)

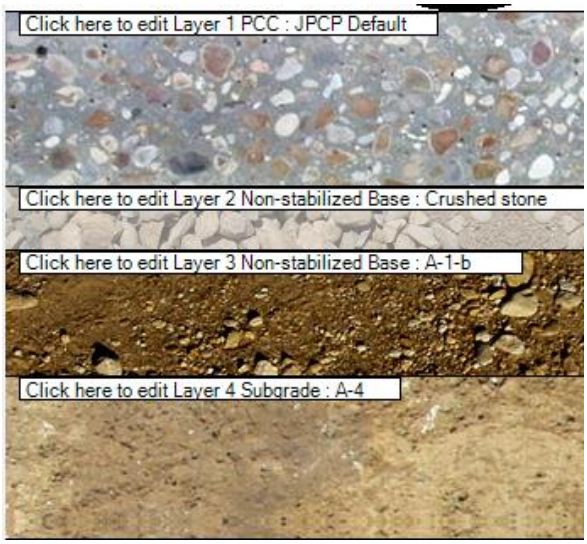

Class A10:

High Traffic = 2000 Two-way AADTT

Thin Pavement = 225mm

Strong Subgrade = 66.6Mpa/8.50% OMC Sandy Silt Soil (A-4)

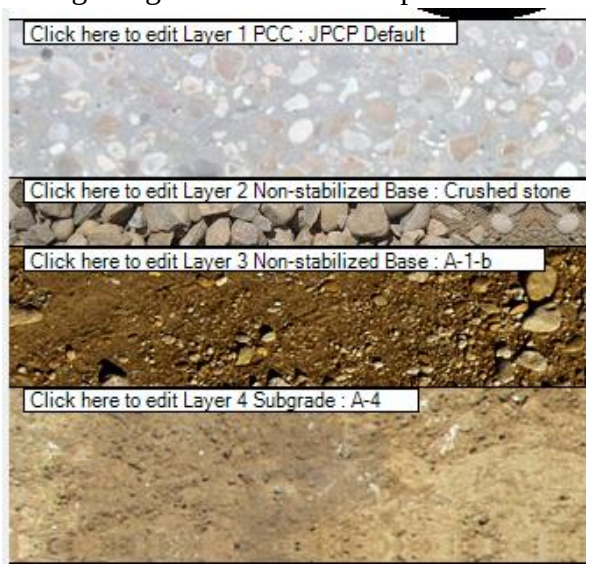

Class A11:

High Traffic = 2000 Two-way AADTT

Thin Pavement = 225mm

Average Subgrade = 73.1Mpa/13% OMC Sandy Clay Soil (A-6)

Class A12:

High Traffic = 2000 Two-way AADTT

Thin Pavement = 225mm

Weak Subgrade = 35Mpa/23.80% OMC High Plastic Clay Soil (A-7-6)

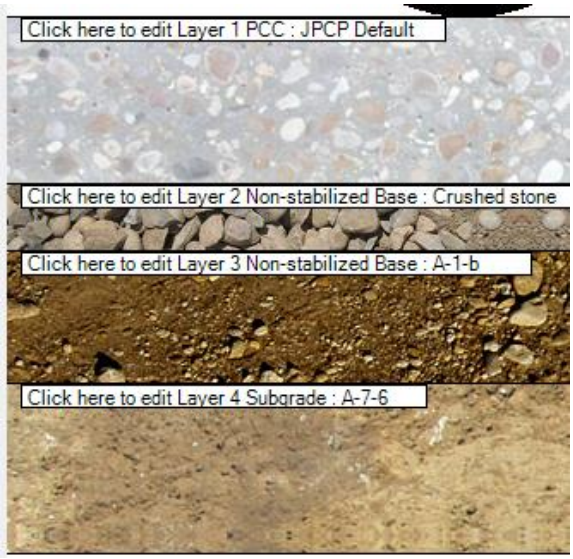

Class A13:

High Traffic = 2000 Two-way AADTT

Average Pavement = 250mm

Weak Subgrade = 35Mpa/23.80% OMC High Plastic Clay Soil (A-7-6)

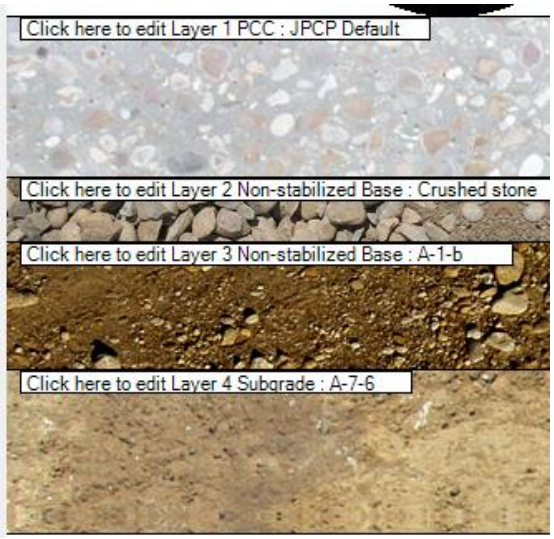

Class A14:

High Traffic = 2000 Two-way AADTT

Medium Pavement = 250mm

Average Subgrade = 73.1Mpa/13% OMC Sandy Clay Soil (A-6)

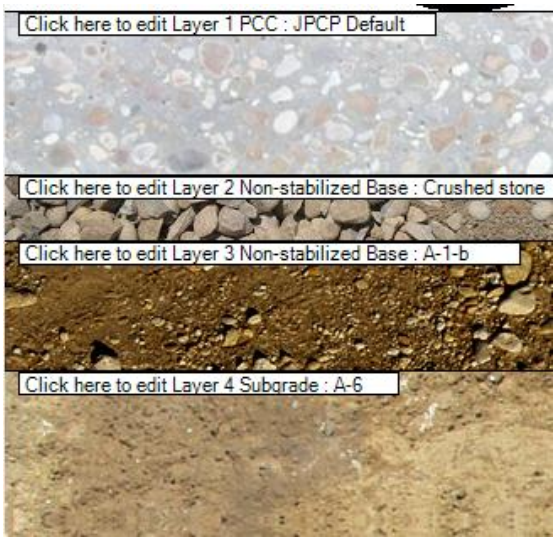

Class A15:

High Traffic = 2000 Two-way AADTT

Medium Pavement = 250mm

Strong Subgrade = 66.6Mpa/8.50% OMC Sandy Silt Soil (A-4)

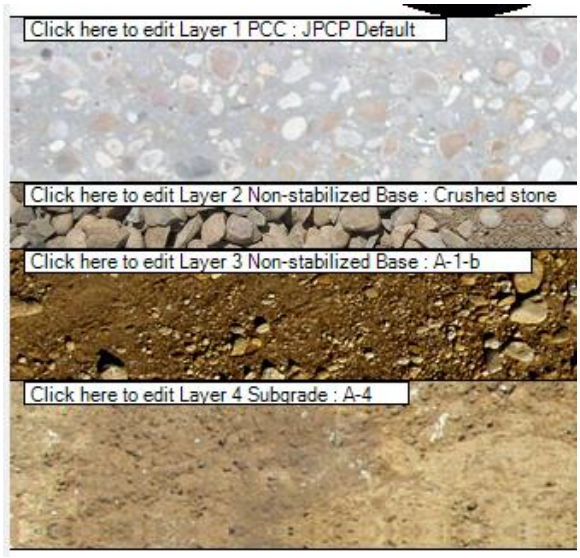

Class A16:

High Traffic = 2000 Two-way AADTT

Thick Pavement = 275mm

Weak Subgrade = 35Mpa/23.80% OMC High Plastic Clay Soil (A-7-6)

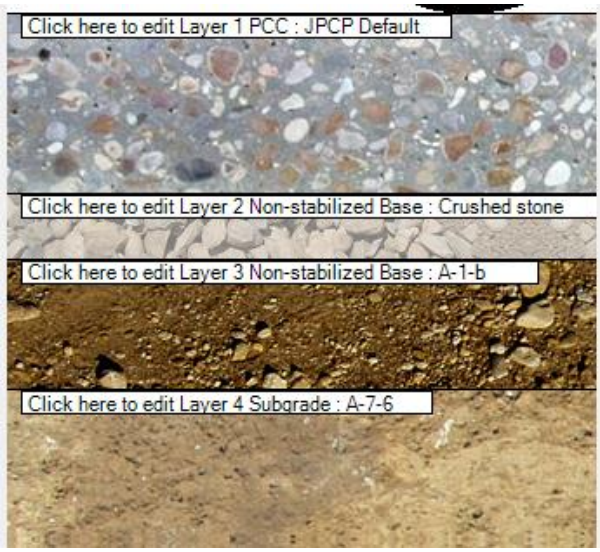

Class A17:

High Traffic = 2000 Two-way AADTT

Thick Pavement = 275mm

Average Subgrade = 73.1Mpa/13% OMC Sandy Clay Soil (A-6)

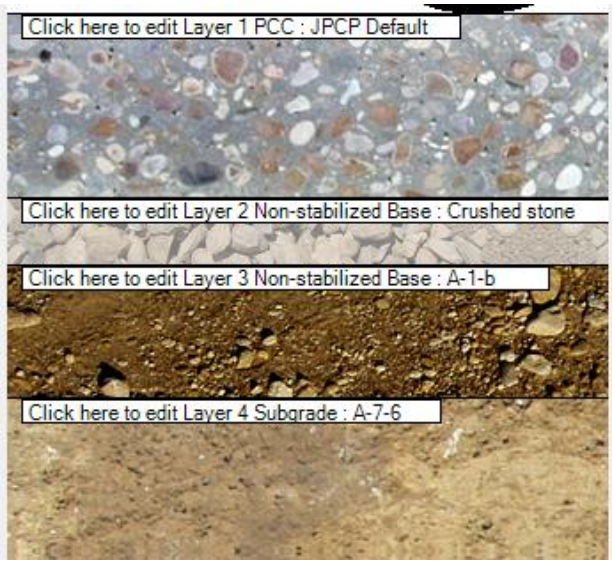

Class A18:

High Traffic = 2000 Two-way AADTT

Thick Pavement = 275mm

Average Subgrade = 66.6Mpa/8.50% OMC Sandy Silt Soil (A-4)

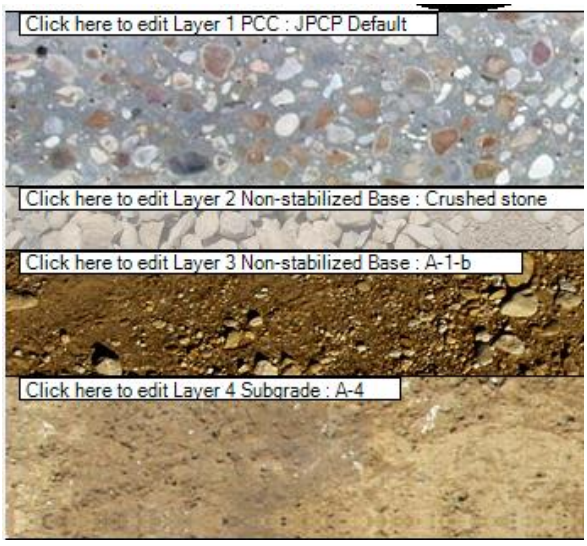

APPENDIX B - Results

Towards a Flood Resilient Pavement System in Canada - A Rigid Pavement Design Approach – Manitoba Case Study

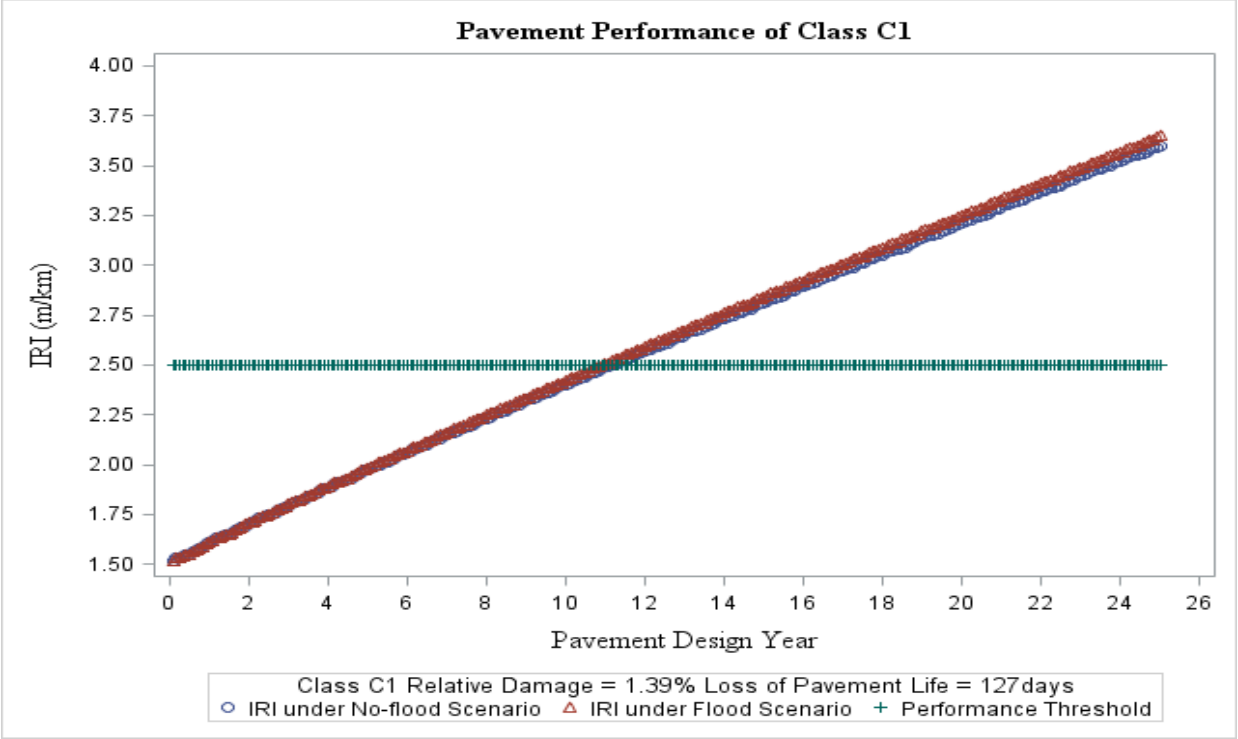
Pavement Performance of Class C1
IRI (m/km)
4.00
3.75
3.50
3.25
3.00
2.75
2.50
2.25
2.00
1.75
1.50
0
2
4
6
8
10
12
14
16
18
20
22
24
26
Pavement Design Year
Class C1 Relative Damage = 1.39% Loss of Pavement Life = 127days
IRI under No-flood Scenario
IRI under Flood Scenario
Performance Threshold

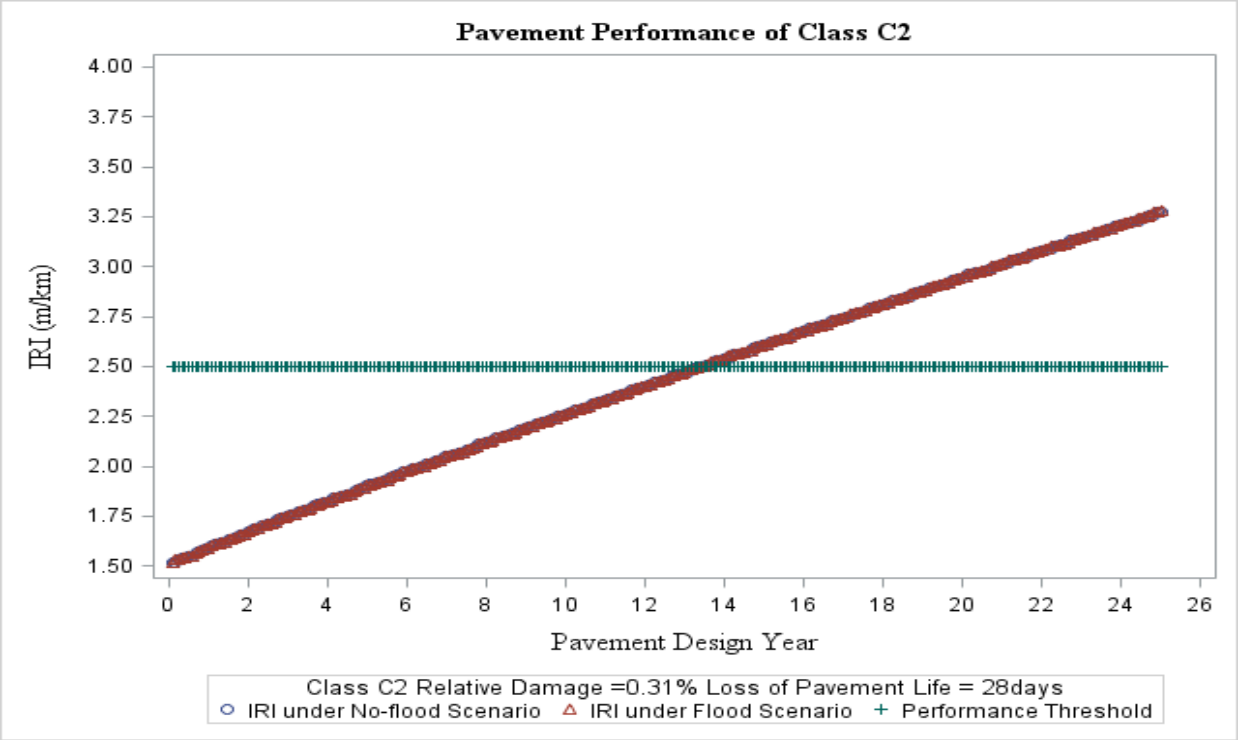
Pavement Performance of Class C2
IRI (m/km)
4.00
3.75
3.50
3.25
3.00
2.75
2.50
2.25
2.00
1.75
1.50
0
2
4
6
8
10
12
14
16
18
20
22
24
26
Pavement Design Year
Class C2 Relative Damage =0.31% Loss of Pavement Life = 28days
IRI under No-flood Scenario
IRI under Flood Scenario
Performance Threshold

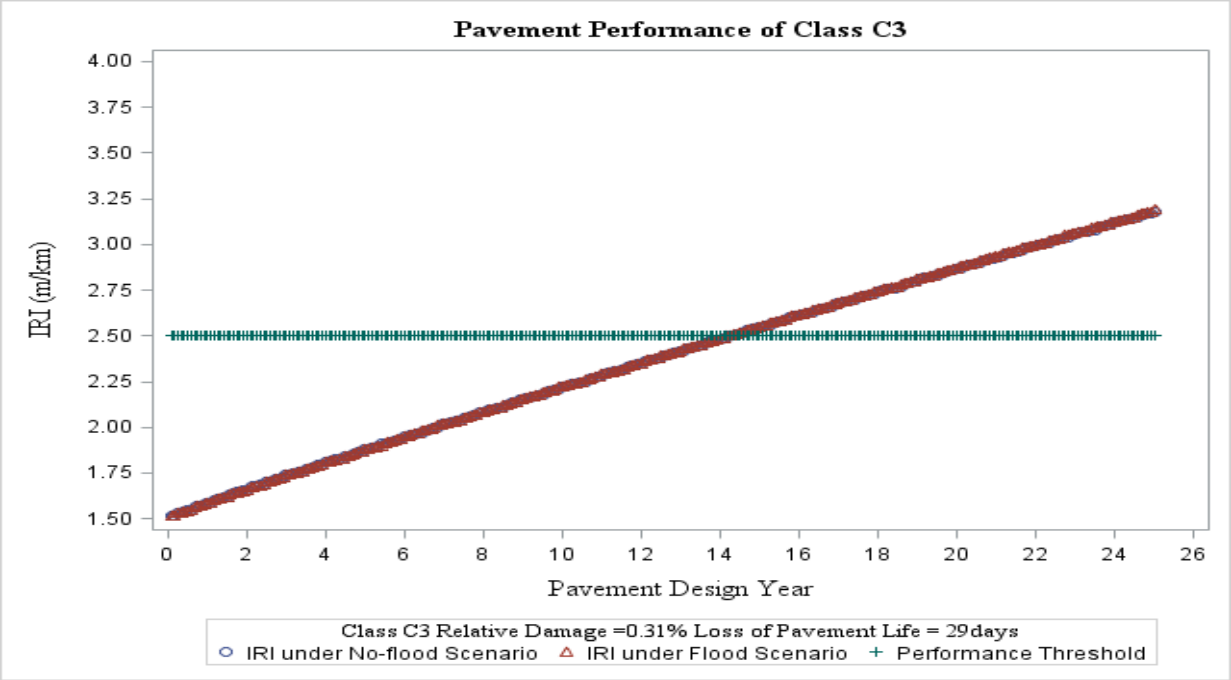
Pavement Performance of Class C3
IRI (m/km)
4.00
3.75
3.50
3.25
3.00
2.75
2.50
2.25
2.00
1.75
1.50
0
2
4
6
8
10
12
14
16
18
20
22
24
26
Pavement Design Year
Class C3 Relative Damage =0.31% Loss of Pavement Life = 29days
IRI under No-flood Scenario
IRI under Flood Scenario
Performance Threshold

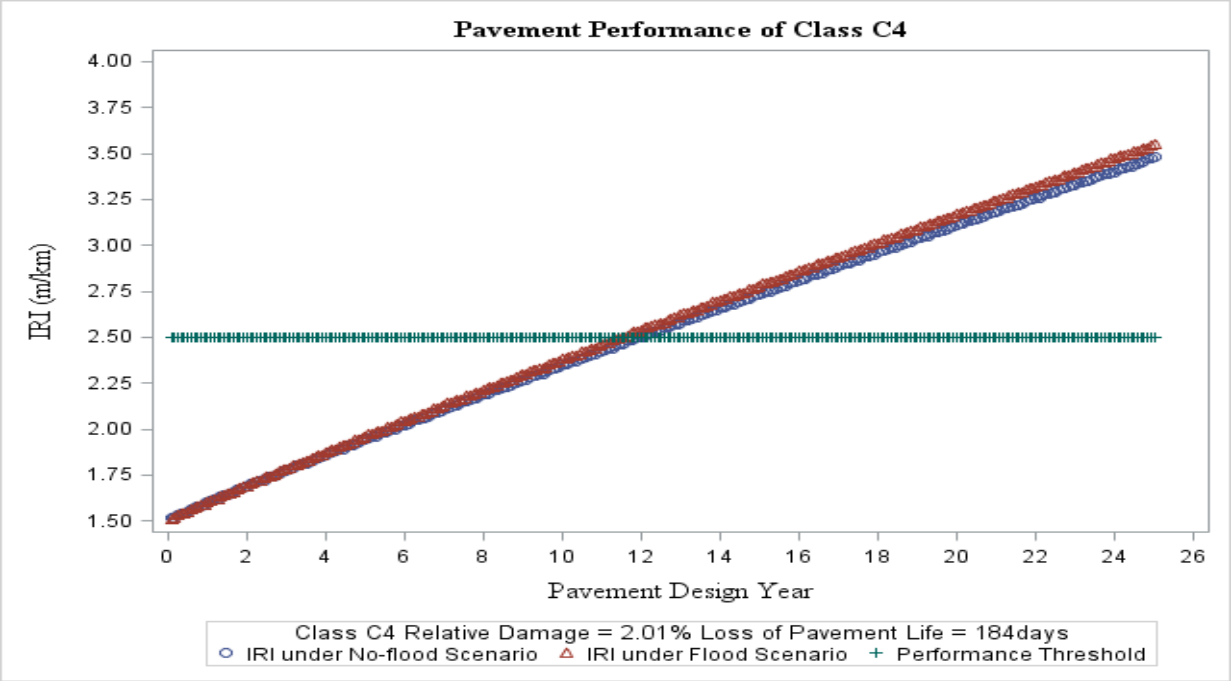
Pavement Performance of Class C4
IRI (m/km)
4.00
3.75
3.50
3.25
3.00
2.75
2.50
2.25
2.00
1.75
1.50
0
2
4
6
8
10
12
14
16
18
20
22
24
26
Pavement Design Year
Class C4 Relative Damage = 2.01% Loss of Pavement Life = 184days
IRI under No-flood Scenario
IRI under Flood Scenario
Performance Threshold

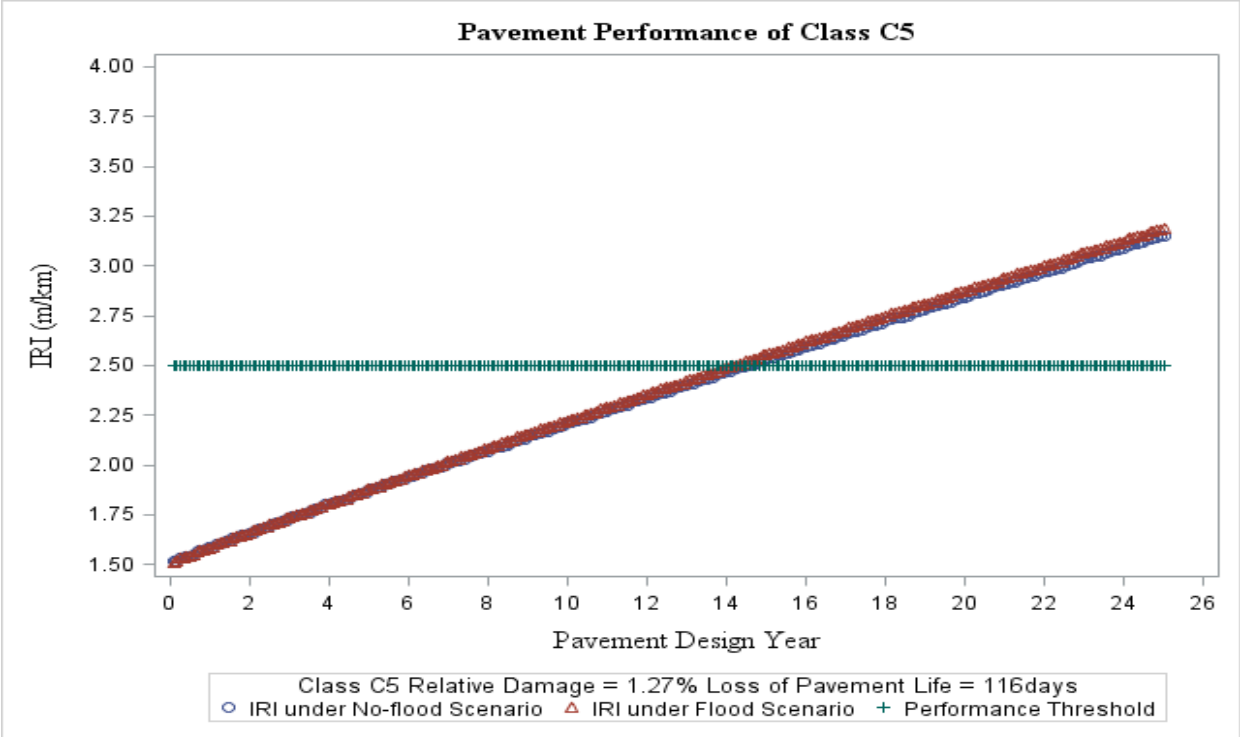
Pavement Performance of Class C5
IRI (m/km)
4.00
3.75
3.50
3.25
3.00
2.75
2.50
2.25
2.00
1.75
1.50
0
2
4
6
8
10
12
14
16
18
20
22
24
26
Pavement Design Year
Class C5 Relative Damage = 1.27% Loss of Pavement Life = 116days
IRI under No-flood Scenario
IRI under Flood Scenario
Performance Threshold

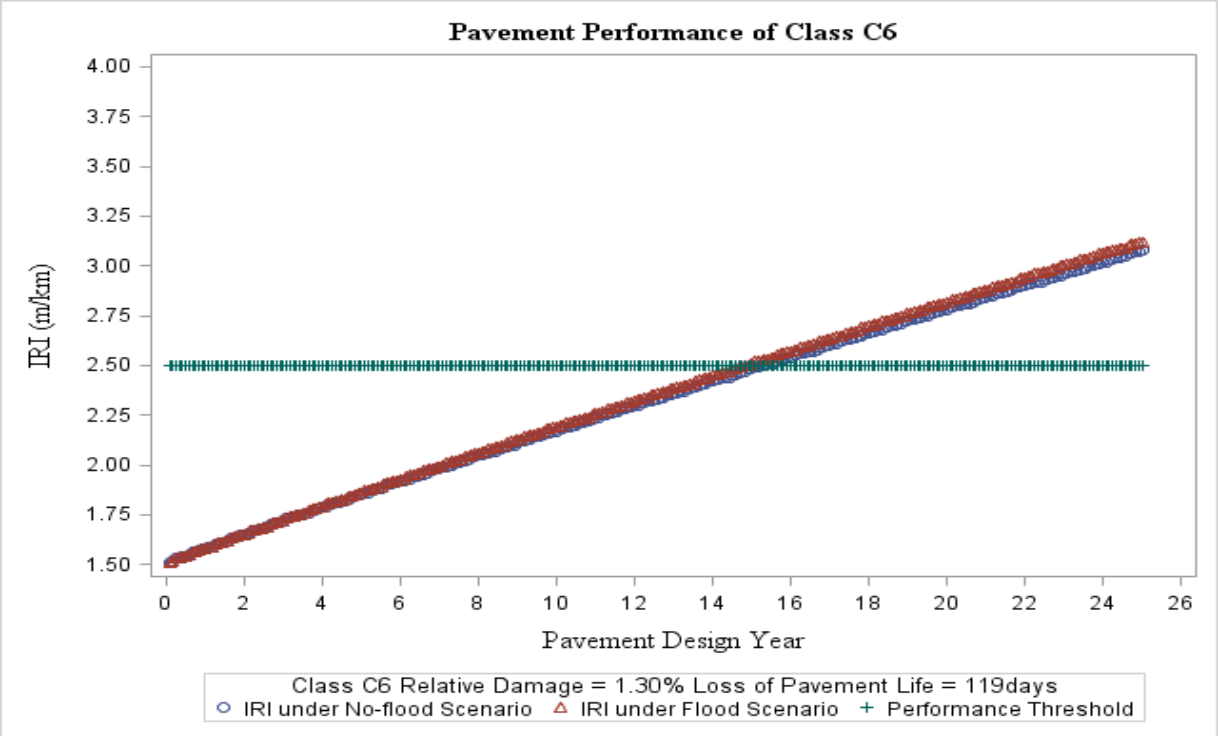
Pavement Performance of Class C6
IRI (m/km)
4.00
3.75
3.50
3.25
3.00
2.75
2.50
2.25
2.00
1.75
1.50
0
2
4
6
8
10
12
14
16
18
20
22
24
26
Pavement Design Year
Class C6 Relative Damage = 1.30% Loss of Pavement Life = 119days
IRI under No-flood Scenario
IRI under Flood Scenario
Performance Threshold

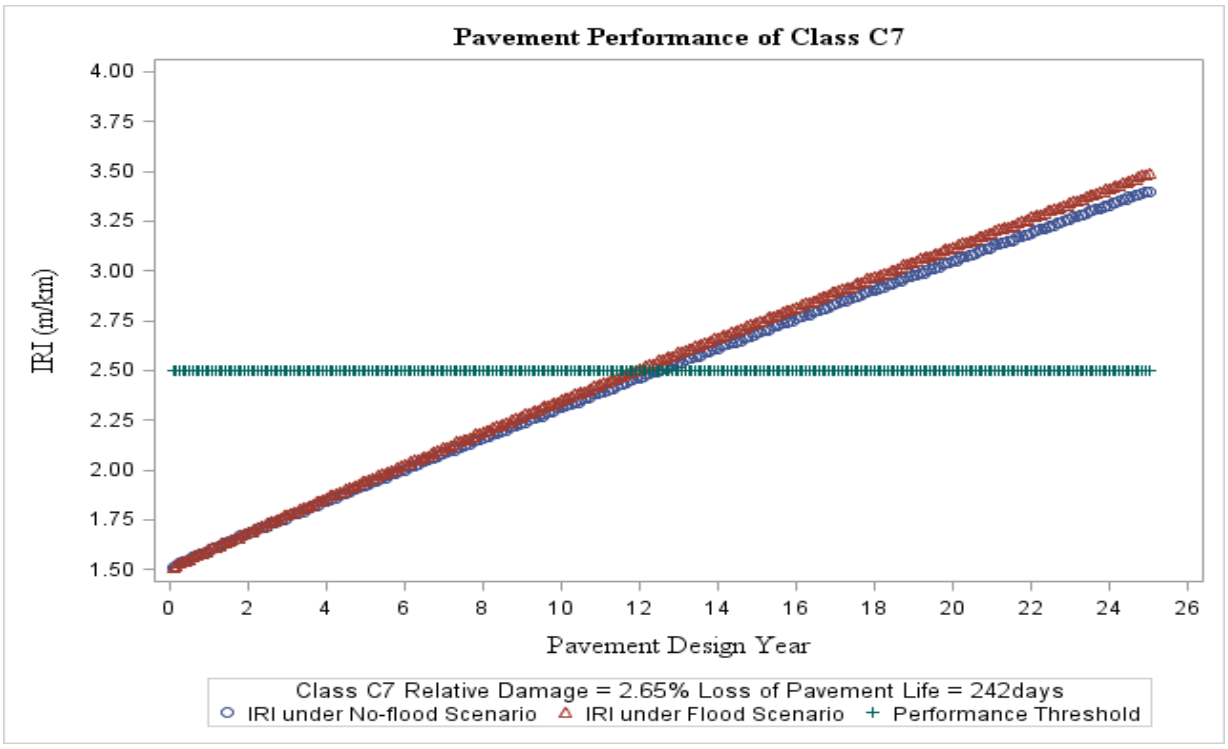
Pavement Performance of Class C7
IRI (m/km)
4.00
3.75
3.50
3.25
3.00
2.75
2.50
2.25
2.00
1.75
1.50
0
2
4
6
8
10
12
14
16
18
20
22
24
26
Pavement Design Year
Class C7 Relative Damage = 2.65% Loss of Pavement Life = 242days
IRI under No-flood Scenario
IRI under Flood Scenario
Performance Threshold

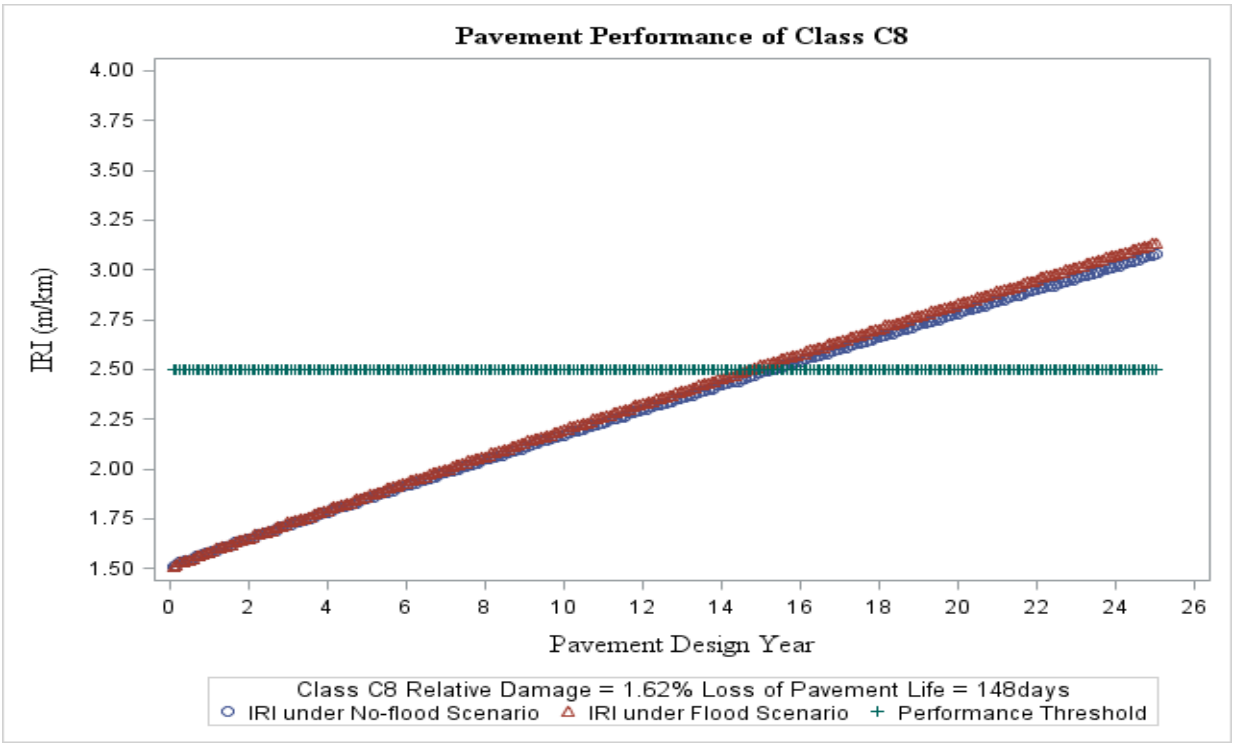
Pavement Performance of Class C8
IRI (m/km)
4.00
3.75
3.50
3.25
3.00
2.75
2.50
2.25
2.00
1.75
1.50
0
2
4
6
8
10
12
14
16
18
20
22
24
26
Pavement Design Year
Class C8 Relative Damage = 1.62% Loss of Pavement Life = 148days
IRI under No-flood Scenario
IRI under Flood Scenario
Performance Threshold

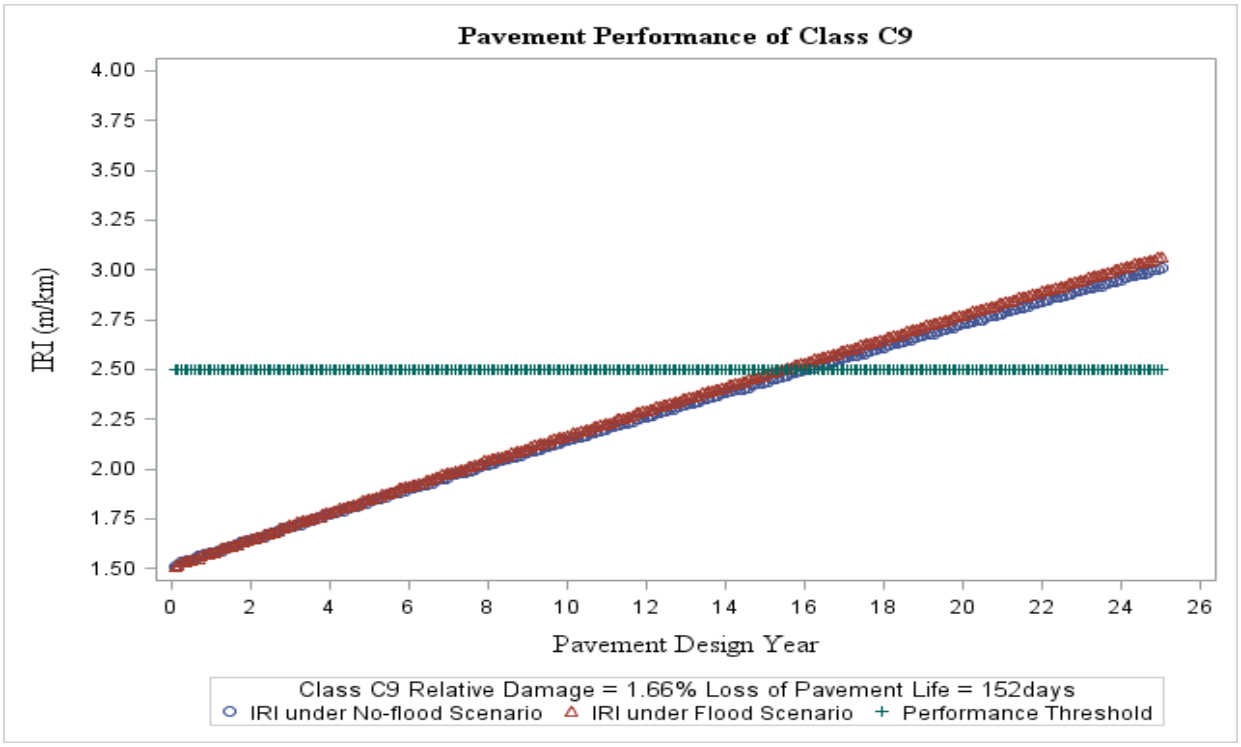
Pavement Performance of Class C9
IRI (m/km)
4.00
3.75
3.50
3.25
3.00
2.75
2.50
2.25
2.00
1.75
1.50
0
2
4
6
8
10
12
14
16
18
20
22
24
26
Pavement Design Year
Class C9 Relative Damage = 1.66% Loss of Pavement Life = 152days
IRI under No-flood Scenario
IRI under Flood Scenario
Performance Threshold

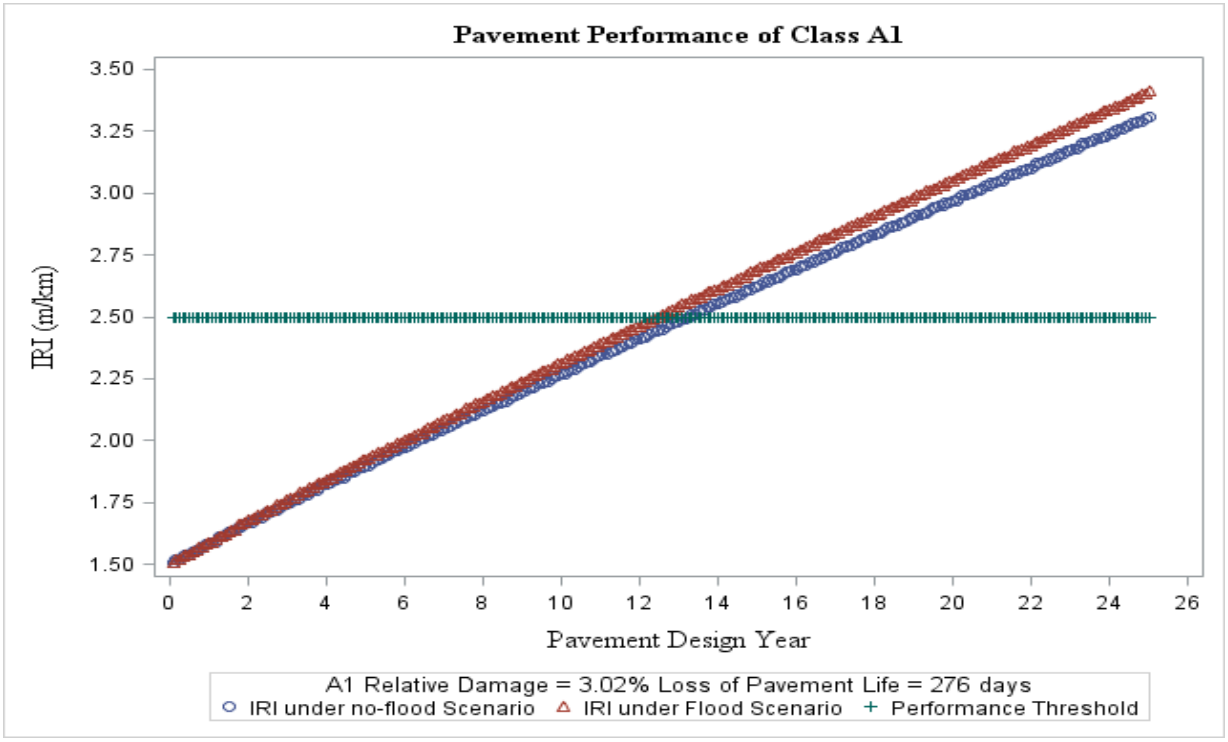
Pavement Performance of Class A1
IRI (m/km)
3.50
3.25
3.00
2.75
2.50
2.25
2.00
1.75
1.50
0
2
4
6
8
10
12
14
16
18
20
22
24
26
Pavement Design Year
A1 Relative Damage = 3.02% Loss of Pavement Life = 276 days
IRI under no-flood Scenario
IRI under Flood Scenario
Performance Threshold

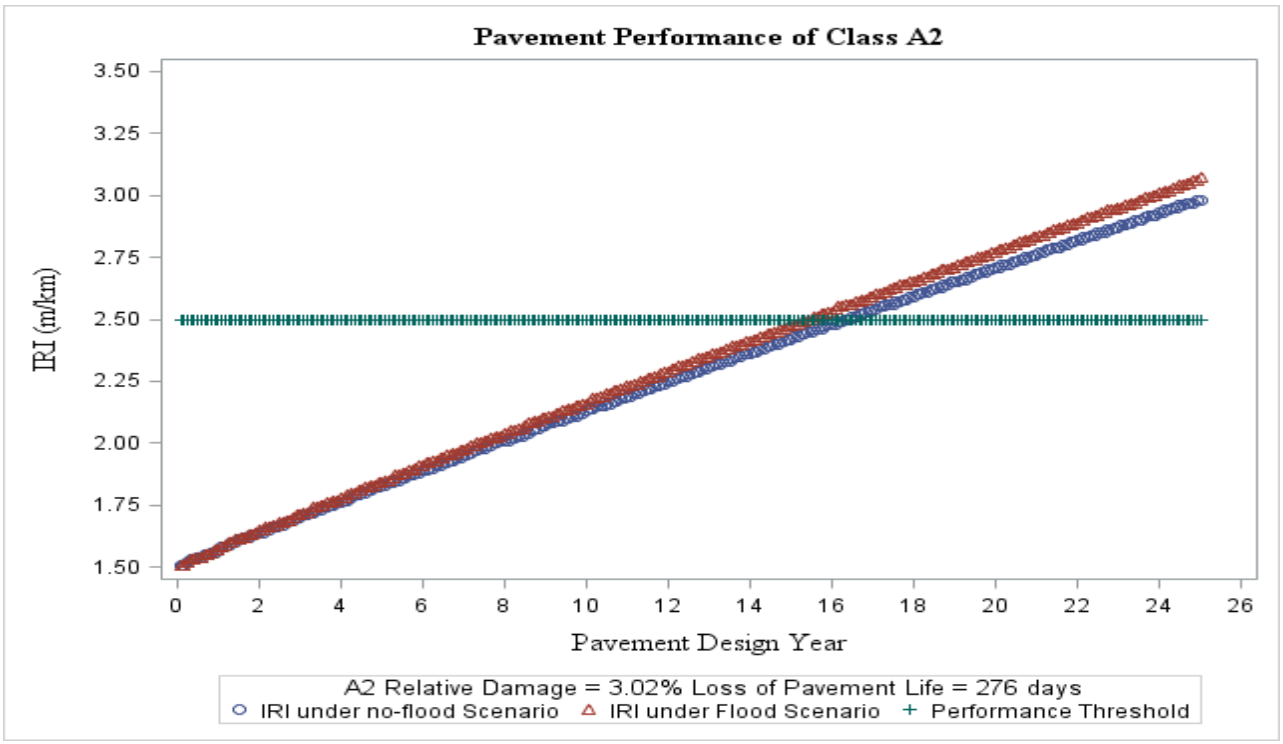
Pavement Performance of Class A2
IRI (m/km)
3.50
3.25
3.00
2.75
2.50
2.25
2.00
1.75
1.50
0
2
4
6
8
10
12
14
16
18
20
22
24
26
Pavement Design Year
A2 Relative Damage = 3.02% Loss of Pavement Life = 276 days
IRI under no-flood Scenario
IRI under Flood Scenario
Performance Threshold

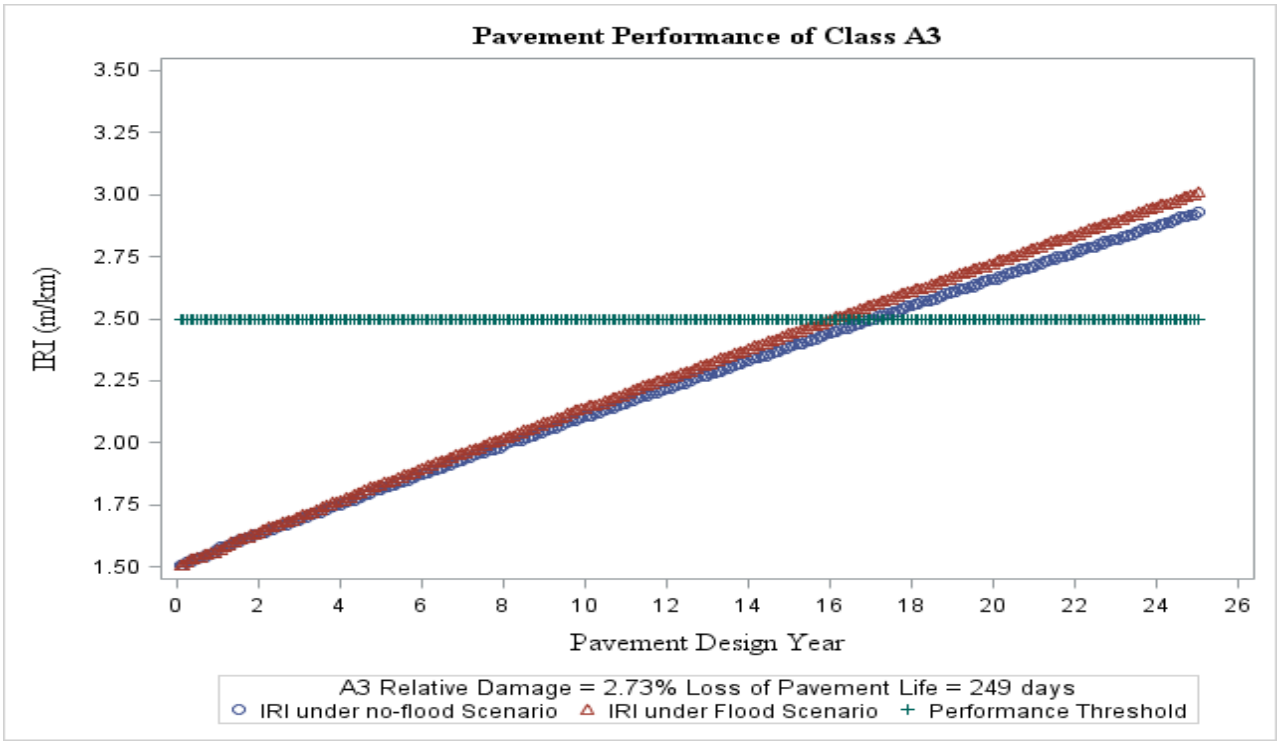
Pavement Performance of Class A3
IRI (m/km)
3.50
3.25
3.00
2.75
2.50
2.25
2.00
1.75
1.50
0
2
4
6
8
10
12
14
16
18
20
22
24
26
Pavement Design Year
A3 Relative Damage = 2.73% Loss of Pavement Life = 249 days
IRI under no-flood Scenario
IRI under Flood Scenario
Performance Threshold

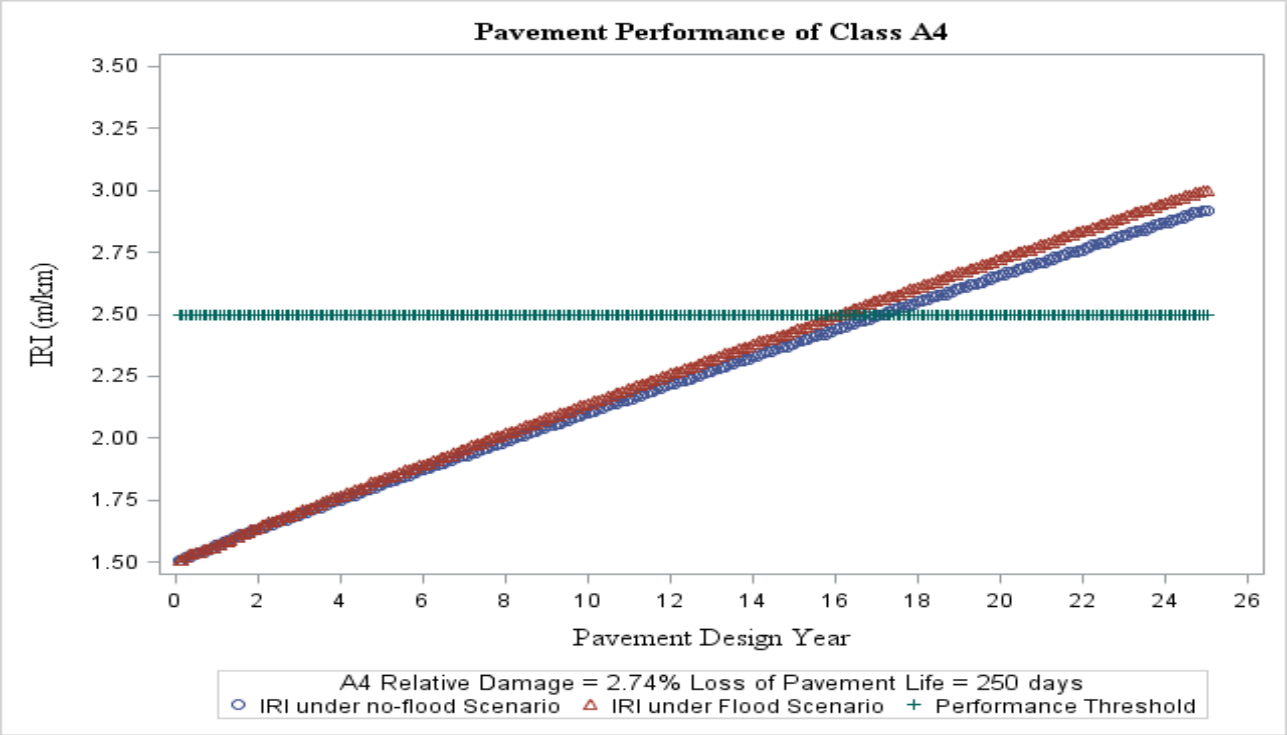
Pavement Performance of Class A4
IRI (m/km)
3.50
3.25
3.00
2.75
2.50
2.25
2.00
1.75
1.50
0
2
4
6
8
10
12
14
16
18
20
22
24
26
Pavement Design Year
A4 Relative Damage = 2.74% Loss of Pavement Life = 250 days
IRI under no-flood Scenario
IRI under Flood Scenario
Performance Threshold

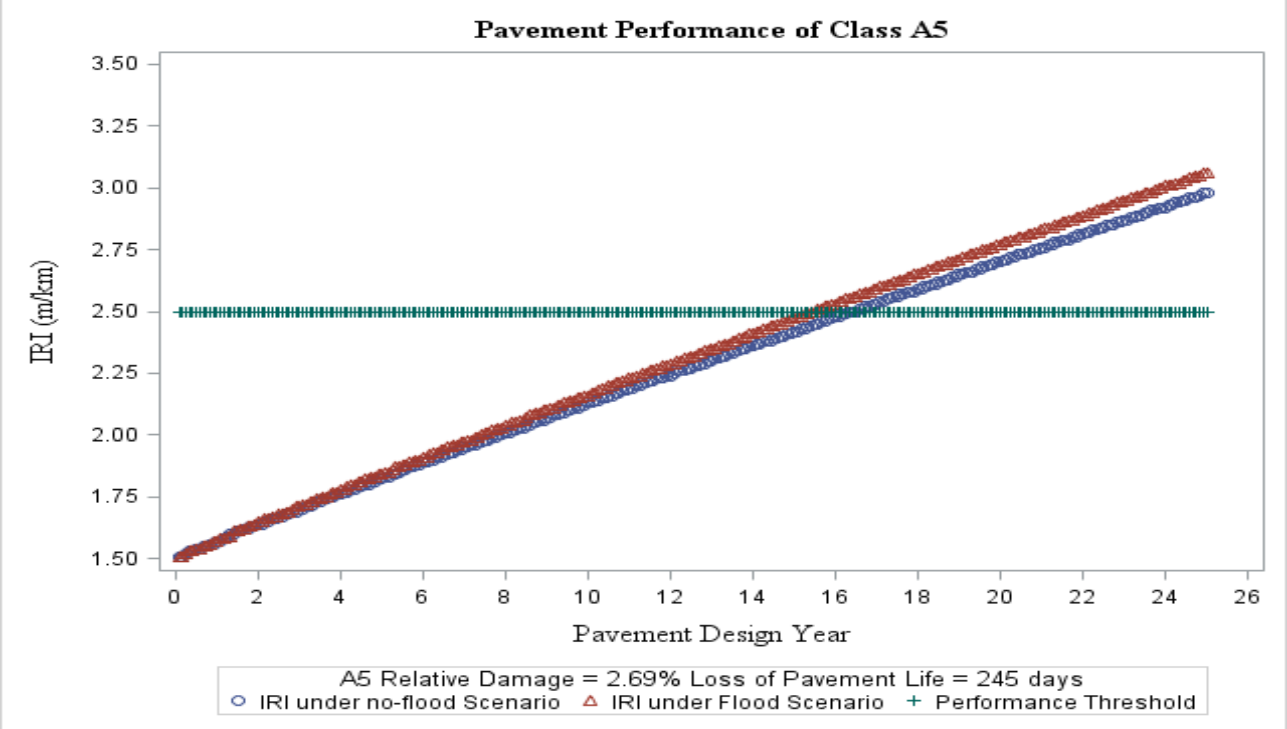
Pavement Performance of Class A5
IRI (m/km)
3.50
3.25
3.00
2.75
2.50
2.25
2.00
1.75
1.50
0
2
4
6
8
10
12
14
16
18
20
22
24
26
Pavement Design Year
A5 Relative Damage = 2.69% Loss of Pavement Life = 245 days
IRI under no-flood Scenario
IRI under Flood Scenario
Performance Threshold

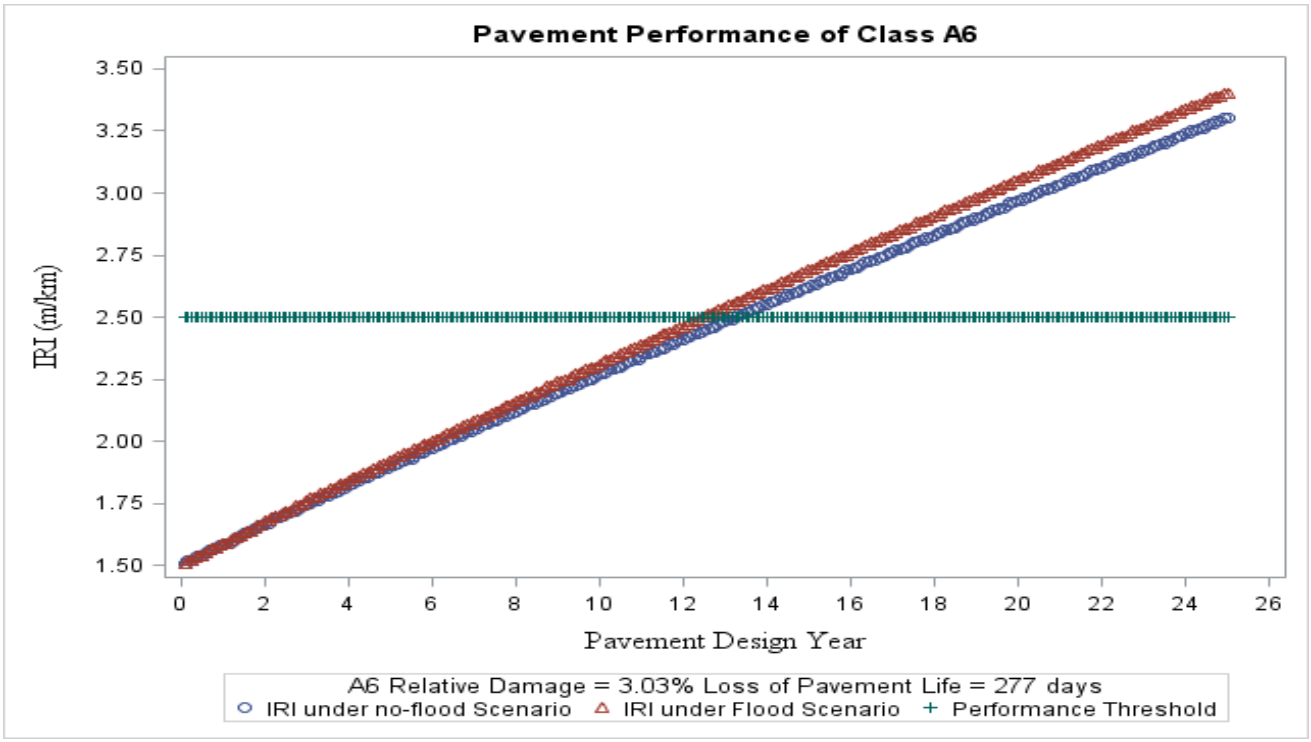
Pavement Performance of Class A6
IRI (m/km)
3.50
3.25
3.00
2.75
2.50
2.25
2.00
1.75
1.50
0
2
4
6
8
10
12
14
16
18
20
22
24
26
Pavement Design Year
A6 Relative Damage = 3.03% Loss of Pavement Life = 277 days
IRI under no-flood Scenario
IRI under Flood Scenario
Performance Threshold

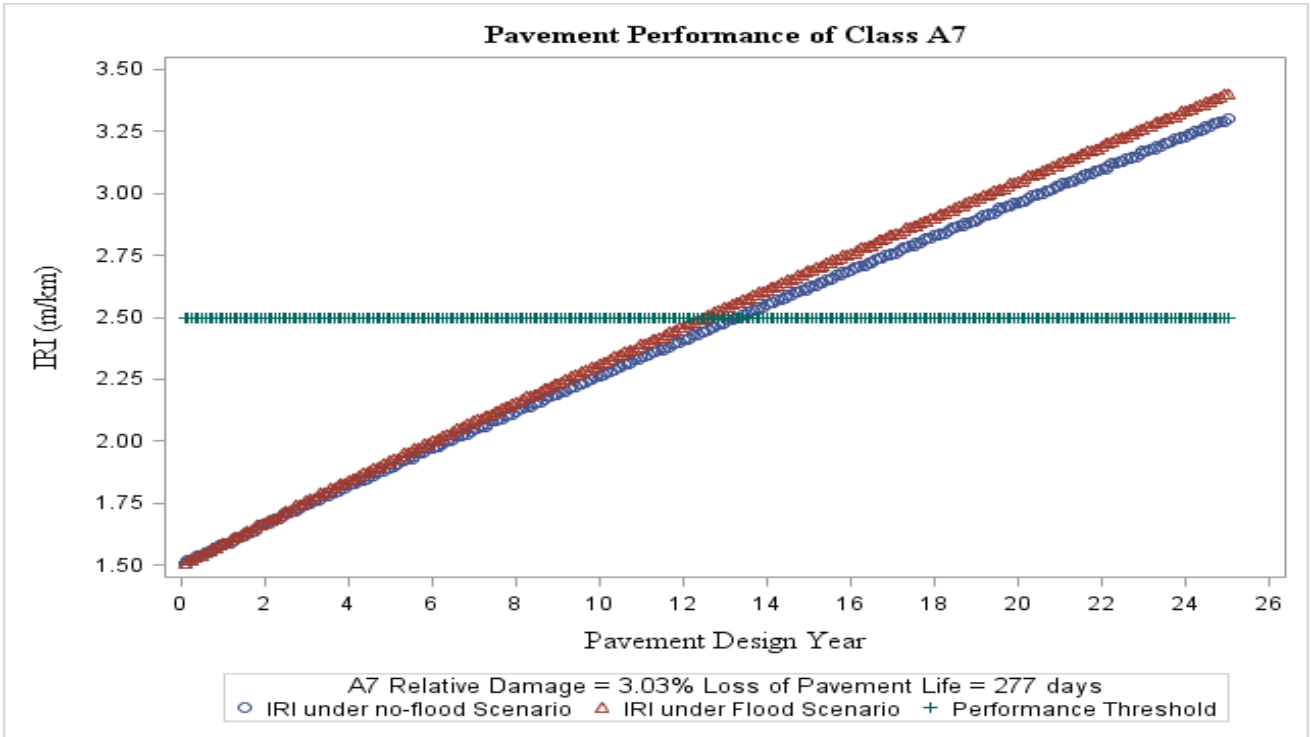
Pavement Performance of Class A7
IRI (m/km)
3.50
3.25
3.00
2.75
2.50
2.25
2.00
1.75
1.50
0
2
4
6
8
10
12
14
16
18
20
22
24
26
Pavement Design Year
A7 Relative Damage = 3.03% Loss of Pavement Life = 277 days
IRI under no-flood Scenario
IRI under Flood Scenario
Performance Threshold

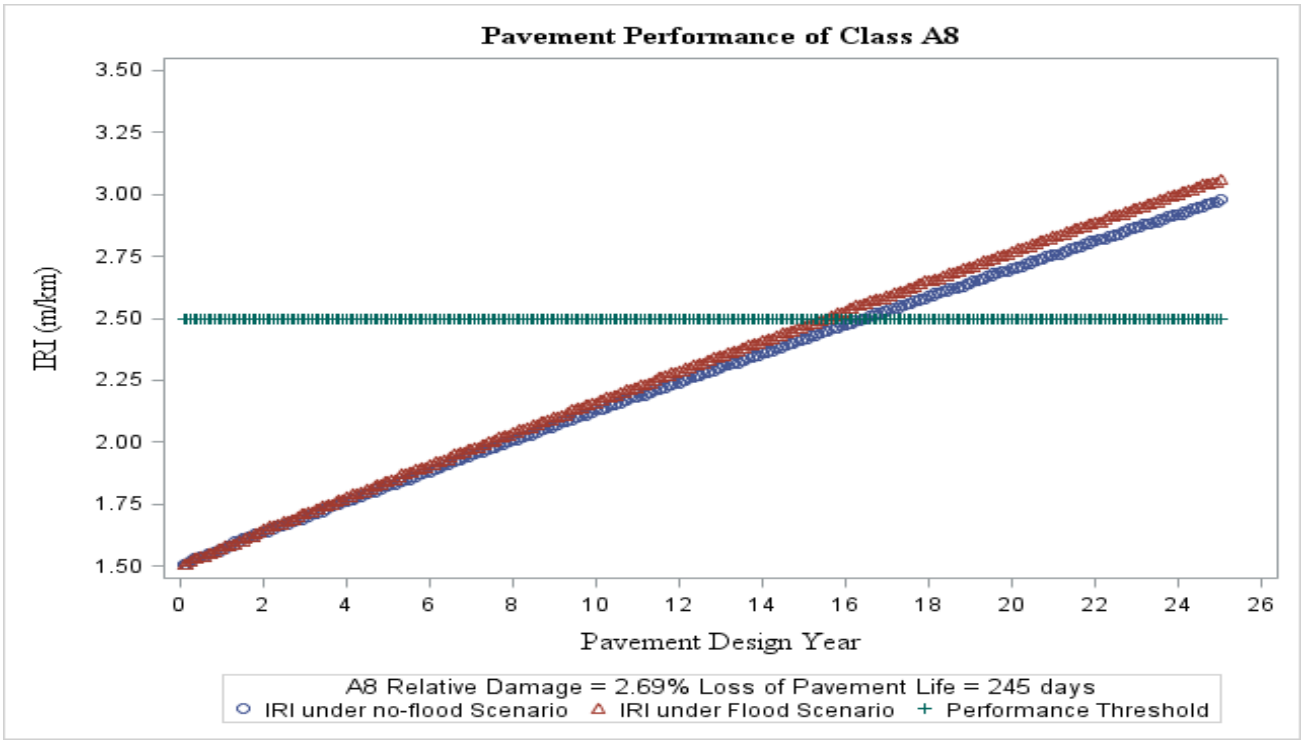
Pavement Performance of Class A8
IRI (m/km)
3.50
3.25
3.00
2.75
2.50
2.25
2.00
1.75
1.50
0
2
4
6
8
10
12
14
16
18
20
22
24
26
Pavement Design Year
A8 Relative Damage = 2.69% Loss of Pavement Life = 245 days
IRI under no-flood Scenario
IRI under Flood Scenario
Performance Threshold

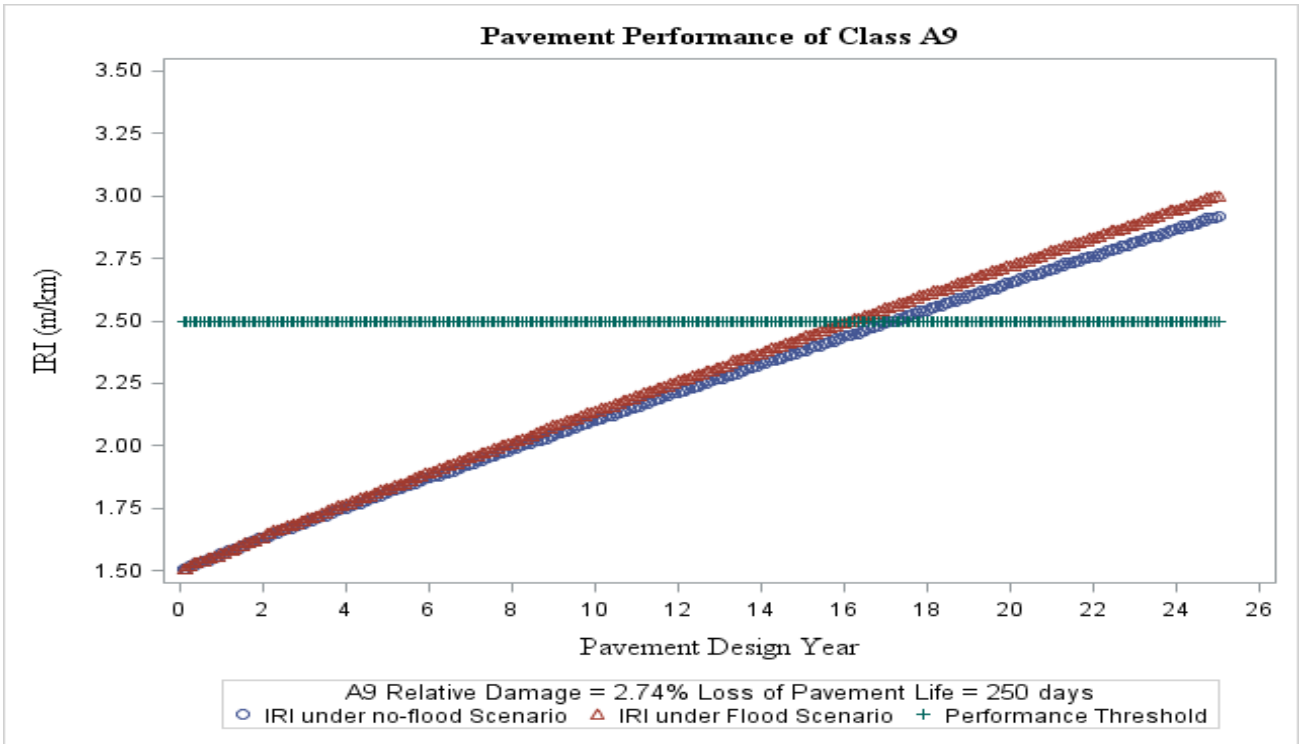
Pavement Performance of Class A9
IRI (m/km)
3.50
3.25
3.00
2.75
2.50
2.25
2.00
1.75
1.50
0
2
4
6
8
10
12
14
16
18
20
22
24
26
Pavement Design Year
A9 Relative Damage = 2.74% Loss of Pavement Life = 250 days
IRI under no-flood Scenario
IRI under Flood Scenario
Performance Threshold

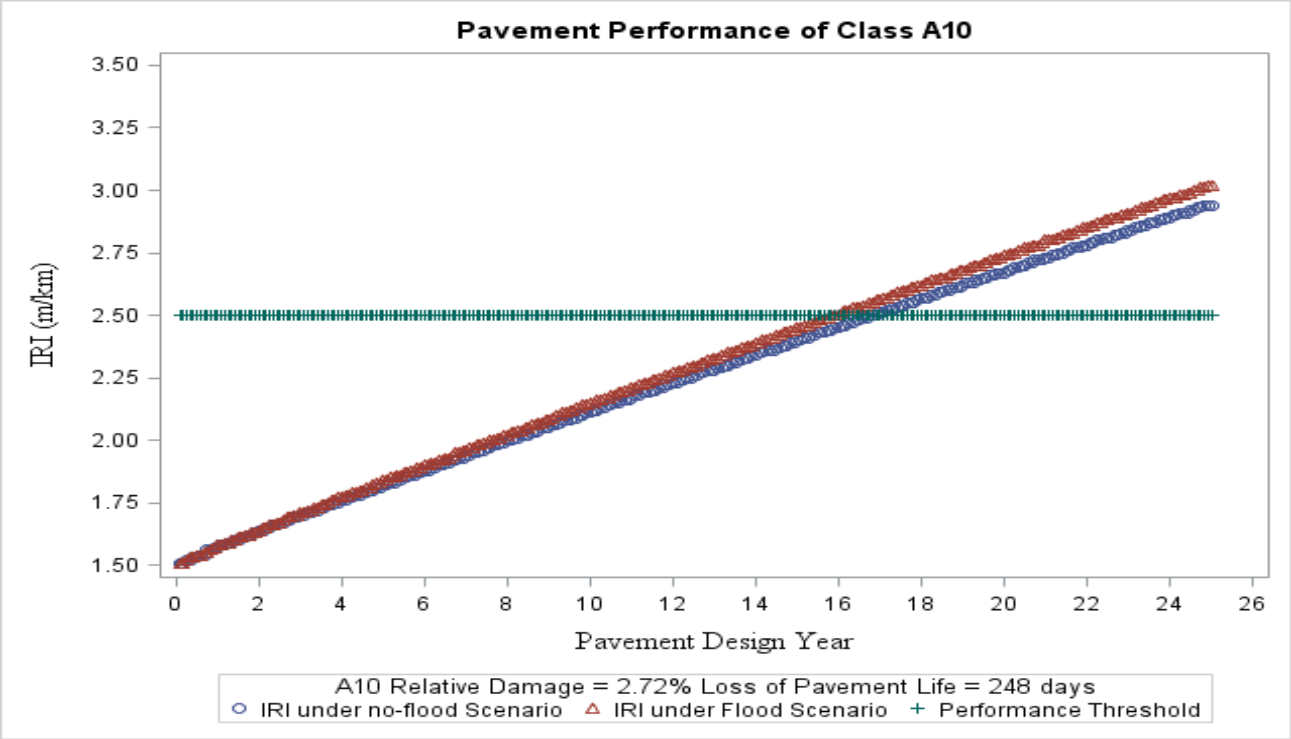
Pavement Performance of Class A10
IRI (m/km)
3.50
3.25
3.00
2.75
2.50
2.25
2.00
1.75
1.50
0
2
4
6
8
10
12
14
16
18
20
22
24
26
Pavement Design Year
A10 Relative Damage = 2.72% Loss of Pavement Life = 248 days
IRI under no-flood Scenario
IRI under Flood Scenario
Performance Threshold

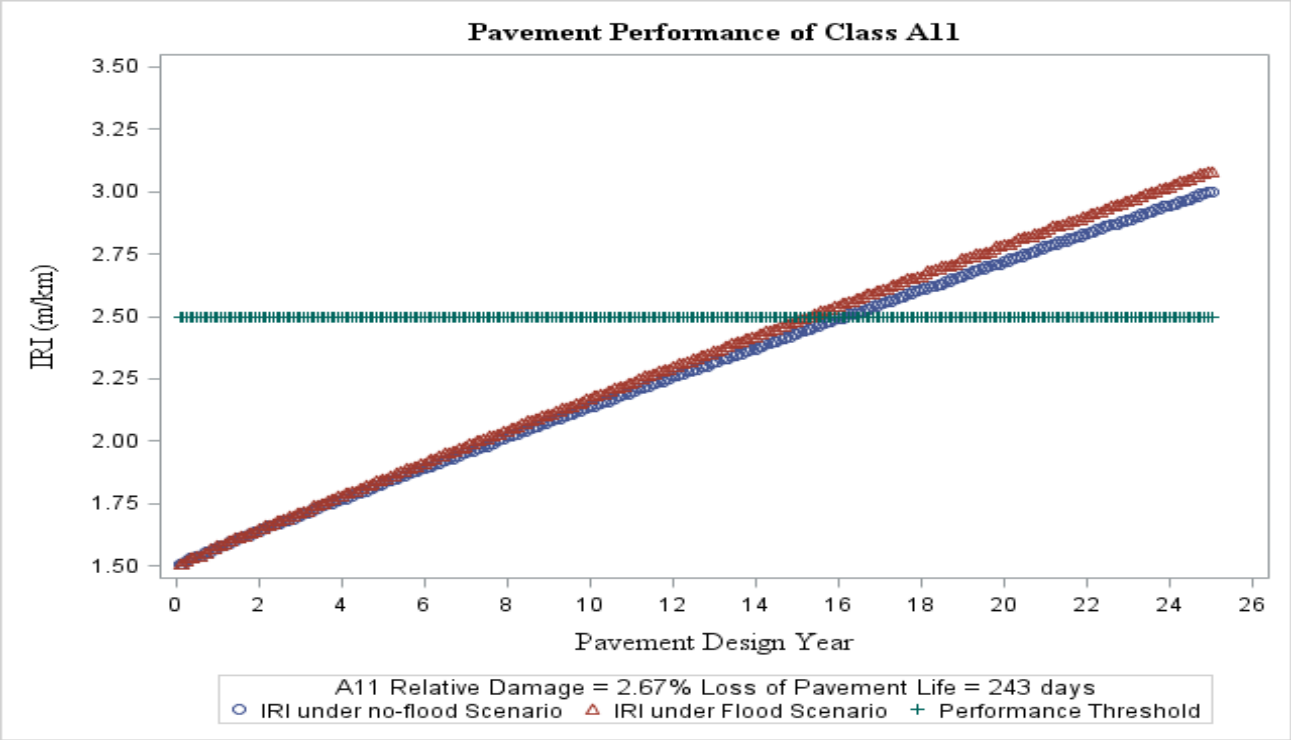
Pavement Performance of Class A11
IRI (m/km)
3.50
3.25
3.00
2.75
2.50
2.25
2.00
1.75
1.50
0
2
4
6
8
10
12
14
16
18
20
22
24
26
Pavement Design Year
A11 Relative Damage = 2.67% Loss of Pavement Life = 243 days
IRI under no-flood Scenario
IRI under Flood Scenario
Performance Threshold

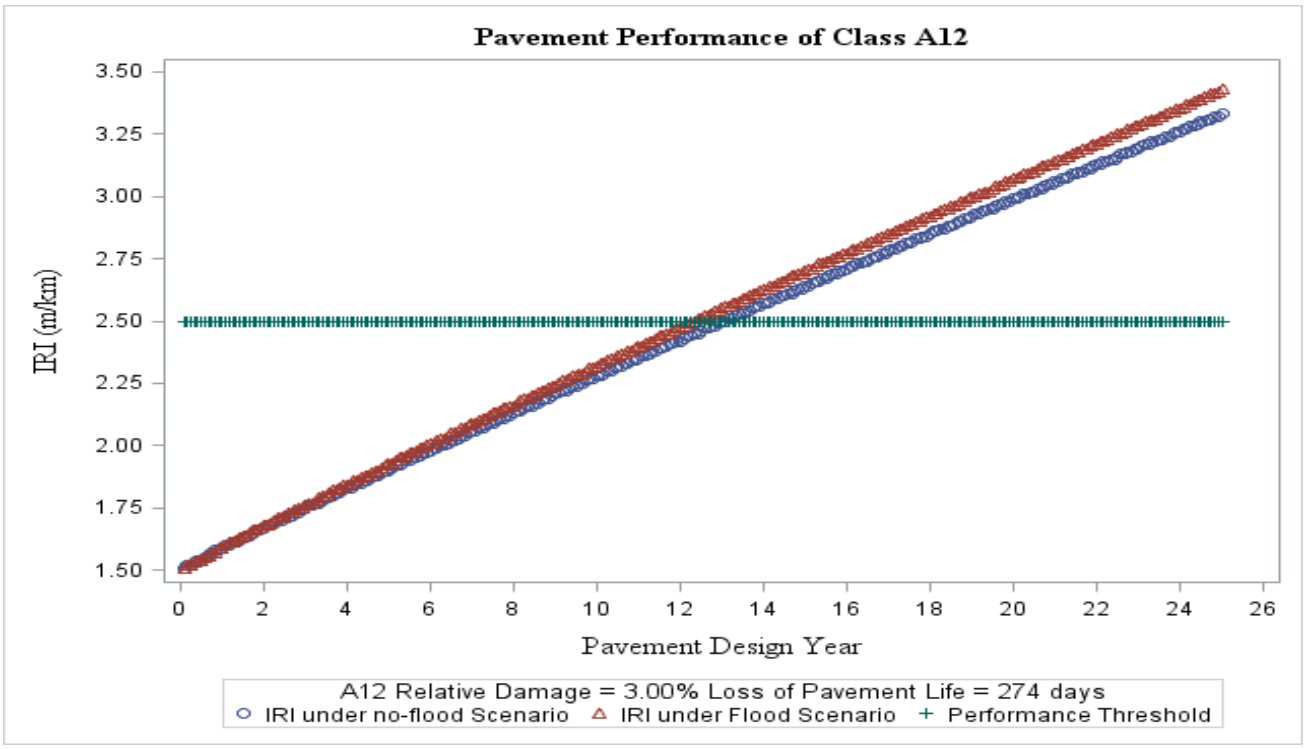
Pavement Performance of Class A12
IRI (m/km)
3.50
3.25
3.00
2.75
2.50
2.25
2.00
1.75
1.50
0
2
4
6
8
10
12
14
16
18
20
22
24
26
Pavement Design Year
A12 Relative Damage = 3.00% Loss of Pavement Life = 274 days
IRI under no-flood Scenario
IRI under Flood Scenario
Performance Threshold

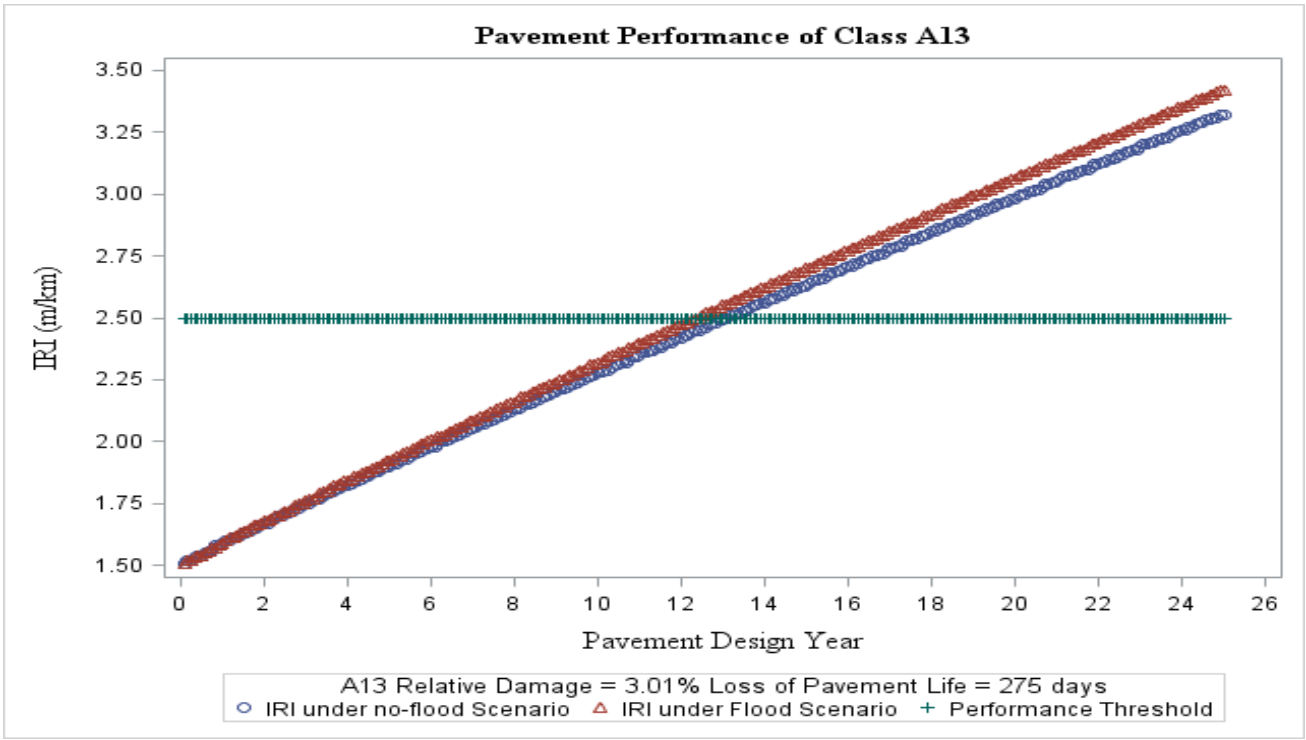
Pavement Performance of Class A13
IRI (m/km)
3.50
3.25
3.00
2.75
2.50
2.25
2.00
1.75
1.50
0
2
4
6
8
10
12
14
16
18
20
22
24
26
Pavement Design Year
A13 Relative Damage = 3.01% Loss of Pavement Life = 275 days
IRI under no-flood Scenario
IRI under Flood Scenario
Performance Threshold

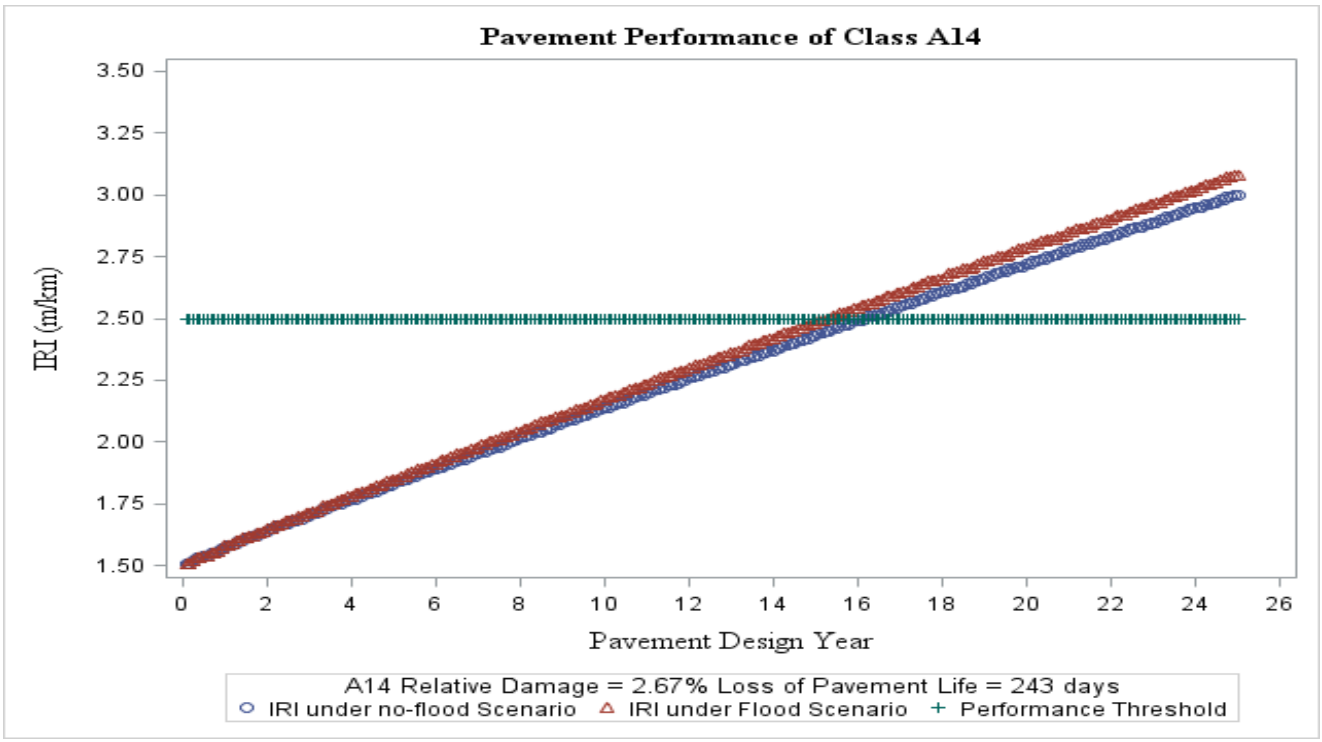
Pavement Performance of Class A14
IRI (m/km)
3.50
3.25
3.00
2.75
2.50
2.25
2.00
1.75
1.50
0
2
4
6
8
10
12
14
16
18
20
22
24
26
Pavement Design Year
A14 Relative Damage = 2.67% Loss of Pavement Life = 243 days
IRI under no-flood Scenario
IRI under Flood Scenario
Performance Threshold

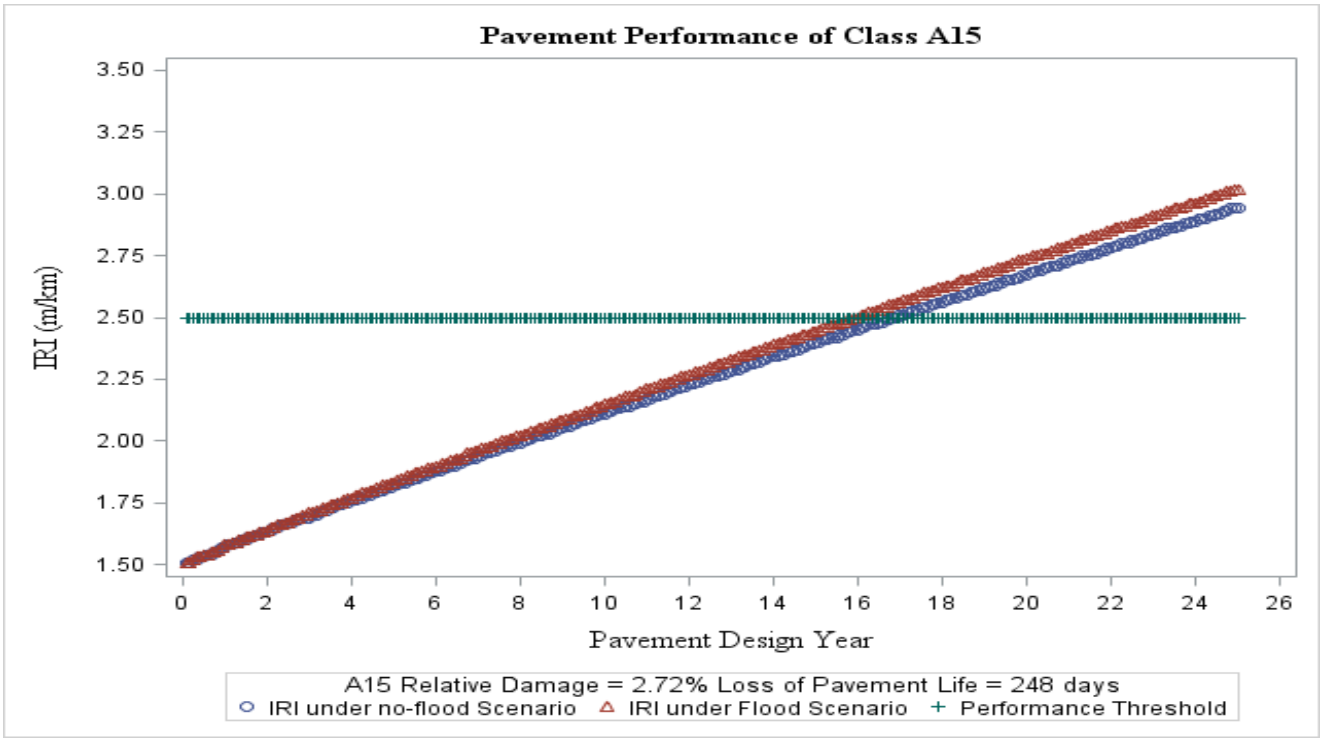
Pavement Performance of Class A15
IRI (m/km)
3.50
3.25
3.00
2.75
2.50
2.25
2.00
1.75
1.50
0
2
4
6
8
10
12
14
16
18
20
22
24
26
Pavement Design Year
A15 Relative Damage = 2.72% Loss of Pavement Life = 248 days
IRI under no-flood Scenario
IRI under Flood Scenario
Performance Threshold

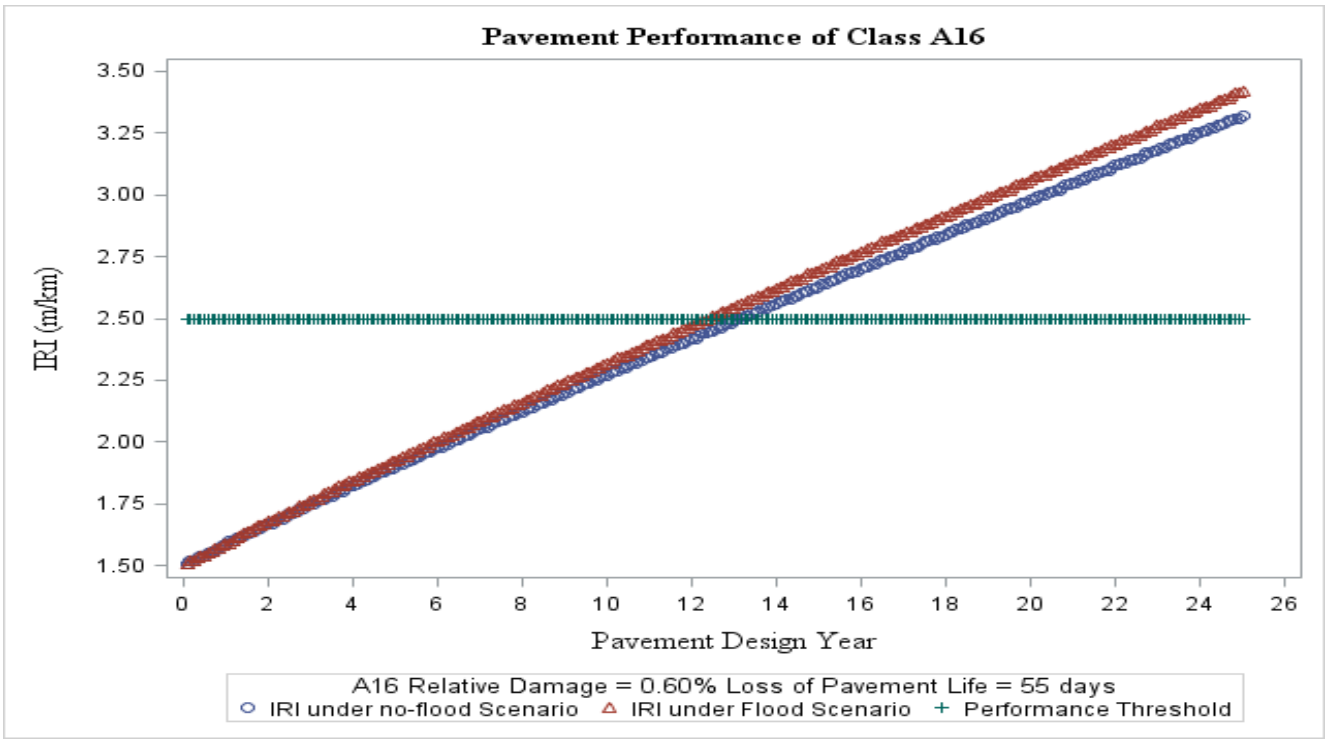
Pavement Performance of Class A16
IRI (m/km)
3.50
3.25
3.00
2.75
2.50
2.25
2.00
1.75
1.50
0
2
4
6
8
10
12
14
16
18
20
22
24
26
Pavement Design Year
A16 Relative Damage = 0.60% Loss of Pavement Life = 55 days
IRI under no-flood Scenario
IRI under Flood Scenario
Performance Threshold

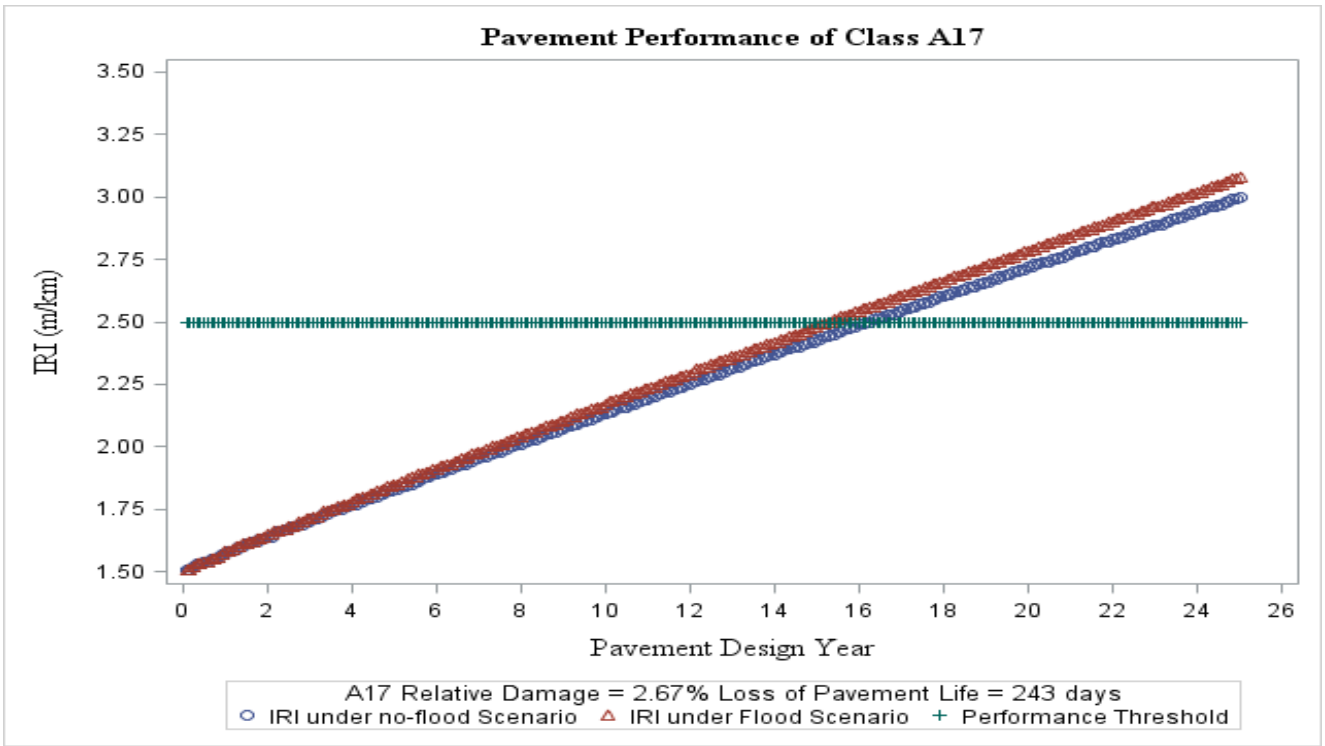
Pavement Performance of Class A17
IRI (m/km)
3.50
3.25
3.00
2.75
2.50
2.25
2.00
1.75
1.50
0
2
4
6
8
10
12
14
16
18
20
22
24
26
Pavement Design Year
A17 Relative Damage = 2.67% Loss of Pavement Life = 243 days
IRI under no-flood Scenario
IRI under Flood Scenario
Performance Threshold

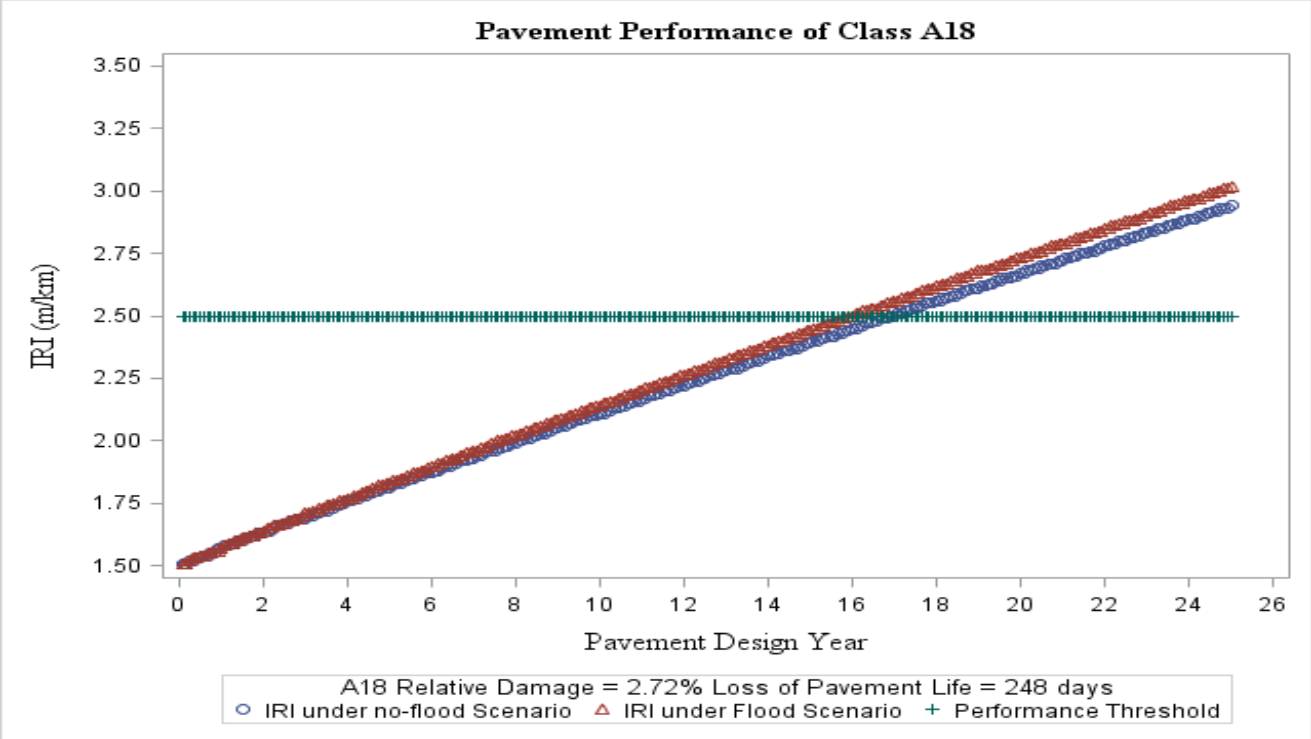
Pavement Performance of Class A18
IRI (m/km)
3.50
3.25
3.00
2.75
2.50
2.25
2.00
1.75
1.50
0
2
4
6
8
10
12
14
16
18
20
22
24
26
Pavement Design Year
A18 Relative Damage = 2.72% Loss of Pavement Life = 248 days
IRI under no-flood Scenario
IRI under Flood Scenario
Performance Threshold

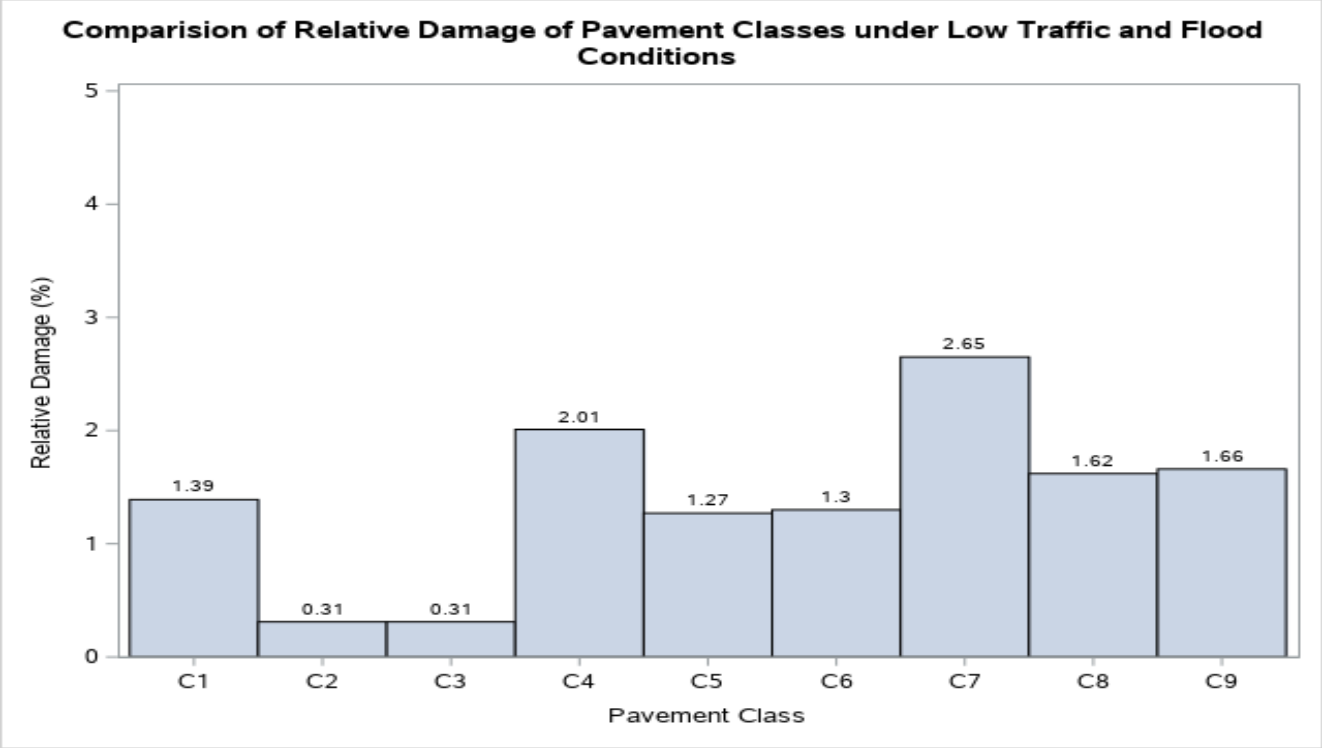
Comparision of Relative Damage of Pavement Classes under Low Traffic and Flood Conditions
Relative Damage (%)
0
1
2
3
4
5
1.39
0.31
0.31
2.01
1.27
1.3
2.65
1.62
1.66
C1
C2
C3
C4
C5
C6
C7
C8
C9
Pavement Class

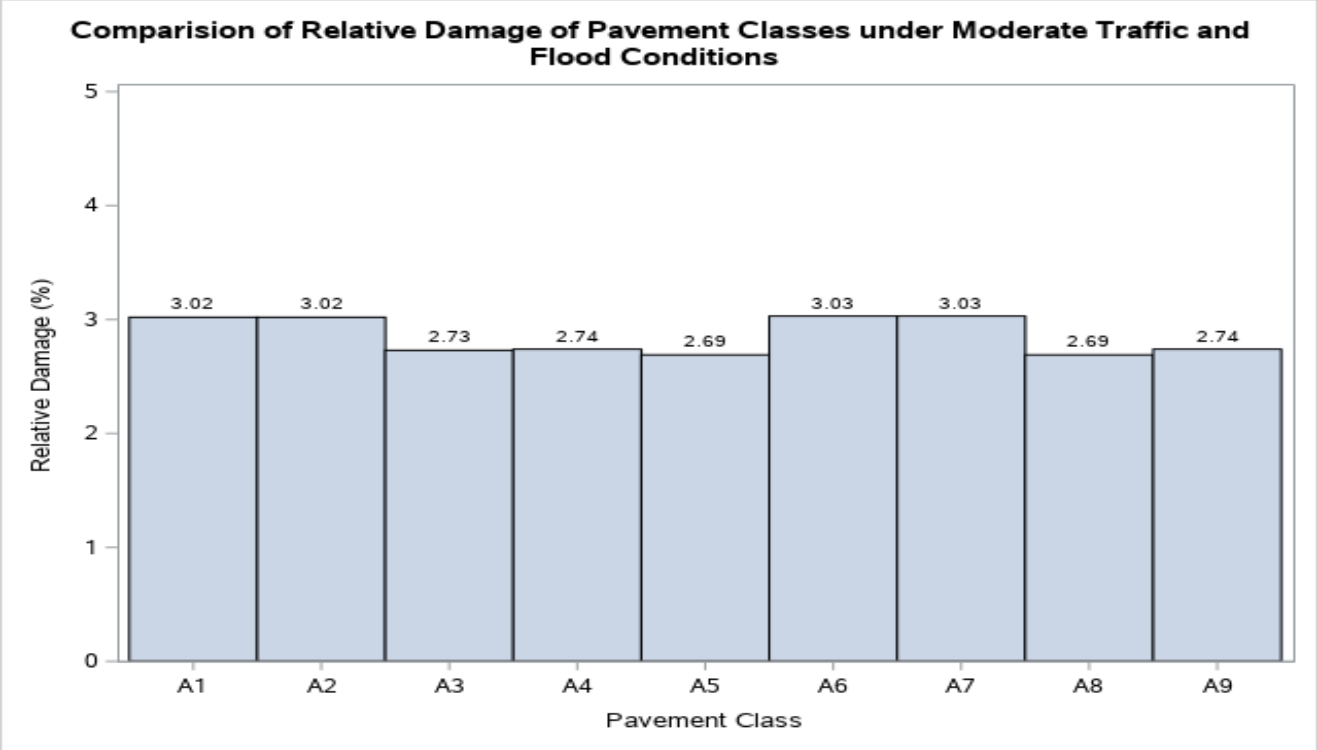
Comparision of Relative Damage of Pavement Classes under Moderate Traffic and Flood Conditions
Relative Damage (%)
0
1
2
3
4
5
3.02
3.02
2.73
2.74
2.69
3.03
3.03
2.69
2.74
A1
A2
A3
A4
A5
A6
A7
A8
A9
Pavement Class

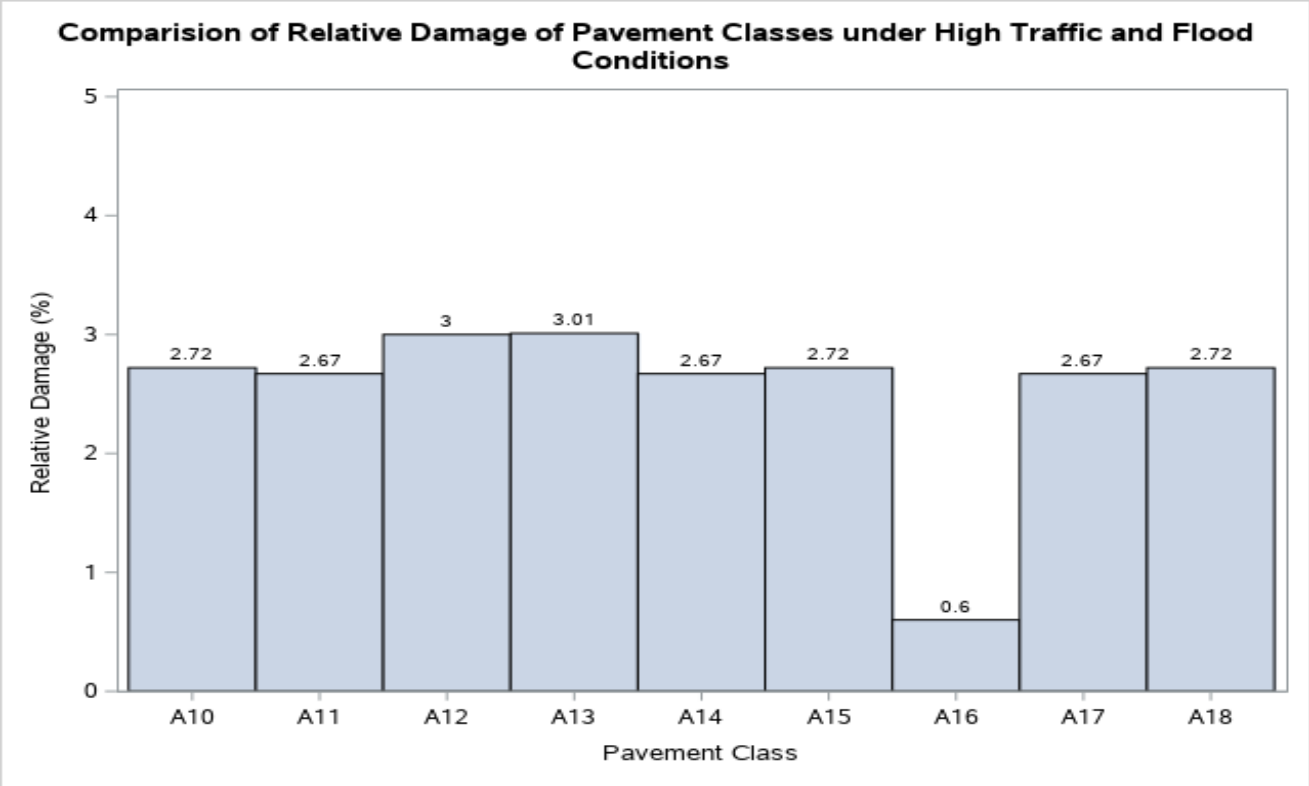
Comparision of Relative Damage of Pavement Classes under High Traffic and Flood Conditions
Relative Damage (%)
0
1
2
3
4
5
2.72
2.67
3
3.01
2.67
2.72
0.6
2.67
2.72
A10
A11
A12
A13
A14
A15
A16
A17
A18
Pavement Class

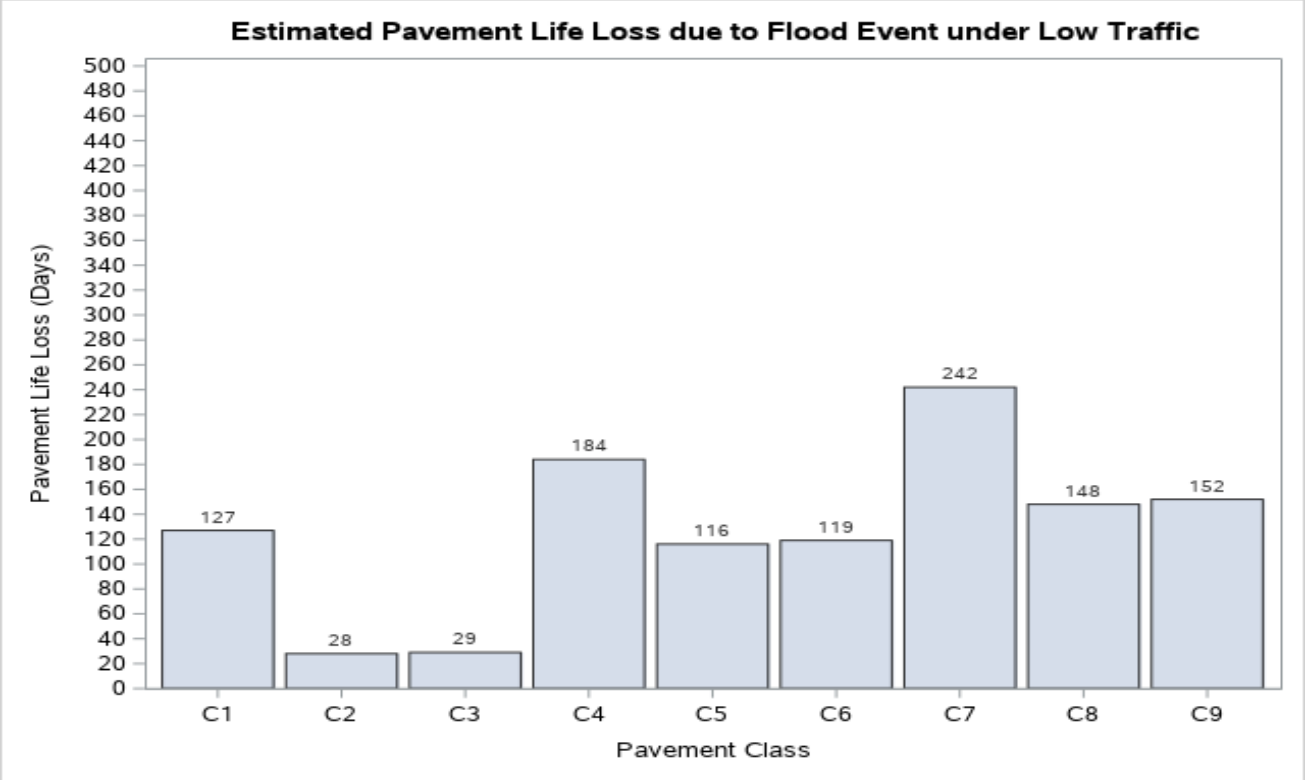
Estimated Pavement Life Loss due to Flood Event under Low Traffic
Pavement Life Loss (Days)
0
20
40
60
80
100
120
140
160
180
200
220
240
260
280
300
320
340
360
380
400
420
440
460
480
500
127
28
29
184
116
119
242
148
152
C1
C2
C3
C4
C5
C6
C7
C8
C9
Pavement Class

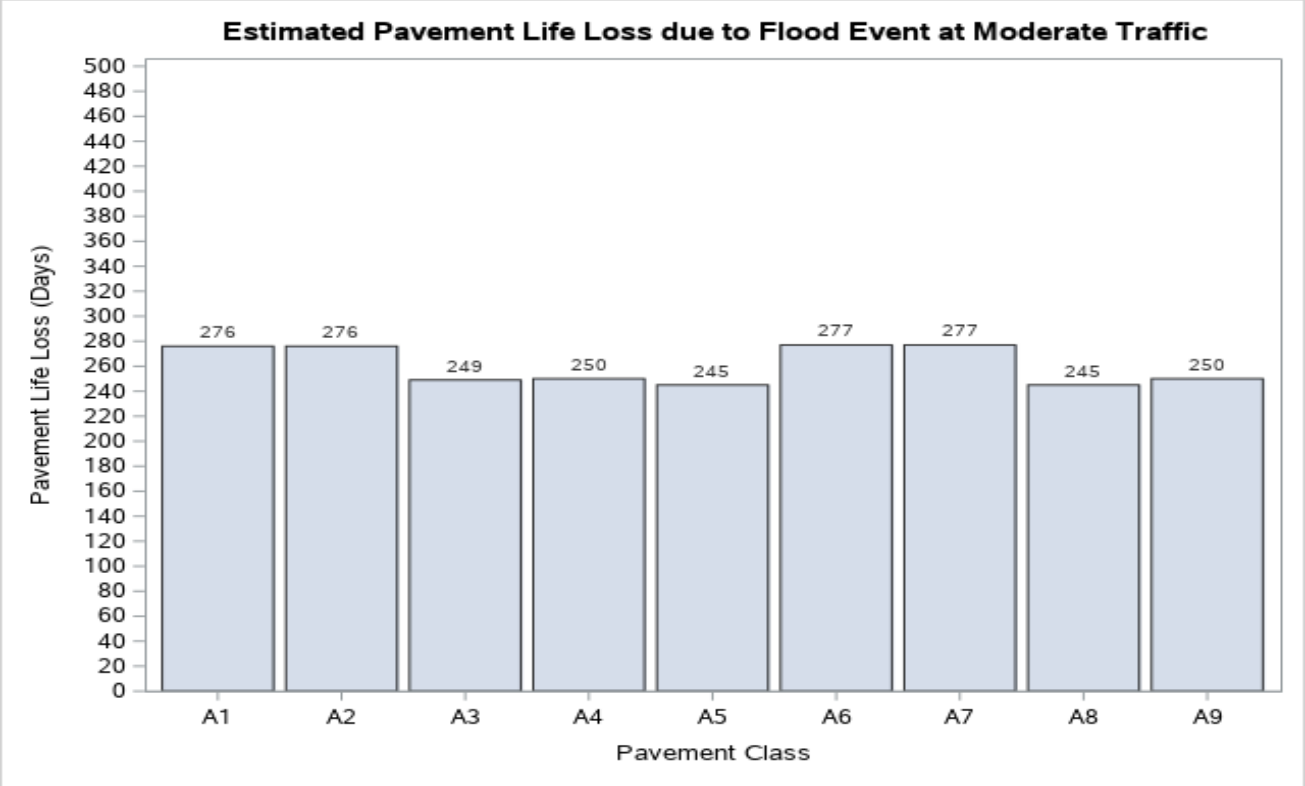
Estimated Pavement Life Loss due to Flood Event at Moderate Traffic
Pavement Life Loss (Days)
500
480
460
440
420
400
380
360
340
320
300
280
260
240
220
200
180
160
140
120
100
80
60
40
20
0
276
276
249
250
245
277
277
245
250
A1
A2
A3
A4
A5
A6
A7
A8
A9
Pavement Class

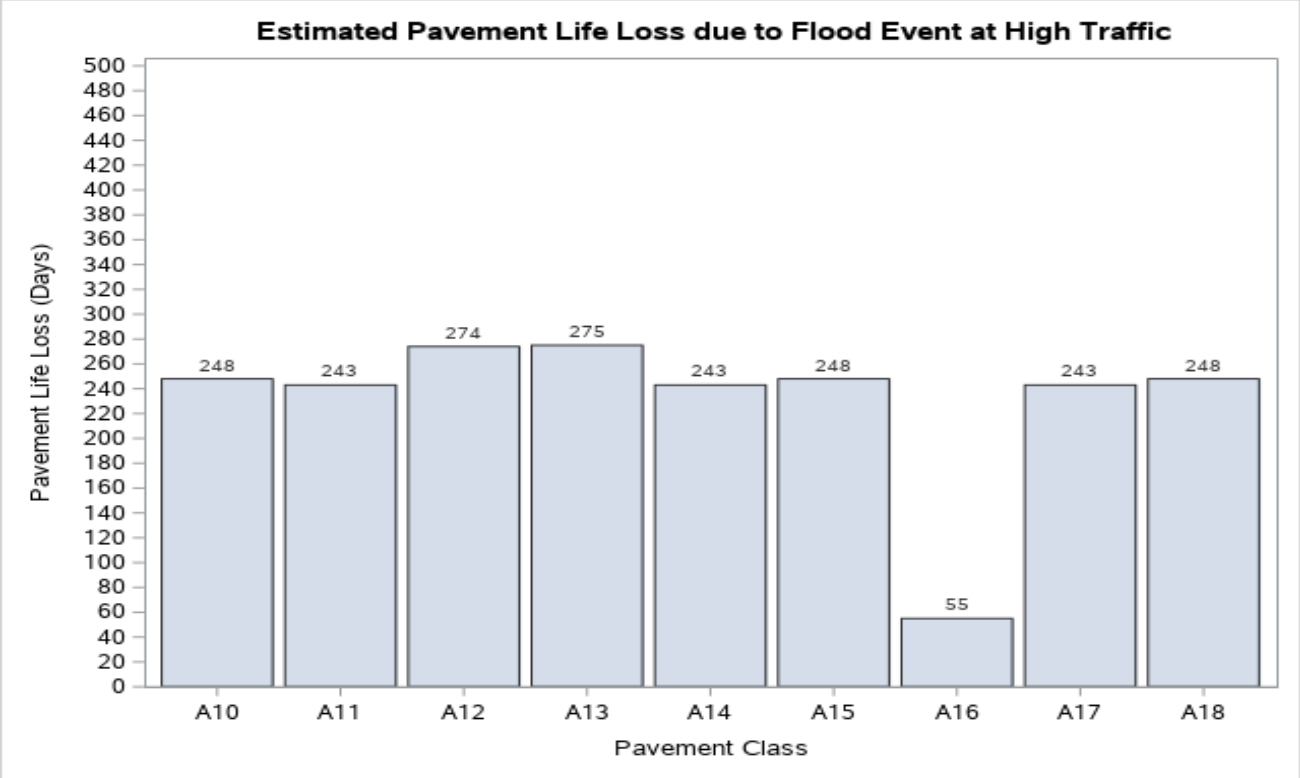
Estimated Pavement Life Loss due to Flood Event at High Traffic
Pavement Life Loss (Days)
500
480
460
440
420
400
380
360
340
320
300
280
260
240
220
200
180
160
140
120
100
80
60
40
20
0
248
243
274
275
243
248
55
243
248
A10
A11
A12
A13
A14
A15
A16
A17
A18
Pavement Class

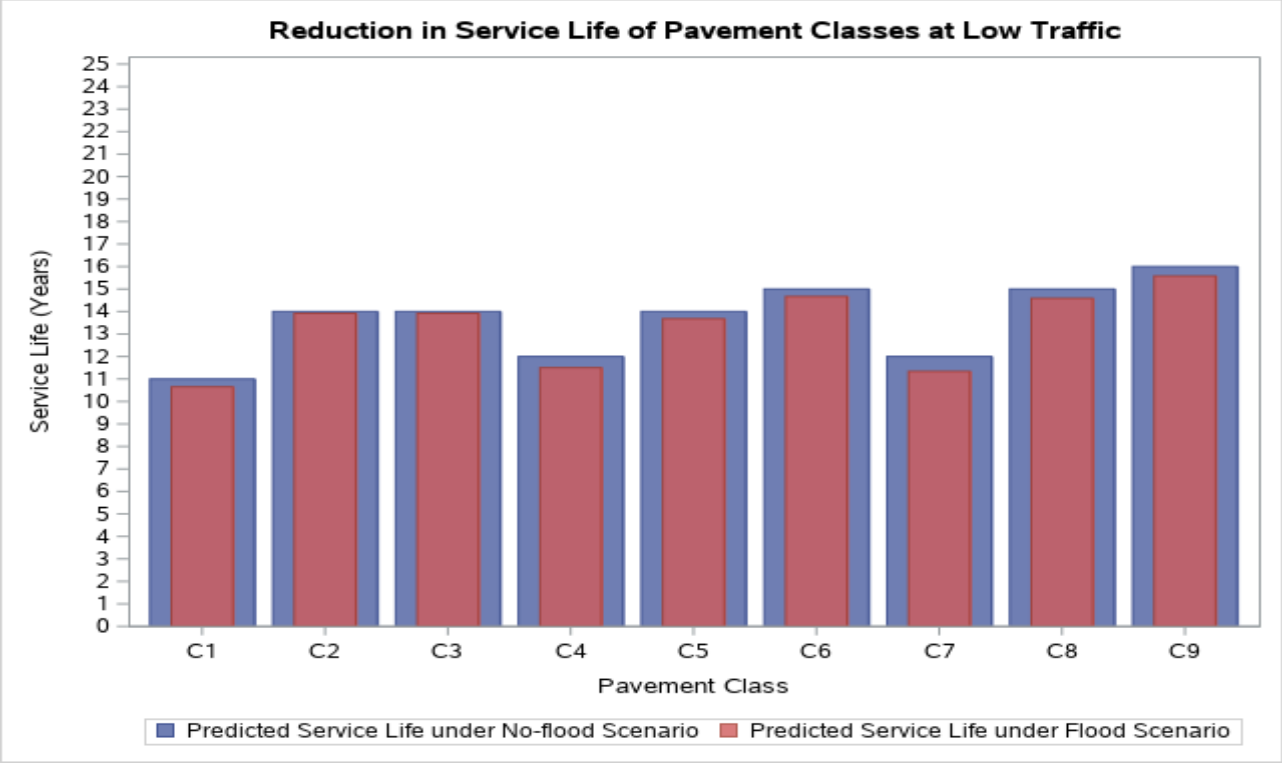
Reduction in Service Life of Pavement Classes at Low Traffic
Service Life (Years)
0 1 2 3 4 5 6 7 8 9 10 11 12 13 14 15 16 17 18 19 20 21 22 23 24 25
C1 C2 C3 C4 C5 C6 C7 C8 C9
Pavement Class
Predicted Service Life under No-flood Scenario
Predicted Service Life under Flood Scenario

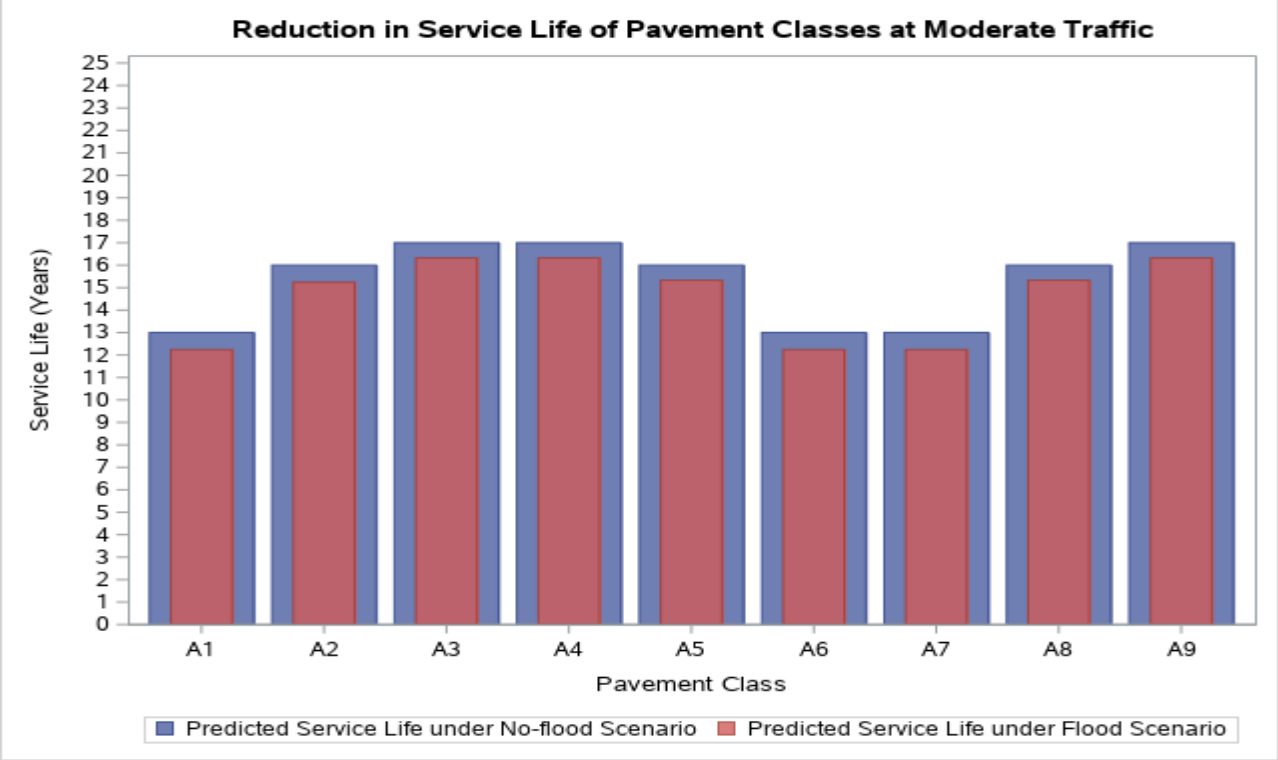
Reduction in Service Life of Pavement Classes at Moderate Traffic
Service Life (Years)
0 1 2 3 4 5 6 7 8 9 10 11 12 13 14 15 16 17 18 19 20 21 22 23 24 25
A1 A2 A3 A4 A5 A6 A7 A8 A9
Pavement Class
Predicted Service Life under No-flood Scenario
Predicted Service Life under Flood Scenario

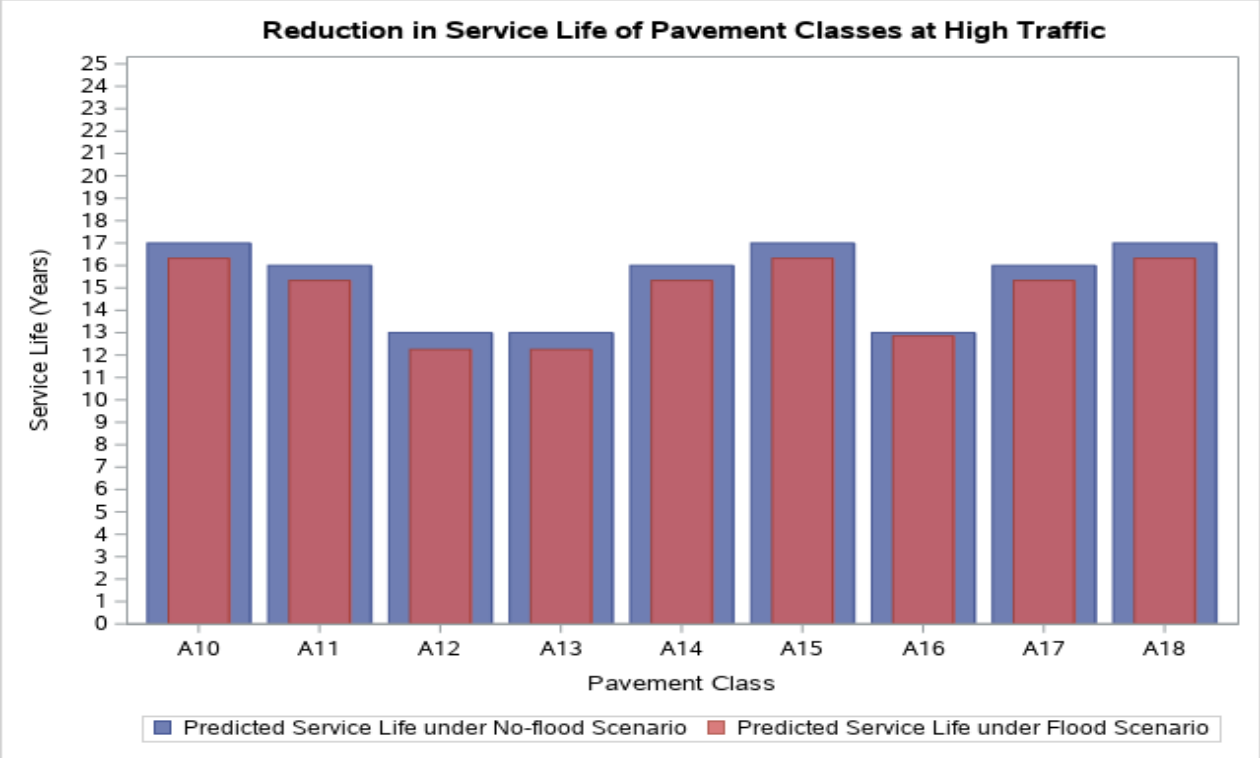
Reduction in Service Life of Pavement Classes at High Traffic
Service Life (Years)
0
1
2
3
4
5
6
7
8
9
10
11
12
13
14
15
16
17
18
19
20
21
22
23
24
25
A10
A11
A12
A13
A14
A15
A16
A17
A18
Pavement Class
Predicted Service Life under No-flood Scenario
Predicted Service Life under Flood Scenario